



A hyperelastic extended Kirchhoff–Love shell model with out-of-plane normal stress: I. Out-of-plane deformation

Yasutoshi Taniguchi¹ · Kenji Takizawa¹ · Yuto Otoguro² · Tayfun E. Tezduyar^{3,4}

Received: 2 February 2022 / Accepted: 17 March 2022 / Published online: 23 April 2022
© The Author(s) 2022

Abstract

This is the first part of a two-part article on a hyperelastic extended Kirchhoff–Love shell model with out-of-plane normal stress. We present the derivation of the new model, with focus on the mechanics of the out-of-plane deformation. Accounting for the out-of-plane normal stress distribution in the out-of-plane direction affects the accuracy in calculating the deformed-configuration out-of-plane position, and consequently the nonlinear response of the shell. The improvement is beyond what we get from accounting for the out-of-plane deformation mapping. By accounting for the out-of-plane normal stress, the traction acting on the shell can be specified on the upper and lower surfaces separately. With that, the new model is free from the “midsurface” location in terms of specifying the traction. We also present derivations related to the variation of the kinetic energy and the form of specifying the traction and moment acting on the upper and lower surfaces and along the edges. We present test computations for unidirectional plate bending, plate saddle deformation, and pressurized cylindrical and spherical shells. We use the neo-Hookean and Fung’s material models, for the compressible- and incompressible-material cases, and with the out-of-plane normal stress and without, which is the plane-stress case.

Keywords Kirchhoff–Love shell model · Hyperelastic material · Out-of-plane normal stress · Out-of-plane deformation mapping · Neo-Hookean material model · Fung’s material model

1 Introduction

A shell formulation based on the Kirchhoff–Love shell theory and isogeometric discretization was introduced in [1–3]. It has the advantage of not requiring rotational degrees of freedom. Extension to general hyperelastic material can be found in [4,5]. The formulation has been successfully used in computation of a good number of challenging

problems, including wind-turbine fluid–structure interaction (FSI) [3,6–10], bioinspired flapping-wing aerodynamics [11], bioprosthetic heart valves [12–16], fatigue and damage [17–22], and design [23,24].

We are introducing a hyperelastic extended Kirchhoff–Love shell model with out-of-plane normal stress. In the first part of a two-part article, we present the derivation of the model, with focus on the mechanics of the out-of-plane deformation. To determine the out-of-plane stress, we solve the linear-momentum-balance equation in the out-of-plane direction. Accounting for the out-of-plane normal stress distribution in the out-of-plane direction affects the accuracy in calculating the deformed-configuration out-of-plane position, and consequently the nonlinear response of the shell. The improvement is beyond what was achieved with the new model’s precursor [5] by accounting for the out-of-plane deformation mapping.

A good number of shell models were presented earlier in the finite element context (see, for example, [25–31]), with significant effort in bending representation. The model in [28] is based on a mixed formulation. The model in [31] is based on a discontinuous-Galerkin type approximation

✉ Kenji Takizawa
Kenji.Takizawa@tafsm.org

Tayfun E. Tezduyar
tezduyar@tafsm.org

¹ Department of Modern Mechanical Engineering, Waseda University, 3-4-1 Ookubo, Shinjuku-ku, Tokyo 169-8555, Japan

² Department of Mechanical Engineering, Faculty of Science and Technology, Tokyo University of Science, 2641 Yamazaki, Noda-shi, Chiba-ken 278-8510, Japan

³ Mechanical Engineering, Rice University – MS 321, 6100 Main Street, Houston, TX 77005, USA

⁴ Faculty of Science and Engineering, Waseda University, 3-4-1 Ookubo, Shinjuku-ku, Tokyo 169-8555, Japan

to weakly enforce C^1 continuity. The model in [30] is a TUBA family element, which has displacement derivatives as unknowns to attain C^1 continuity in the displacement. The model we are introducing here is similar to the model in [25], which uses only one parameter to represent the out-of-plane deformation. Most of the other shell formulations, including some based on the Reissner–Mindlin theory, use the plane-stress assumption. The models in [26,27], based on the Reissner–Mindlin theory, are, however, without the plane-stress assumption, in the finite element context.

Continuing what was started with its precursor, the model introduced here is extending the range of applicability of the Kirchhoff–Love shell theory to the situations where the Kirchhoff–Love shell kinematics is still valid yet the thickness or the curvature change is significant enough to make a difference in the response. Fung’s material model has different versions. In the version used in [13], the first invariant of the Cauchy–Green deformation tensor appears in a squared form. In the version used in this article, as in [5], it appears without being squared, and this version has been used in a number of arterial FSI computations [32–39] with the continuum model.

By accounting for the out-of-plane normal stress, the traction acting on the shell can be specified on the upper and lower surfaces separately. This enables not only more accuracy in the linear-momentum balance in the out-of-plane direction, but also representation of the moment the shear tractions on the upper and lower surfaces generate around the midsurface. With separate out-of-plane tractions on the upper and lower surfaces, for example, we can accurately model cases that might have nonzero net force even when those out-of-plane tractions have equal magnitudes and opposite directions. The net force would be nonzero because the upper and lower surfaces would have different areas due to the curvature. To accurately account for the moment generated by the separate shear tractions on the upper and lower surfaces, we improve the rotational kinematics in the model.

We note that accounting for the out-of-plane stress improves the out-of-plane deformation mapping also in cases with no traction on the upper or lower surfaces and no body force. Those would be the cases when the shell deformation is driven by the displacements and slopes specified along the edges of the shell.

We also would like to note that the level of accuracy we are striving for in representing the tractions on the upper and lower surfaces would be meaningful in an FSI computation only if the flow solution method can deliver those tractions with a comparable level of accuracy. That level of flow solution accuracy, especially in representing the shear stress, requires moving-mesh methods [9], where the high mesh resolution near solid surfaces follows the fluid–solid interface as it moves. That is now possible even in flow computations with actual contact between solid surfaces or some

other topology change. The Space–Time Topology Change method [40] enabled that. We can both represent the actual contact and have high-fidelity, moving-mesh flow solution near the solid surfaces.

Our test computations are based on solving the linear-momentum-balance equation in the out-of-plane direction with finite element discretization. The computed problems are unidirectional plate bending, plate saddle deformation, and pressurized cylindrical and spherical shells. We use the neo-Hookean and Fung’s material models, for the compressible- and incompressible-material cases, and with the out-of-plane normal stress and without, which is the plane-stress case.

In Sect. 2, we provide the definitions and concepts used in the shell model, including the notations and main assumptions. In Sect. 3, we derive the weak form from the virtual-work principle and express the corresponding strong form. In Sect. 4, we describe the solution technique for the out-of-plane deformation, which is meant to be used only for the test computations in Sect. 5. The concluding remarks are given in Sect. 6. In the Appendix, we provide some supplemental derivations and the constitutive models.

2 Hyperelastic shell model

2.1 Kinematics

Let $\Omega_t \subset \mathbb{R}^{n_{sd}}$ be the spatial domain with boundary Γ_t at time $t \in (0, T)$, where n_{sd} is the number of space dimensions. Here, we assume $n_{sd} = 3$. The subscript t indicates the time-dependence of the domain.

We split the domain as $\Omega_t = \bar{\Gamma}_t \times (h_{th})_t$, where $\bar{\Gamma}_t$ represents the midsurface, which is parametrized by $n_{pd} = n_{sd} - 1$, with n_{pd} being the number of parametric dimensions. The remaining parametric direction is the out-of-plane direction, which we will explain a little later in this section. The symbol $(h_{th})_t$ will represent both the shell thickness and the domain in the out-of-plane direction, depending on the context. With the position $\bar{\mathbf{x}} \in \bar{\Gamma}_t$, we define a natural coordinate system:

$$\bar{\mathbf{g}}_\alpha \equiv \frac{\partial \bar{\mathbf{x}}}{\partial \xi^\alpha} \quad (1)$$

$$= \bar{\mathbf{x}}_{,\alpha}, \quad (2)$$

where $\alpha = 1, \dots, n_{pd}$ and ξ^α represents the parametric space. Figure 1 shows a schematic shell domain. We note that this parametric space is only for representing the neighborhood around a point. With a range $-1 \leq \xi^\alpha \leq 1$ and without loss of generality, it can be seen as a parent finite element domain. The out-of-plane direction is

$$\bar{\mathbf{n}} \equiv \bar{\mathbf{g}}_3 \quad (3)$$

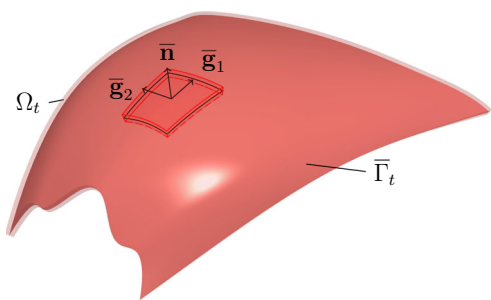


Fig. 1 A schematic shell domain Ω_t at current configuration and the midsurface $\bar{\Gamma}_t$. The black-framed region is for showing the parametric space used in representing the neighborhood around a point. With a range $-1 \leq \xi^\alpha \leq 1$, the parametric space can be seen as a parent finite element domain. The basis vectors of the natural coordinate system are also shown in the figure

$$= \frac{\bar{\mathbf{g}}_1 \times \bar{\mathbf{g}}_2}{\|\bar{\mathbf{g}}_1 \times \bar{\mathbf{g}}_2\|}. \tag{4}$$

The components of the metric tensor are

$$\bar{g}_{\alpha\beta} = \bar{\mathbf{g}}_\alpha \cdot \bar{\mathbf{g}}_\beta, \tag{5}$$

and this is known as the first fundamental form. We also work with the contravariant components of the metric tensor $\bar{g}^{\alpha\beta}$ and the contravariant basis vectors $\bar{\mathbf{g}}^\alpha$ (see Appendix A for their relationship to $\bar{g}_{\alpha\beta}$ and $\bar{\mathbf{g}}_\alpha$).

A position $\mathbf{x} \in \Omega_t$ is represented as

$$\mathbf{x} = \bar{\mathbf{x}} + \bar{\mathbf{n}}\xi^3, \tag{6}$$

where $\xi^3 \in (h_{th})_t = [(\xi^3)^-, (\xi^3)^+]$. Along ξ^3 , the basis vectors are represented as

$$\mathbf{g}_\alpha \equiv \mathbf{x}_{,\alpha} \tag{7}$$

$$= \bar{\mathbf{g}}_\alpha + \bar{\mathbf{n}}_{,\alpha}\xi^3 \tag{8}$$

$$= \bar{\mathbf{g}}_\alpha + \bar{\kappa}_{\alpha\gamma}\bar{\mathbf{g}}^\gamma\xi^3, \tag{9}$$

where

$$\bar{\kappa}_{\alpha\gamma} \equiv \frac{1}{2}(\bar{\mathbf{g}}_\alpha \cdot \bar{\mathbf{n}}_{,\gamma} + \bar{\mathbf{g}}_\gamma \cdot \bar{\mathbf{n}}_{,\alpha}). \tag{10}$$

See Appendix B.1 for the lines between Eqs. (8) and (9). With that, the metric tensor components in 3D space are

$$g_{\alpha\beta} = \mathbf{g}_\alpha \cdot \mathbf{g}_\beta \tag{11}$$

$$= \bar{g}_{\alpha\beta} + 2\bar{\kappa}_{\alpha\beta}\xi^3 + \bar{\omega}_{\alpha\beta}(\xi^3)^2, \tag{12}$$

where

$$\bar{\omega}_{\alpha\beta} \equiv \bar{\mathbf{n}}_{,\alpha} \cdot \bar{\mathbf{n}}_{,\beta} \tag{13}$$

$$= \bar{\kappa}_{\alpha\gamma}\bar{g}^{\gamma\delta}\bar{\kappa}_{\delta\beta}. \tag{14}$$

Remark 1 The symbols $\bar{\kappa}_{\alpha\beta}$ and $\bar{\omega}_{\alpha\beta}$ are for notational convenience.

We note that the curvature tensor is defined by

$$\bar{\boldsymbol{\kappa}} = \bar{\kappa}_{\alpha\beta}\bar{\mathbf{g}}^\alpha\bar{\mathbf{g}}^\beta, \tag{15}$$

and the square of the curvature tensor is the tensor version of $\bar{\omega}_{\alpha\beta}$:

$$\bar{\boldsymbol{\kappa}} \cdot \bar{\boldsymbol{\kappa}} = \bar{\omega}_{\alpha\beta}\bar{\mathbf{g}}^\alpha\bar{\mathbf{g}}^\beta, \tag{16}$$

We also use the dual basis system with $g^{\alpha\beta}$ and \mathbf{g}^α (see Appendix A for their relationship to $g_{\alpha\beta}$ and \mathbf{g}_α).

We now provide similar definitions and derivations for the undeformed configuration $\bar{\mathbf{X}} \in \bar{\Gamma}_0$. We start with the basis vectors

$$\bar{\mathbf{G}}_\alpha = \frac{\partial \bar{\mathbf{X}}}{\partial \xi_0^\alpha} \tag{17}$$

$$= \bar{\mathbf{X}}_{,\alpha}, \tag{18}$$

where $\xi_0^\alpha = \xi^\alpha$, and

$$\bar{\mathbf{N}} \equiv \bar{\mathbf{G}}_3 \tag{19}$$

$$= \frac{\bar{\mathbf{G}}_1 \times \bar{\mathbf{G}}_2}{\|\bar{\mathbf{G}}_1 \times \bar{\mathbf{G}}_2\|}. \tag{20}$$

We also again work with the contravariant components of the metric tensor $\bar{G}^{\alpha\beta}$ and the contravariant basis vectors $\bar{\mathbf{G}}^\alpha$ (see Appendix A for their relationship to $\bar{G}_{\alpha\beta}$ and $\bar{\mathbf{G}}_\alpha$).

A position $\mathbf{X} \in \Omega_0$ is expressed as

$$\mathbf{X} = \bar{\mathbf{X}} + \bar{\mathbf{N}}\xi_0^3, \tag{21}$$

where $\xi_0^3 \in (h_{th})_0 = [(\xi_0^3)^-, (\xi_0^3)^+]$. Similar to what we had for the current configuration, along ξ_0^3 , the basis vectors are represented as

$$\mathbf{G}_\alpha \equiv \mathbf{X}_{,\alpha} \tag{22}$$

$$= \bar{\mathbf{G}}_\alpha + \bar{\mathbf{N}}_{,\alpha}\xi_0^3 \tag{23}$$

$$= \bar{\mathbf{G}}_\alpha + \bar{K}_{\alpha\gamma}\bar{\mathbf{G}}^\gamma\xi_0^3, \tag{24}$$

where

$$\bar{K}_{\alpha\gamma} \equiv \frac{1}{2}(\bar{\mathbf{G}}_\alpha \cdot \bar{\mathbf{N}}_{,\gamma} + \bar{\mathbf{G}}_\gamma \cdot \bar{\mathbf{N}}_{,\alpha}). \tag{25}$$

The lines between Eqs. (23) and (24) are the deformed-configuration counterpart of the lines between Eqs. (8) and (9). The metric tensor components in 3D space are

$$G_{\alpha\beta} = \mathbf{G}_\alpha \cdot \mathbf{G}_\beta \tag{26}$$

$$= \bar{G}_{\alpha\beta} + 2\bar{K}_{\alpha\beta}\xi_0^3 + \bar{\Omega}_{\alpha\beta} (\xi_0^3)^2, \tag{27}$$

where

$$\bar{\Omega}_{\alpha\beta} \equiv \bar{\mathbf{N}}_{,\alpha} \cdot \bar{\mathbf{N}}_{,\beta} \tag{28}$$

$$= \bar{K}_{\alpha\gamma} \bar{G}^{\gamma\delta} \bar{K}_{\delta\beta}. \tag{29}$$

We also again use the dual basis system with $G^{\alpha\beta}$ and \mathbf{G}^α (see Appendix A for their relationship to $G_{\alpha\beta}$ and \mathbf{G}_α).

2.1.1 Deformation gradient tensor

The deformation gradient tensor \mathbf{F} is defined from

$$d\mathbf{x} = \mathbf{F} \cdot d\mathbf{X}, \tag{30}$$

which implies

$$\mathbf{g}_\alpha d\xi^\alpha + \bar{\mathbf{n}} d\xi^3 = \mathbf{F} \cdot (\mathbf{G}_\alpha d\xi^\alpha + \bar{\mathbf{N}} d\xi^3). \tag{31}$$

Using the relationship $\xi^\alpha = \xi_0^\alpha$ and introducing

$$\lambda_3 = \frac{d\xi^3}{d\xi_0^3}, \tag{32}$$

we can write

$$\mathbf{F} = \mathbf{g}_\alpha \mathbf{G}^\alpha + \lambda_3 \bar{\mathbf{n}} \bar{\mathbf{N}}. \tag{33}$$

2.1.2 Cauchy–Green deformation tensor

The Cauchy–Green deformation tensor is defined as

$$\mathbf{C} \equiv \mathbf{F}^T \cdot \mathbf{F}, \tag{34}$$

which is

$$\mathbf{C} = (\mathbf{G}^\alpha \mathbf{g}_\alpha + \lambda_3 \bar{\mathbf{N}} \bar{\mathbf{n}}) \cdot (\mathbf{g}_\beta \mathbf{G}^\beta + \lambda_3 \bar{\mathbf{n}} \bar{\mathbf{N}}) \tag{35}$$

$$= g_{\alpha\beta} \mathbf{G}^\alpha \mathbf{G}^\beta + \lambda_3^2 \bar{\mathbf{N}} \bar{\mathbf{N}}, \tag{36}$$

and the determinant of \mathbf{C} gives the square of $J = \det \mathbf{F}$:

$$J^2 = \det \mathbf{C} \tag{37}$$

$$= \frac{A^2}{A_0^2} \lambda_3^2, \tag{38}$$

$$A^2 = \det [g_{\alpha\beta}], \tag{39}$$

$$A_0^2 = \det [G_{\alpha\beta}]. \tag{40}$$

2.1.3 Green–Lagrange strain tensor

The Green–Lagrange strain tensor is defined as

$$\mathbf{E} = \frac{1}{2} (\mathbf{C} - \mathbf{I}), \tag{41}$$

where \mathbf{I} is the identity tensor, and one of the ways to express it is

$$\mathbf{I} = G_{\alpha\beta} \mathbf{G}^\alpha \mathbf{G}^\beta + \bar{\mathbf{N}} \bar{\mathbf{N}}. \tag{42}$$

We can then write \mathbf{E} as

$$\mathbf{E} = \frac{1}{2} (\mathbf{C} - (G_{\alpha\beta} \mathbf{G}^\alpha \mathbf{G}^\beta + \bar{\mathbf{N}} \bar{\mathbf{N}})) \tag{43}$$

$$= \frac{1}{2} (g_{\alpha\beta} - G_{\alpha\beta}) \mathbf{G}^\alpha \mathbf{G}^\beta + \frac{1}{2} (\lambda_3^2 - 1) \bar{\mathbf{N}} \bar{\mathbf{N}}. \tag{44}$$

The covariant components of the in-plane strain tensor are

$$E_{\alpha\beta} = \frac{1}{2} (g_{\alpha\beta} - G_{\alpha\beta}) \tag{45}$$

$$= \frac{1}{2} \underbrace{(\bar{g}_{\alpha\beta} - \bar{G}_{\alpha\beta})}_{\bar{\varepsilon}_{\alpha\beta}} + (\bar{\kappa}_{\alpha\beta} \xi^3 - \bar{K}_{\alpha\beta} \xi_0^3) + \frac{1}{2} \left(\bar{\omega}_{\alpha\beta} (\xi^3)^2 - \bar{\Omega}_{\alpha\beta} (\xi_0^3)^2 \right). \tag{46}$$

The symbol $\bar{\varepsilon}_{\alpha\beta}$ here represents what is typically identified as the membrane strain. That is only part of the membrane strain in our model. The normal component associated with the out-of-plane direction is

$$E_{33} = \frac{1}{2} (\lambda_3^2 - 1). \tag{47}$$

Remark 2 The term of Eq. (46) that is quadratic in ξ^3 and ξ_0^3 was omitted in [5] as a higher-order term. We retain that here.

2.2 The strain-energy density function

We express the strain-energy density function as

$$\varphi = \varphi(\mathbf{E}). \tag{48}$$

The second Piola–Kirchhoff stress tensor,

$$\mathbf{S} = S^{\alpha\beta} \mathbf{G}_\alpha \mathbf{G}_\beta + S^{33} \bar{\mathbf{N}} \bar{\mathbf{N}}, \tag{49}$$

is obtained from

$$\mathbf{S} \equiv \frac{\partial \varphi}{\partial \mathbf{E}}, \tag{50}$$

and from that and Eq. (41),

$$\mathbf{S} = 2 \frac{\partial \varphi}{\partial \mathbf{C}}. \tag{51}$$

The Cauchy stress tensor, defined in the current configuration, can be obtained from

$$\boldsymbol{\sigma} = J^{-1} \mathbf{F} \cdot \mathbf{S} \cdot \mathbf{F}^T. \tag{52}$$

3 Variational formulation

The variations of the internal and kinetic energies are expressed as

$$\delta U = \int_{\Omega_0} \delta \mathbf{E} : \mathbf{S} d\Omega, \tag{53}$$

$$\delta T = - \int_{\Omega_0} \delta \mathbf{x} \cdot \rho_0 \ddot{\mathbf{x}} d\Omega, \tag{54}$$

where ρ_0 is the density at the undeformed configuration. The principle of virtual work can then be written as

$$\delta U - \delta T - \delta W_{\text{ext}} = 0, \tag{55}$$

where δW_{ext} is the external-force virtual work, explained more later.

Remark 3 We note that in [9] (Section 1.2.2), $-\delta W_{\text{int}}$ is used in place of δU .

Remark 4 We also note that in [9] (Section 1.2.2), the variation of the kinetic energy, expressed in terms of the acceleration, is part of the external-force virtual work. Here we keep that separate. With this separation, Eq. (55) can be seen as d’Alembert’s principle.

Remark 5 With the displacement expressed as $\mathbf{y} = \mathbf{x} - \mathbf{X}$, we can do the substitutions $\dot{\mathbf{x}} = \dot{\mathbf{y}}$ and $\ddot{\mathbf{x}} = \ddot{\mathbf{y}}$.

3.1 Admissible variations

The variation of \mathbf{x} is obtained by taking the variation of Eq. (6):

$$\delta \mathbf{x} = \delta \bar{\mathbf{x}} + \delta \bar{\mathbf{n}} \xi^3 + \bar{\mathbf{n}} \delta \xi^3. \tag{56}$$

The variation $\delta \bar{\mathbf{x}}$ represents the virtual displacement of the midsurface, $\delta \bar{\mathbf{n}}$ represents the rotation of the midsurface (see Appendix B.2), and $\delta \xi^3$ represents the virtual displacement in the out-of-plane direction, relative to the midsurface.

From the variation of Eqs. (8) and (32), we obtain

$$\delta \mathbf{g}_\alpha = \delta \bar{\mathbf{g}}_\alpha + \delta \bar{\mathbf{n}}_{,\alpha} \xi^3 + \bar{\mathbf{n}}_{,\alpha} \delta \xi^3, \tag{57}$$

$$\delta \lambda_3 = \frac{d(\delta \xi^3)}{d\xi_0^3}. \tag{58}$$

The variation of \mathbf{E} can be obtained by taking the variation of Eqs. (46) and (47):

$$\begin{aligned} \delta E_{\alpha\beta} &= \delta \bar{e}_{\alpha\beta} + \delta \bar{\kappa}_{\alpha\beta} \xi^3 \\ &\quad + \frac{1}{2} \delta \bar{\omega}_{\alpha\beta} (\xi^3)^2 + \delta \xi^3 (\bar{\kappa}_{\alpha\beta} + \bar{\omega}_{\alpha\beta} \xi^3), \end{aligned} \tag{59}$$

$$\delta E_{33} = \lambda_3 \delta \lambda_3. \tag{60}$$

Remark 6 In [5], only the first two terms of Eq. (59) were present.

The expressions for the three variations in Eq. (59) can be written, from Eqs. (46), (10) and (13), as

$$\delta \bar{e}_{\alpha\beta} = \frac{1}{2} (\bar{\mathbf{g}}_\alpha \cdot \delta \bar{\mathbf{g}}_\beta + \bar{\mathbf{g}}_\beta \cdot \delta \bar{\mathbf{g}}_\alpha), \tag{61}$$

$$\begin{aligned} \delta \bar{\kappa}_{\alpha\beta} &= \frac{1}{2} (\bar{\mathbf{n}}_{,\alpha} \cdot \delta \bar{\mathbf{g}}_\beta + \bar{\mathbf{g}}_\alpha \cdot \delta \bar{\mathbf{n}}_{,\beta} \\ &\quad + \bar{\mathbf{n}}_{,\beta} \cdot \delta \bar{\mathbf{g}}_\alpha + \bar{\mathbf{g}}_\beta \cdot \delta \bar{\mathbf{n}}_{,\alpha}), \end{aligned} \tag{62}$$

$$\delta \bar{\omega}_{\alpha\beta} = \bar{\mathbf{n}}_{,\alpha} \cdot \delta \bar{\mathbf{n}}_{,\beta} + \bar{\mathbf{n}}_{,\beta} \cdot \delta \bar{\mathbf{n}}_{,\alpha}. \tag{63}$$

Remark 7 As can be seen from the expressions in Eqs. (61), (62) and (63), the three variations are not independent. The variation $\delta \bar{\omega}_{\alpha\beta}$ can be expressed in terms of $\delta \bar{e}_{\alpha\beta}$ and $\delta \bar{\kappa}_{\alpha\beta}$. That can be done by first taking the variation of Eq. (14):

$$\delta \bar{\omega}_{\alpha\beta} = \delta \bar{\kappa}_{\alpha\gamma} \bar{g}^{\gamma\delta} \bar{\kappa}_{\delta\beta} + \bar{\kappa}_{\alpha\gamma} \bar{g}^{\gamma\delta} \delta \bar{\kappa}_{\delta\beta} + \bar{\kappa}_{\alpha\gamma} \delta \bar{g}^{\gamma\delta} \bar{\kappa}_{\delta\beta}. \tag{64}$$

Next, $\delta \bar{g}^{\gamma\delta}$ is written as

$$\delta \bar{g}^{\gamma\delta} = -\bar{g}^{\gamma\eta} \delta \bar{g}_{\eta\kappa} \bar{g}^{\kappa\delta}, \tag{65}$$

which can be derived by taking the variation of

$$\bar{g}^{\gamma\eta} \bar{g}_{\eta\kappa} = \delta_\kappa^\gamma. \tag{66}$$

As the last steps, from Eqs. (65) and (66), we write

$$\delta \bar{g}^{\gamma\delta} = -2\bar{g}^{\gamma\eta} \delta \bar{e}_{\eta\kappa} \bar{g}^{\kappa\delta}, \tag{67}$$

substitute that into Eq. (64), and obtain

$$\begin{aligned} \delta \bar{\omega}_{\alpha\beta} &= \delta \bar{\kappa}_{\alpha\gamma} \bar{g}^{\gamma\delta} \bar{\kappa}_{\delta\beta} + \bar{\kappa}_{\alpha\gamma} \bar{g}^{\gamma\delta} \delta \bar{\kappa}_{\delta\beta} \\ &\quad - 2\bar{\kappa}_{\alpha\gamma} \bar{g}^{\gamma\eta} \delta \bar{e}_{\eta\kappa} \bar{g}^{\kappa\delta} \bar{\kappa}_{\delta\beta}. \end{aligned} \tag{68}$$

3.2 Variation of the strain energy

In one of the ways to express the variation of the strain energy, we start with

$$\delta E = \frac{1}{2} (\delta \mathbf{F}^T \cdot \mathbf{F} + \mathbf{F}^T \cdot \delta \mathbf{F}) \tag{69}$$

$$= \frac{1}{2} \left((\mathbf{F}^T \cdot \delta \mathbf{F})^T + \mathbf{F}^T \cdot \delta \mathbf{F} \right). \tag{70}$$

Because \mathbf{S} is a symmetric tensor, we simply write

$$\delta E : \mathbf{S} = (\delta \mathbf{F}^T \cdot \mathbf{F}) : \mathbf{S}. \tag{71}$$

Substituting Eq. (33), its variation, and Eq. (49) into this, we get

$$\delta E : \mathbf{S} = \delta \mathbf{g}_\alpha \cdot \mathbf{g}_\beta S^{\alpha\beta} + \delta \lambda_3 \lambda_3 S^{33}. \tag{72}$$

Substituting Eq. (57) into that, we obtain

$$\delta E : \mathbf{S} = \delta \bar{\mathbf{g}}_\alpha \cdot S^{\alpha\beta} \mathbf{g}_\beta + \delta \bar{\mathbf{n}}_{,\alpha} \cdot S^{\alpha\beta} \mathbf{g}_\beta \xi^3 + \delta \xi^3 \bar{\mathbf{n}}_{,\alpha} \cdot S^{\alpha\beta} \mathbf{g}_\beta + \delta \lambda_3 \lambda_3 S^{33}. \tag{73}$$

We perform the integration in Eq. (53) with the integrand given by Eq. (73):

$$\begin{aligned} \delta U &= \int_{\bar{\Gamma}_0} \delta \bar{\mathbf{g}}_\alpha \cdot \int_{(h_{th})_0} \mathbf{g}_\beta S^{\alpha\beta} \frac{A_0}{A_0} d\xi^3 d\Gamma \\ &+ \int_{\bar{\Gamma}_0} \delta \bar{\mathbf{n}}_{,\alpha} \cdot \int_{(h_{th})_0} \xi^3 \mathbf{g}_\beta S^{\alpha\beta} \frac{A_0}{A_0} d\xi^3 d\Gamma \\ &+ \int_{\bar{\Gamma}_0} \bar{\mathbf{n}}_{,\alpha} \cdot \int_{(h_{th})_0} \delta \xi^3 \mathbf{g}_\beta S^{\alpha\beta} \frac{A_0}{A_0} d\xi^3 d\Gamma \\ &+ \int_{\bar{\Gamma}_0} \bar{\mathbf{n}} \cdot \int_{(h_{th})_0} \delta \lambda_3 \lambda_3 \bar{\mathbf{n}} S^{33} \frac{A_0}{A_0} d\xi^3 d\Gamma. \end{aligned} \tag{74}$$

We define \mathbf{p}^α as

$$\mathbf{p}^\alpha = \mathbf{g}_\beta S^{\alpha\beta} \frac{A_0}{A_0}, \tag{75}$$

its integration along $(h_{th})_0$ as

$$\hat{\mathbf{p}}_0^\alpha = \int_{(h_{th})_0} \mathbf{p}^\alpha d\xi^3, \tag{76}$$

and its first moment as

$$\hat{\mathbf{p}}_1^\alpha = \int_{(h_{th})_0} \xi^3 \mathbf{p}^\alpha d\xi^3. \tag{77}$$

With these definitions, we write Eq. (74) in a simpler form:

$$\delta U = \int_{\bar{\Gamma}_0} \delta \bar{\mathbf{g}}_\alpha \cdot \hat{\mathbf{p}}_0^\alpha d\Gamma$$

$$\begin{aligned} &+ \int_{\bar{\Gamma}_0} \delta \bar{\mathbf{n}}_{,\alpha} \cdot \hat{\mathbf{p}}_1^\alpha d\xi^3 d\Gamma \\ &+ \int_{\bar{\Gamma}_0} \bar{\mathbf{n}}_{,\alpha} \cdot \int_{(h_{th})_0} \delta \xi^3 \mathbf{p}^\alpha d\xi^3 d\Gamma \\ &+ \int_{\bar{\Gamma}_0} \bar{\mathbf{n}} \cdot \int_{(h_{th})_0} \delta \lambda_3 \lambda_3 \bar{\mathbf{n}} S^{33} \frac{A_0}{A_0} d\xi^3 d\Gamma. \end{aligned} \tag{78}$$

We also express δU in an alternative form by using Eqs. (59), (60) and (49) in Eq. (53):

$$\begin{aligned} \delta U &= \int_{\bar{\Gamma}_0} \delta \bar{\varepsilon}_{\alpha\beta} \hat{S}_\varepsilon^{\alpha\beta} d\Gamma \\ &+ \int_{\bar{\Gamma}_0} \delta \bar{\kappa}_{\alpha\beta} \hat{S}_\kappa^{\alpha\beta} d\Gamma \\ &+ \int_{\bar{\Gamma}_0} \frac{1}{2} \delta \bar{\omega}_{\alpha\beta} \hat{S}_\omega^{\alpha\beta} d\Gamma \\ &+ \int_{\bar{\Gamma}_0} \bar{\kappa}_{\alpha\beta} \int_{(h_{th})_0} \delta \xi^3 S^{\alpha\beta} \frac{A_0}{A_0} d\xi^3 d\Gamma \\ &+ \int_{\bar{\Gamma}_0} \bar{\omega}_{\alpha\beta} \int_{(h_{th})_0} \delta \xi^3 \xi^3 S^{\alpha\beta} \frac{A_0}{A_0} d\xi^3 d\Gamma \\ &+ \int_{\bar{\Gamma}_0} \int_{(h_{th})_0} \delta \lambda_3 \lambda_3 S^{33} \frac{A_0}{A_0} d\xi^3 d\Gamma, \end{aligned} \tag{79}$$

where the zeroth, first, and second moments of the contravariant components of \mathbf{S} are given as

$$\hat{S}_\varepsilon^{\alpha\beta} = \int_{(h_{th})_0} S^{\alpha\beta} \frac{A_0}{A_0} d\xi^3, \tag{80}$$

$$\hat{S}_\kappa^{\alpha\beta} = \int_{(h_{th})_0} \xi^3 S^{\alpha\beta} \frac{A_0}{A_0} d\xi^3, \tag{81}$$

$$\hat{S}_\omega^{\alpha\beta} = \int_{(h_{th})_0} (\xi^3)^2 S^{\alpha\beta} \frac{A_0}{A_0} d\xi^3. \tag{82}$$

Remark 8 In [5], the third integral in Eq. (79) was omitted.

Remark 9 The fourth, fifth, and sixth integrals in Eq. (79) are the contributions to the virtual work in the out-of-plane direction, which will be explained more in Sect. 3.5.

3.3 Variation of the kinetic energy

Performing the integration in Eq. (54), we get

$$\delta T = - \int_{\bar{\Gamma}_0} \int_{(h_{th})_0} \delta \mathbf{x} \cdot \rho_0 \ddot{\mathbf{y}} \frac{A_0}{A_0} d\xi^3 d\Gamma. \tag{83}$$

Substituting Eq. (56) into this, we obtain

$$\begin{aligned} \delta T &= - \int_{\bar{\Gamma}_0} \delta \bar{\mathbf{x}} \cdot \hat{\mathbf{m}}_0 d\Gamma - \int_{\bar{\Gamma}_0} \delta \bar{\mathbf{n}} \cdot \hat{\mathbf{m}}_1 d\Gamma \\ &- \int_{\bar{\Gamma}_0} \int_{(h_{th})_0} \delta \xi^3 \rho_0 \bar{\mathbf{n}} \cdot \ddot{\mathbf{y}} \frac{A_0}{A_0} d\xi^3 d\Gamma, \end{aligned} \tag{84}$$

where

$$\hat{\mathbf{m}}_0 = \int_{(h_{th})_0} \rho_0 \ddot{\mathbf{y}} \frac{A_0}{A_0} d\xi^3, \tag{85}$$

$$\hat{\mathbf{m}}_1 = \int_{(h_{th})_0} \xi^3 \rho_0 \dot{\mathbf{y}} \frac{A_0}{A_0} d\xi^3. \tag{86}$$

Remark 10 We note that

$$\delta \bar{\mathbf{n}} \cdot \hat{\mathbf{m}}_1 = \delta \bar{\mathbf{r}} \cdot (\bar{\mathbf{n}} \times \hat{\mathbf{m}}_1), \tag{87}$$

where

$$\delta \bar{\mathbf{r}} \equiv \bar{\mathbf{g}}^\beta \times \delta \bar{\mathbf{g}}_\beta, \tag{88}$$

and $\bar{\mathbf{n}} \times \hat{\mathbf{m}}_1$ represents the time derivative of the angular momentum. The derivation of Eq. (87) is given in Appendix B.3. This rearrangement may make it easier to see the fundamental mechanics in the term.

Remark 11 The second integral in Eq. (84) is related to the time derivative of the angular momentum. It was included in [41], but we did not see other papers that explicitly mention the inclusion of the term.

The acceleration is written as

$$\ddot{\mathbf{y}} = \frac{d^2 (\bar{\mathbf{y}} + \bar{\mathbf{n}} \xi^3)}{dt^2} \tag{89}$$

$$= \ddot{\bar{\mathbf{y}}} + \ddot{\bar{\mathbf{n}}} \xi^3 + 2 \dot{\bar{\mathbf{n}}} \dot{\xi}^3 + \bar{\mathbf{n}} \ddot{\xi}^3. \tag{90}$$

Remark 12 We omit the time derivatives of ξ^3 :

$$\ddot{\mathbf{y}} \approx \ddot{\bar{\mathbf{y}}} + \ddot{\bar{\mathbf{n}}} \xi^3. \tag{91}$$

Otherwise they need to be stored. We see this approximation as a quasi-steady-state assumption.

With that, approximated forms of Eqs. (85) and (86) are written as

$$\hat{\mathbf{m}}_0 = \ddot{\bar{\mathbf{y}}} \hat{m}_0 + \ddot{\bar{\mathbf{n}}} \hat{m}_1, \tag{92}$$

$$\hat{\mathbf{m}}_1 = \ddot{\bar{\mathbf{y}}} \hat{m}_1 + \ddot{\bar{\mathbf{n}}} \hat{m}_2, \tag{93}$$

where

$$\hat{m}_0 = \int_{(h_{th})_0} \rho_0 \frac{A_0}{A_0} d\xi^3, \tag{94}$$

$$\hat{m}_1 = \int_{(h_{th})_0} \xi^3 \rho_0 \frac{A_0}{A_0} d\xi^3, \tag{95}$$

$$\hat{m}_2 = \int_{(h_{th})_0} (\xi^3)^2 \rho_0 \frac{A_0}{A_0} d\xi^3. \tag{96}$$

In the third term of Eq. (84), the integration along $(h_{th})_0$ can be written, with Eq. (91), as

$$\int_{(h_{th})_0} \delta \xi^3 \rho_0 \bar{\mathbf{n}} \cdot \ddot{\mathbf{y}} \frac{A_0}{A_0} d\xi^3 = \bar{\mathbf{n}} \cdot \ddot{\bar{\mathbf{y}}} \delta \hat{m}_1 + \bar{\mathbf{n}} \cdot \ddot{\bar{\mathbf{n}}} \frac{1}{2} \delta \hat{m}_2 \tag{97}$$

$$= \bar{\mathbf{n}} \cdot \ddot{\bar{\mathbf{y}}} \delta \hat{m}_1 - \frac{1}{2} \|\dot{\bar{\mathbf{n}}}\|^2 \delta \hat{m}_2, \tag{98}$$

where

$$\delta \hat{m}_1 = \int_{(h_{th})_0} \delta \xi^3 \rho_0 \frac{A_0}{A_0} d\xi^3, \tag{99}$$

$$\delta \hat{m}_2 = 2 \int_{(h_{th})_0} \delta \xi^3 \xi^3 \rho_0 \frac{A_0}{A_0} d\xi^3, \tag{100}$$

which are the variation of Eqs. (95) and (96). From Eqs. (97) to (98), we used

$$\bar{\mathbf{n}} \cdot \ddot{\bar{\mathbf{n}}} = - \|\dot{\bar{\mathbf{n}}}\|^2, \tag{101}$$

which can be obtained from $\bar{\mathbf{n}} \cdot \dot{\bar{\mathbf{n}}} = 0$.

Remark 13 The second term in Eq. (98) represents the effect of the centripetal acceleration.

Remark 14 Because we omitted $\dot{\xi}^3$ in obtaining Eq. (91), the Coriolis effect is neglected in Eq. (98).

Substituting Eq. (98) into Eq. (84), we obtain

$$\begin{aligned} \delta T = & - \int_{\bar{\Gamma}_0} \delta \bar{\mathbf{x}} \cdot \hat{\mathbf{m}}_0 d\Gamma - \int_{\bar{\Gamma}_0} \delta \bar{\mathbf{n}} \cdot \hat{\mathbf{m}}_1 d\Gamma \\ & - \int_{\bar{\Gamma}_0} \left(\bar{\mathbf{n}} \cdot \ddot{\bar{\mathbf{y}}} \delta \hat{m}_1 - \frac{1}{2} \|\dot{\bar{\mathbf{n}}}\|^2 \delta \hat{m}_2 \right) d\Gamma. \end{aligned} \tag{102}$$

3.4 The external virtual work

We separate δW_{ext} into three parts:

$$\delta W_{\text{ext}} = \delta W_{\text{exbody}} + \delta W_{\text{exsurf}} + \delta W_{\text{exedge}}, \tag{103}$$

where

$$\delta W_{\text{exbody}} = \int_{\bar{\Gamma}_0} \int_{(h_{th})_0} \delta \mathbf{x} \cdot \rho_0 \mathbf{f} \frac{A_0}{A_0} d\xi^3 d\Gamma, \tag{104}$$

$$\delta W_{\text{exsurf}} = \int_{\Gamma_t^-} \delta \mathbf{x} \cdot \mathbf{h} d\Gamma + \int_{\Gamma_t^+} \delta \mathbf{x} \cdot \mathbf{h} d\Gamma, \tag{105}$$

$$\delta W_{\text{exedge}} = \int_{(h_{th})_t} \int_{S_t} \delta \mathbf{x} \cdot \mathbf{h} dS d\xi^3. \tag{106}$$

Here S_t (see Fig. 2) is the edge line that traverses the edge surface as ξ^3 varies from $(\xi^3)^-$ to $(\xi^3)^+$. The symbol \mathbf{h} represents the traction, for all surfaces, including the edge surfaces.

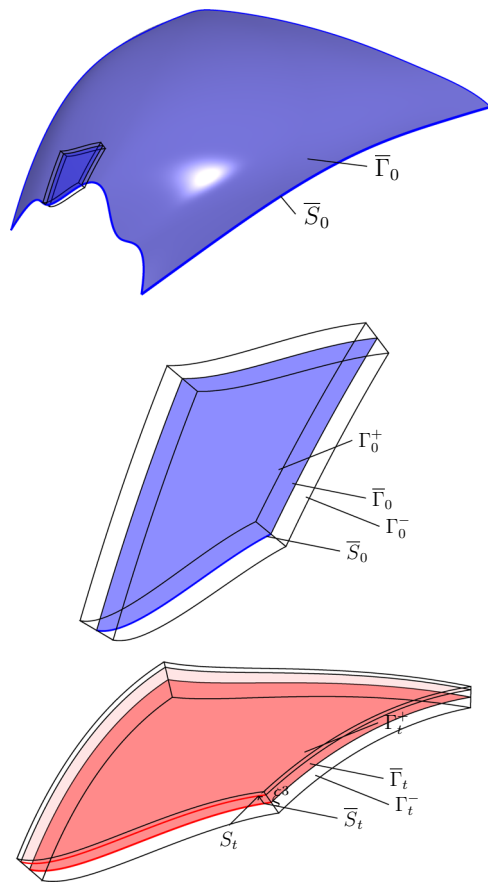


Fig. 2 A schematic undeformed-shell mid-surface $\bar{\Gamma}_0$ with edge \bar{S}_0 and how a piece is cut from the shell domain to show the edge surface details (top). Enlarged view of the cut piece, showing also the upper and lower surfaces Γ_0^+ and Γ_0^- (middle). Deformed-configuration cut piece, with $\bar{\Gamma}_t, \bar{S}_t, \Gamma_t^+$, and Γ_t^- denoting the deformed-configuration counterparts of $\bar{\Gamma}_0, \bar{S}_0, \Gamma_0^+$, and Γ_0^- , and the edge line S_t that traverses the edge surface as ξ^3 varies from $(\xi^3)^-$ to $(\xi^3)^+$ (bottom)

Substituting Eq. (56) into Eq. (104) and using Eqs. (94), (95) and (99), we obtain

$$\delta W_{\text{exbody}} = \int_{\bar{\Gamma}_0} \delta \bar{\mathbf{x}} \cdot \mathbf{f} \hat{m}_0 d\Gamma + \int_{\bar{\Gamma}_0} \delta \bar{\mathbf{n}} \cdot \mathbf{f} \hat{m}_1 d\Gamma + \int_{\bar{\Gamma}_0} \bar{\mathbf{n}} \cdot \mathbf{f} \delta \hat{m}_1 d\Gamma. \tag{107}$$

Substituting Eq. (56) into Eq. (105), we obtain

$$\delta W_{\text{exsurf}} = \int_{\bar{\Gamma}_0} \delta \bar{\mathbf{x}} \cdot (\hat{\mathbf{h}}_0^- + \hat{\mathbf{h}}_0^+) d\Gamma + \int_{\bar{\Gamma}_0} \delta \bar{\mathbf{n}} \cdot (\hat{\mathbf{h}}_1^- + \hat{\mathbf{h}}_1^+) d\Gamma + \int_{\bar{\Gamma}_0} \left(\left(\delta \xi^3 \hat{p}^- \right) \Big|_{(\xi^3)^-} - \left(\delta \xi^3 \hat{p}^+ \right) \Big|_{(\xi^3)^+} \right) d\Gamma, \tag{108}$$

$$\hat{\mathbf{h}}_0^- = \left(\mathbf{h} \frac{A}{A_0} \right) \Big|_{(\xi^3)^-}, \tag{109}$$

$$\hat{\mathbf{h}}_0^+ = \left(\mathbf{h} \frac{A}{A_0} \right) \Big|_{(\xi^3)^+}, \tag{110}$$

$$\hat{\mathbf{h}}_1^- = \left(\xi^3 \mathbf{h} \frac{A}{A_0} \right) \Big|_{(\xi^3)^-}, \tag{111}$$

$$\hat{\mathbf{h}}_1^+ = \left(\xi^3 \mathbf{h} \frac{A}{A_0} \right) \Big|_{(\xi^3)^+}, \tag{112}$$

and the normal tractions as

$$\hat{p}^- = \hat{\mathbf{h}}_0^- \cdot \bar{\mathbf{n}}, \tag{113}$$

$$\hat{p}^+ = -\hat{\mathbf{h}}_0^+ \cdot \bar{\mathbf{n}}. \tag{114}$$

We note that we can see \hat{p} as the pressure brought to the midsurface by using the area ratios.

Remark 15 In Eq. (108), there are three integrals. In [5], only the first integral was considered, and even in that, the evaluations were not based on the actual upper and lower surfaces as how it was done with Eqs. (109) and (110). The tractions acting on the upper and lower surfaces were treated as if they were acting on the midsurface. Not being able to use the correct surfaces was a consequence of the plane-stress assumption.

Remark 16 The terms in the second line of Eq. (108) can be written as $\delta \bar{\mathbf{n}} \cdot \hat{\mathbf{h}}_1^- = \delta \bar{\mathbf{r}} \cdot (\bar{\mathbf{n}} \times \hat{\mathbf{h}}_1^-)$ and $\delta \bar{\mathbf{n}} \cdot \hat{\mathbf{h}}_1^+ = \delta \bar{\mathbf{r}} \cdot (\bar{\mathbf{n}} \times \hat{\mathbf{h}}_1^+)$ (see Appendix B.3). We note that $\bar{\mathbf{n}} \times \hat{\mathbf{h}}_1^-$ and $\bar{\mathbf{n}} \times \hat{\mathbf{h}}_1^+$ represent the moment. Again these rearrangements may make it easier to see the fundamental mechanics in the terms. In a typical shell formulation, the distance between the upper and lower surfaces is not taken into account. Therefore, the tractions on those surfaces, even when they have shear components, do not produce moment.

For the representation at the edges, we introduce a unit vector $\bar{\mathbf{T}}$ along \bar{S}_0 (see Fig. 3). The contravariant components are denoted as

$$\bar{T}^\alpha = \bar{\mathbf{T}} \cdot \mathbf{G}^\alpha. \tag{115}$$

We map $\bar{\mathbf{T}}$ from the midsurface to the ξ_0^3 surface with edge S_0 , and make a unit vector from that:

$$\mathbf{T} \equiv \frac{\bar{T}^\alpha \mathbf{G}_\alpha}{\| \bar{T}^\alpha \mathbf{G}_\alpha \|}. \tag{116}$$

Using Eqs. (24), (26) and (27), \mathbf{T} can be expressed as

$$\mathbf{T} = \frac{\bar{\mathbf{T}} + \bar{T}^\alpha \bar{K}_{\alpha\beta} \bar{\mathbf{G}}^\beta \xi_0^3}{\sqrt{1 + (2\bar{K}_{\gamma\delta} + \bar{\Omega}_{\gamma\delta} \xi_0^3) \xi_0^3 \bar{T}^\gamma \bar{T}^\delta}}, \tag{117}$$

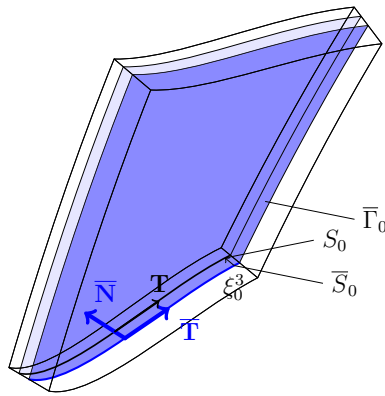


Fig. 3 The cut piece in Fig. 2 (middle) with the unit vectors $\bar{\mathbf{N}}$, $\bar{\mathbf{T}}$, and \mathbf{T}

and its contravariant components are denoted as

$$T^\alpha = \mathbf{T} \cdot \mathbf{G}^\alpha \tag{118}$$

$$= \frac{\bar{T}^\alpha}{\sqrt{1 + (2\bar{K}_{\gamma\delta} + \bar{\Delta}_{\gamma\delta}\xi_0^3)\xi_0^3\bar{T}^\gamma\bar{T}^\delta}}. \tag{119}$$

We note that the numerator of Eq. (119) is coming from the numerator Eq. (116). For notational convenience, we define

$$L_0 \equiv \frac{1}{\sqrt{\mathbf{G}^\alpha\mathbf{G}^\alpha : \mathbf{T}\mathbf{T}}} \tag{120}$$

$$= \frac{1}{\sqrt{(T^1)^2 + (T^2)^2}} \tag{121}$$

$$= \frac{\sqrt{1 + (2\bar{K}_{\alpha\beta} + \bar{\Delta}_{\alpha\beta}\xi_0^3)\xi_0^3\bar{T}^\alpha\bar{T}^\beta}}{\sqrt{(\bar{T}^1)^2 + (\bar{T}^2)^2}}. \tag{122}$$

From Eqs. (121) to (122), we used Eq. (119). We use the symbol \bar{L}_0 to denote L_0 at the midsurface, obtained by setting $\xi_0^3 = 0$:

$$\bar{L}_0 = \frac{1}{\sqrt{(\bar{T}^1)^2 + (\bar{T}^2)^2}}. \tag{123}$$

This can be seen as the length counterpart of A_0 given in Eq. (40). Using Eqs. (119), (122) and (123), we get

$$T^\alpha = \frac{\bar{L}_0}{L_0}\bar{T}^\alpha. \tag{124}$$

Similarly, we introduce unit vectors $\bar{\mathbf{t}}$ and \mathbf{t} along \bar{S}_t and S_t (see Fig. 4). The stretch λ_T along S_0 is obtained from

$$\lambda_T\mathbf{t} = \mathbf{g}_\alpha\mathbf{G}^\alpha \cdot \mathbf{T} \tag{125}$$

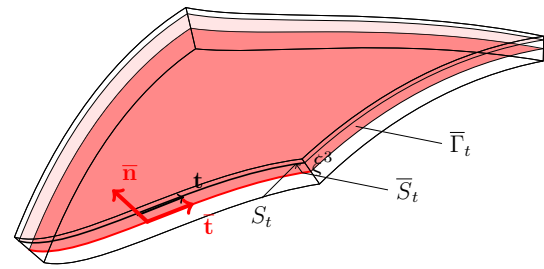


Fig. 4 The cut piece in Fig. 2 (bottom) with the unit vectors $\bar{\mathbf{n}}$, $\bar{\mathbf{t}}$, and \mathbf{t}

$$= \mathbf{g}_\alpha T^\alpha. \tag{126}$$

Taking the inner product of \mathbf{g}^α with both sides of Eq. (126), we obtain

$$\lambda_T t^\alpha = T^\alpha. \tag{127}$$

Because \mathbf{t} is a unit vector, $g_{\alpha\beta}t^\alpha t^\beta = 1$ can be used to calculate λ_T as

$$\lambda_T = \sqrt{g_{\alpha\beta}T^\alpha T^\beta}. \tag{128}$$

Similar to what we did for the undeformed configuration, we define

$$L \equiv \frac{1}{\sqrt{(t^1)^2 + (t^2)^2}}, \tag{129}$$

which is the length counterpart of A given in Eq. (39). Using Eqs. (129), (127) and (121), we get

$$L = \lambda_T L_0, \tag{130}$$

and at the midsurface,

$$\bar{L} = \bar{\lambda}_T \bar{L}_0. \tag{131}$$

We now define a unit outward normal vector for S_0 :

$$\mathbf{B} = \mathbf{T} \times \bar{\mathbf{N}}, \tag{132}$$

and for \bar{S}_0 :

$$\bar{\mathbf{B}} = \bar{\mathbf{T}} \times \bar{\mathbf{N}}. \tag{133}$$

Figure 5 shows the unit vectors $\bar{\mathbf{B}}$ and \mathbf{B} and the rest of the unit vectors in the undeformed configuration.

Then, corresponding to \mathbf{B} , we introduce a unit vector \mathbf{b} in the deformed configuration, and the stretch in the direction of \mathbf{B} is obtained from

$$\lambda_B\mathbf{b} = \mathbf{g}_\alpha\mathbf{G}^\alpha \cdot \mathbf{B}. \tag{134}$$

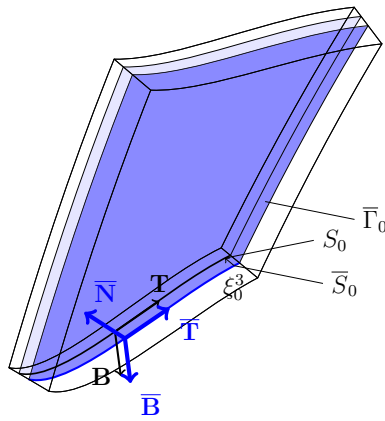


Fig. 5 The cut piece in Fig. 3 with the unit vectors $\bar{\mathbf{B}}$ and \mathbf{B}

With Eq. (134) and $\|\mathbf{b}\| = 1$, the stretch can be written as

$$\lambda_B = \sqrt{g_{\alpha\beta} \mathbf{G}^\alpha \mathbf{G}^\beta : \mathbf{B} \mathbf{B}}. \tag{135}$$

We use the symbols $\bar{\mathbf{b}}$ and $\bar{\lambda}_B$ to denote \mathbf{b} and λ_B at midsurface:

$$\bar{\lambda}_B \bar{\mathbf{b}} = \bar{\mathbf{g}}_\alpha \bar{\mathbf{G}}^\alpha \cdot \bar{\mathbf{B}}, \tag{136}$$

and similarly write the stretch $\bar{\lambda}_B$ as

$$\bar{\lambda}_B = \sqrt{\bar{g}_{\alpha\beta} \bar{\mathbf{G}}^\alpha \bar{\mathbf{G}}^\beta : \bar{\mathbf{B}} \bar{\mathbf{B}}}. \tag{137}$$

Remark 17 We note that, unlike $\bar{\mathbf{B}}$, the unit vector $\bar{\mathbf{b}}$ is not necessarily normal to \bar{S}_t , and therefore $\bar{\mathbf{t}} \cdot \bar{\mathbf{b}}$ does not have to be zero. To overcome the difficulty with using non-orthogonal basis vectors, we introduce the dual basis vectors:

$$\bar{\mathbf{t}}^* = \frac{\bar{\mathbf{n}} \times \bar{\mathbf{b}}}{(\bar{\mathbf{b}} \times \bar{\mathbf{t}}) \cdot \bar{\mathbf{n}}}, \tag{138}$$

$$\bar{\mathbf{b}}^* = \frac{\bar{\mathbf{t}} \times \bar{\mathbf{n}}}{(\bar{\mathbf{b}} \times \bar{\mathbf{t}}) \cdot \bar{\mathbf{n}}}. \tag{139}$$

We refer to Appendix C.1 for more on these.

Figure 6 shows the vectors $\bar{\mathbf{t}}^*$ and $\bar{\mathbf{b}}^*$, the unit vector $\bar{\mathbf{b}}$, and some of earlier-defined unit vectors in the deformed configuration.

With the ratio of the lengths along S_t and \bar{S}_t being L/\bar{L} , we change the order of the integration in Eq. (106):

$$\delta W_{\text{exedge}} = \int_{\bar{S}_t} \int_{(h_{th})_t} \delta \mathbf{x} \cdot \mathbf{h} \frac{L}{\bar{L}} d\xi^3 dS. \tag{140}$$

With the ratio of the lengths along \bar{S}_t and \bar{S}_0 being \bar{L}/\bar{L}_0 and with Eq. (130), we transform the first integration from the

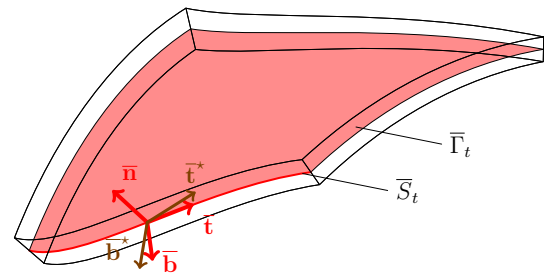


Fig. 6 The cut piece in Fig. 4 with the unit vector $\bar{\mathbf{b}}$ and the dual basis vectors $\bar{\mathbf{t}}^*$ and $\bar{\mathbf{b}}^*$

current to undeformed configuration:

$$\delta W_{\text{exedge}} = \int_{\bar{S}_0} \int_{(h_{th})_t} \delta \mathbf{x} \cdot \mathbf{h} \lambda_T \frac{L_0}{L_0} d\xi^3 dS. \tag{141}$$

Using Eq. (32), we transform the second integration from the current to undeformed configuration:

$$\delta W_{\text{exedge}} = \int_{\bar{S}_0} \int_{(h_{th})_0} \delta \mathbf{x} \cdot \mathbf{h} \lambda_T \lambda_3 \frac{L_0}{L_0} d\xi^3 dS. \tag{142}$$

Substituting Eq. (56) into this, we get

$$\begin{aligned} \delta W_{\text{exedge}} = & \int_{\bar{S}_0} \delta \bar{\mathbf{x}} \cdot \int_{(h_{th})_0} \mathbf{h} \lambda_T \lambda_3 \frac{L_0}{L_0} d\xi^3 dS \\ & + \int_{\bar{S}_0} \delta \bar{\mathbf{n}} \cdot \int_{(h_{th})_0} \xi^3 \mathbf{h} \lambda_T \lambda_3 \frac{L_0}{L_0} d\xi^3 dS \\ & + \int_{\bar{S}_0} \bar{\mathbf{n}} \cdot \int_{(h_{th})_0} \delta \xi^3 \mathbf{h} \lambda_T \lambda_3 \frac{L_0}{L_0} d\xi^3 dS. \end{aligned} \tag{143}$$

We define $\hat{\mathbf{h}}_0^e$ as

$$\hat{\mathbf{h}}_0^e = \int_{(h_{th})_0} \mathbf{h} \lambda_T \lambda_3 \frac{L_0}{L_0} d\xi^3, \tag{144}$$

and its first moment as

$$\hat{\mathbf{h}}_1^e = \int_{(h_{th})_0} \xi^3 \mathbf{h} \lambda_T \lambda_3 \frac{L_0}{L_0} d\xi^3. \tag{145}$$

With these definitions, we write Eq. (143) in a simpler form:

$$\begin{aligned} \delta W_{\text{exedge}} = & \int_{\bar{S}_0} \delta \bar{\mathbf{x}} \cdot \hat{\mathbf{h}}_0^e dS + \int_{\bar{S}_0} \delta \bar{\mathbf{n}} \cdot \hat{\mathbf{h}}_1^e dS \\ & + \int_{\bar{S}_0} \bar{\mathbf{n}} \cdot \int_{(h_{th})_0} \delta \xi^3 \mathbf{h} \lambda_T \lambda_3 d\xi^3 \frac{L_0}{L_0} dS. \end{aligned} \tag{146}$$

We omit the variation of ξ^3 :

$$\delta W_{\text{exedge}} = \int_{\bar{S}_0} \delta \bar{\mathbf{x}} \cdot \hat{\mathbf{h}}_0^e dS + \int_{\bar{S}_0} \delta \bar{\mathbf{n}} \cdot \hat{\mathbf{h}}_1^e dS. \tag{147}$$

Remark 18 The reasons for omitting the variation of ξ^3 in Eq. (146) are, (i) the out-of-plane shear stress is not meant to be represented in this model, and (ii) we already omitted the time derivatives of ξ^3 (see Remark 12).

Remark 19 The second integrand in Eq. (147) can be written as $\delta \bar{\mathbf{n}} \cdot \hat{\mathbf{h}}_1^e = \delta \bar{\mathbf{r}} \cdot (\bar{\mathbf{n}} \times \hat{\mathbf{h}}_1^e)$. We note that $\bar{\mathbf{n}} \times \hat{\mathbf{h}}_1^e$ represents the moment.

3.5 The virtual work in the out-of-plane direction and the corresponding strong form

We substitute δU given by Eq. (79), δT given by Eq. (102), and δW_{ext} given by Eqs. (103), (107), (108) and (147) into Eq. (55), exclude the variations associated with the midsurface, and obtain

$$\begin{aligned} & \int_{\bar{\Gamma}_0} (\bar{\mathbf{n}} \cdot (\ddot{\bar{\mathbf{y}}} - \mathbf{f})) \delta \hat{m}_1 - \frac{1}{2} \|\dot{\bar{\mathbf{n}}}\|^2 \delta \hat{m}_2 \, d\Gamma \\ & + \int_{\bar{\Gamma}_0} \bar{\kappa}_{\alpha\beta} \int_{(h_{\text{th}})_0} \delta \xi^3 S^{\alpha\beta} \frac{A_0}{A_0} d\xi^3 d\Gamma \\ & + \int_{\bar{\Gamma}_0} \bar{\omega}_{\alpha\beta} \int_{(h_{\text{th}})_0} \delta \xi^3 \xi^3 S^{\alpha\beta} \frac{A_0}{A_0} d\xi^3 d\Gamma \\ & + \int_{\bar{\Gamma}_0} \int_{(h_{\text{th}})_0} \delta \lambda_3 \lambda_3 S^{33} \frac{A_0}{A_0} d\xi^3 d\Gamma \\ & = \int_{\bar{\Gamma}_0} \left((\delta \xi^3 \hat{p}^-) \Big|_{(\xi_0^3)^-} - (\delta \xi^3 \hat{p}^+) \Big|_{(\xi_0^3)^+} \right) d\Gamma. \end{aligned} \tag{148}$$

We substitute Eq. (58) into this and consider only the out-of-plane variations at a given midsurface point:

$$\begin{aligned} & \bar{\mathbf{n}} \cdot (\ddot{\bar{\mathbf{y}}} - \mathbf{f}) \delta \hat{m}_1 - \frac{1}{2} \|\dot{\bar{\mathbf{n}}}\|^2 \delta \hat{m}_2 \\ & + \bar{\kappa}_{\alpha\beta} \int_{(h_{\text{th}})_0} \delta \xi^3 S^{\alpha\beta} \frac{A_0}{A_0} d\xi^3 \\ & + \bar{\omega}_{\alpha\beta} \int_{(h_{\text{th}})_0} \delta \xi^3 \xi^3 S^{\alpha\beta} \frac{A_0}{A_0} d\xi^3 \\ & + \int_{(h_{\text{th}})_0} \frac{d(\delta \xi^3)}{d\xi^3} \lambda_3 S^{33} \frac{A_0}{A_0} d\xi^3 \\ & = (\delta \xi^3 \hat{p}^-) \Big|_{(\xi_0^3)^-} - (\delta \xi^3 \hat{p}^+) \Big|_{(\xi_0^3)^+}. \end{aligned} \tag{149}$$

Applying integration by parts to the last integral on the left-hand side, we obtain

$$\begin{aligned} & \bar{\mathbf{n}} \cdot (\ddot{\bar{\mathbf{y}}} - \mathbf{f}) \delta \hat{m}_1 - \frac{1}{2} \|\dot{\bar{\mathbf{n}}}\|^2 \delta \hat{m}_2 \\ & + \bar{\kappa}_{\alpha\beta} \int_{(h_{\text{th}})_0} \delta \xi^3 S^{\alpha\beta} \frac{A_0}{A_0} d\xi^3 \\ & + \bar{\omega}_{\alpha\beta} \int_{(h_{\text{th}})_0} \delta \xi^3 \xi^3 S^{\alpha\beta} \frac{A_0}{A_0} d\xi^3 \end{aligned}$$

$$\begin{aligned} & - \int_{(h_{\text{th}})_0} \delta \xi^3 \frac{d}{d\xi^3} \left(\lambda_3 S^{33} \frac{A_0}{A_0} \right) d\xi^3 \\ & = (\delta \xi^3 (\hat{p}^- + \lambda_3 S^{33} \frac{A_0}{A_0})) \Big|_{(\xi_0^3)^-} \\ & - (\delta \xi^3 (\hat{p}^+ + \lambda_3 S^{33} \frac{A_0}{A_0})) \Big|_{(\xi_0^3)^+}. \end{aligned} \tag{150}$$

We substitute Eqs. (99) and (100) into this, and the equation holds for all admissible $\delta \xi^3$. From that, we obtain the strong form:

$$\begin{aligned} \frac{d}{d\xi^3} \left(\lambda_3 S^{33} \frac{A_0}{A_0} \right) & = (\bar{\kappa}_{\alpha\beta} + \bar{\omega}_{\alpha\beta} \xi^3) S^{\alpha\beta} \frac{A_0}{A_0} \\ & + (\bar{\mathbf{n}} \cdot (\ddot{\bar{\mathbf{y}}} - \mathbf{f}) - \xi^3 \|\dot{\bar{\mathbf{n}}}\|^2) \rho_0 \frac{A_0}{A_0} \\ & \text{in}(h_{\text{th}})_0, \end{aligned} \tag{151}$$

$$\lambda_3 S^{33} \frac{A_0}{A_0} = -\hat{p}^- \quad \text{on } \xi_0^3 = (\xi_0^3)^-, \tag{152}$$

and

$$\lambda_3 S^{33} \frac{A_0}{A_0} = -\hat{p}^+ \quad \text{on } \xi_0^3 = (\xi_0^3)^+. \tag{153}$$

Integrating Eq. (151) from $(\xi_0^3)^-$ to $(\xi_0^3)^+$ and using Eqs. (152) and (153), we obtain

$$\begin{aligned} -\hat{p}^+ + \hat{p}^- & = \int_{(h_{\text{th}})_0} (\bar{\kappa}_{\alpha\beta} + \bar{\omega}_{\alpha\beta} \xi^3) S^{\alpha\beta} \frac{A_0}{A_0} d\xi^3 \\ & + \bar{\mathbf{n}} \cdot (\ddot{\bar{\mathbf{y}}} - \mathbf{f}) \hat{m}_0 - \|\dot{\bar{\mathbf{n}}}\|^2 \hat{m}_1. \end{aligned} \tag{154}$$

We rearrange this equation by substituting for \hat{p}^- and \hat{p}^+ from Eqs. (113) and (114), using the expression for $\hat{S}_\varepsilon^{\alpha\beta}$ and $\hat{S}_\kappa^{\alpha\beta}$ from Eqs. (80) and (81), and using Eqs. (92) and (101):

$$\bar{\mathbf{n}} \cdot (\hat{\mathbf{h}}_0^- + \hat{\mathbf{h}}_0^+) = \bar{\kappa}_{\alpha\beta} \hat{S}_\varepsilon^{\alpha\beta} + \bar{\omega}_{\alpha\beta} \hat{S}_\kappa^{\alpha\beta} + \bar{\mathbf{n}} \cdot (\hat{\mathbf{m}}_0 - \mathbf{f} \hat{m}_0). \tag{155}$$

3.6 The virtual work for the midsurface deformation and the corresponding strong form

We substitute δU given by Eq. (78), δT given by Eq. (102), and δW_{ext} given by Eqs. (103), (107), (108) and (147) into Eq. (55), exclude the out-of-plane variations, and obtain

$$\begin{aligned} & \int_{\bar{\Gamma}_0} \delta \bar{\mathbf{g}}_\alpha \cdot \hat{\mathbf{p}}_0^\alpha d\Gamma - \int_{\bar{\Gamma}_0} \delta \bar{\mathbf{x}} \cdot \hat{\mathbf{f}}_0 d\Gamma \\ & + \int_{\bar{\Gamma}_0} \delta \bar{\mathbf{n}}_{,\alpha} \cdot \hat{\mathbf{p}}_1^\alpha d\Gamma - \int_{\bar{\Gamma}_0} \delta \bar{\mathbf{n}} \cdot \hat{\mathbf{f}}_1 d\Gamma \\ & = \int_{\bar{S}_0} \delta \bar{\mathbf{x}} \cdot \hat{\mathbf{h}}_0^e dS + \int_{\bar{S}_0} \delta \bar{\mathbf{n}} \cdot \hat{\mathbf{h}}_1^e dS, \end{aligned} \tag{156}$$

where

$$\hat{\mathbf{f}}_0 = \hat{\mathbf{h}}_0^- + \hat{\mathbf{h}}_0^+ + \mathbf{f}\hat{m}_0 - \hat{\mathbf{m}}_0, \tag{157}$$

$$\hat{\mathbf{f}}_1 = \hat{\mathbf{h}}_1^- + \hat{\mathbf{h}}_1^+ + \mathbf{f}\hat{m}_1 - \hat{\mathbf{m}}_1. \tag{158}$$

Equation (156) is our weak form for the midsurface representation. To understand it better, we substitute

$$\delta \bar{\mathbf{g}}_\alpha = \delta \bar{\mathbf{x}}_{,\gamma} \bar{\mathbf{G}}^\gamma \cdot \bar{\mathbf{G}}_\alpha, \tag{159}$$

$$\delta \bar{\mathbf{n}}_{,\alpha} = \delta \bar{\mathbf{n}}_{,\gamma} \bar{\mathbf{G}}^\gamma \cdot \bar{\mathbf{G}}_\alpha, \tag{160}$$

into it, apply integration by parts to the first and third integrals, and obtain

$$\begin{aligned} & - \int_{\bar{\Gamma}_0} \delta \bar{\mathbf{x}} \cdot (\hat{\mathbf{f}}_0 + (\hat{\mathbf{p}}_0^\alpha \bar{\mathbf{G}}_\alpha)_{,\gamma} \cdot \bar{\mathbf{G}}^\gamma) d\Gamma \\ & - \int_{\bar{\Gamma}_0} \delta \bar{\mathbf{n}} \cdot (\hat{\mathbf{f}}_1 + (\hat{\mathbf{p}}_1^\alpha \bar{\mathbf{G}}_\alpha)_{,\gamma} \cdot \bar{\mathbf{G}}^\gamma) d\Gamma \\ & = \int_{\bar{S}_0} \delta \bar{\mathbf{x}} \cdot (\hat{\mathbf{h}}_0^e - \hat{\mathbf{p}}_0^\alpha \bar{\mathbf{G}}_\alpha \cdot \bar{\mathbf{B}}) dS \\ & + \int_{\bar{S}_0} \delta \bar{\mathbf{n}} \cdot (\hat{\mathbf{h}}_1^e - \hat{\mathbf{p}}_1^\alpha \bar{\mathbf{G}}_\alpha \cdot \bar{\mathbf{B}}) dS. \end{aligned} \tag{161}$$

We note that, as shown in Fig. 5, the unit outward normal vector for \bar{S}_0 is $\bar{\mathbf{B}}$. With $\delta \bar{\mathbf{n}}$ involving derivatives, we next apply integration by parts to the second and fourth lines of Eq. (161). We do that by using two expressions derived in Appendix C, given by Eqs. (306) and (316). After that, separating $\delta \bar{\mathbf{x}}$ into its normal and tangential components, we obtain

$$\begin{aligned} & - \int_{\bar{\Gamma}_0} \delta \bar{\mathbf{x}} \cdot \bar{\mathbf{n}} \bar{\mathbf{n}} \cdot (\hat{\mathbf{f}}_0 + (\hat{\mathbf{p}}_0^\alpha \bar{\mathbf{G}}_\alpha)_{,\gamma} \cdot \bar{\mathbf{G}}^\gamma) d\Gamma \\ & - \int_{\bar{\Gamma}_0} \delta \bar{\mathbf{x}} \cdot \bar{\mathbf{n}} (\bar{\mathbf{g}}^\beta \cdot (\hat{\mathbf{f}}_1 + (\hat{\mathbf{p}}_1^\alpha \bar{\mathbf{G}}_\alpha)_{,\gamma} \cdot \bar{\mathbf{G}}^\gamma) \bar{\mathbf{G}}_\beta)_{,\delta} \cdot \bar{\mathbf{G}}^\delta d\Gamma \\ & - \int_{\bar{\Gamma}_0} \delta \bar{\mathbf{x}} \cdot \bar{\mathbf{g}}_\delta \bar{\mathbf{g}}^\delta \cdot (\hat{\mathbf{f}}_0 + (\hat{\mathbf{p}}_0^\alpha \bar{\mathbf{G}}_\alpha)_{,\gamma} \cdot \bar{\mathbf{G}}^\gamma) d\Gamma \\ & - \int_{\bar{\Gamma}_0} \delta \bar{\mathbf{x}} \cdot \bar{\boldsymbol{\kappa}} \cdot (\hat{\mathbf{f}}_1 + (\hat{\mathbf{p}}_1^\alpha \bar{\mathbf{G}}_\alpha)_{,\gamma} \cdot \bar{\mathbf{G}}^\gamma) d\Gamma \\ & = \int_{\bar{S}_0} \delta \bar{\mathbf{x}} \cdot \bar{\mathbf{n}} \bar{\mathbf{n}} \cdot (\hat{\mathbf{h}}_0^e - \hat{\mathbf{p}}_0^\alpha \bar{\mathbf{G}}_\alpha \cdot \bar{\mathbf{B}}) dS \\ & - \int_{\bar{S}_0} \delta \bar{\mathbf{x}} \cdot \bar{\mathbf{n}} \frac{1}{\lambda_B} \bar{\mathbf{b}}^\star \cdot (\hat{\mathbf{f}}_1 + (\hat{\mathbf{p}}_1^\alpha \bar{\mathbf{G}}_\alpha)_{,\gamma} \cdot \bar{\mathbf{G}}^\gamma) dS \\ & + \int_{\bar{S}_0} \delta \bar{\mathbf{x}} \cdot \bar{\mathbf{n}} \left(\frac{1}{\lambda_T} \bar{\mathbf{t}}^\star \cdot (\hat{\mathbf{h}}_1^e - \hat{\mathbf{p}}_1^\alpha \bar{\mathbf{G}}_\alpha \cdot \bar{\mathbf{B}}) \right)_{,\gamma} \bar{\mathbf{G}}^\gamma \cdot \bar{\mathbf{T}} dS \\ & + \int_{\bar{S}_0} \delta \bar{\mathbf{x}} \cdot (\bar{\mathbf{t}} \bar{\mathbf{t}}^\star + \bar{\mathbf{b}} \bar{\mathbf{b}}^\star) \cdot (\hat{\mathbf{h}}_0^e - \hat{\mathbf{p}}_0^\alpha \bar{\mathbf{G}}_\alpha \cdot \bar{\mathbf{B}}) dS \\ & + \int_{\bar{S}_0} \delta \bar{\mathbf{x}} \cdot \bar{\boldsymbol{\kappa}} \cdot \bar{\mathbf{t}} \bar{\mathbf{t}}^\star \cdot (\hat{\mathbf{h}}_1^e - \hat{\mathbf{p}}_1^\alpha \bar{\mathbf{G}}_\alpha \cdot \bar{\mathbf{B}}) dS \end{aligned}$$

$$+ \int_{\bar{S}_0} \delta \bar{\mathbf{n}} \cdot \bar{\mathbf{b}} \bar{\mathbf{b}}^\star \cdot (\hat{\mathbf{h}}_1^e - \hat{\mathbf{p}}_1^\alpha \bar{\mathbf{G}}_\alpha \cdot \bar{\mathbf{B}}) dS. \tag{162}$$

We note that $\hat{\mathbf{p}}_0^\alpha$ and $\hat{\mathbf{p}}_1$ have only in-plane components; $\bar{\mathbf{n}} \cdot \hat{\mathbf{p}}_0^\alpha = 0$ and $\bar{\mathbf{n}} \cdot \hat{\mathbf{p}}_1 = 0$ (see Eqs. (75), (76) and (77)). With that, we get

$$\bar{\mathbf{n}} \cdot (\hat{\mathbf{p}}_0^\alpha \bar{\mathbf{G}}_\alpha)_{,\gamma} \cdot \bar{\mathbf{G}}^\gamma = \underbrace{(\bar{\mathbf{n}} \cdot \hat{\mathbf{p}}_0^\alpha \bar{\mathbf{G}}_\alpha)_{,\gamma}}_{=0} \cdot \bar{\mathbf{G}}^\gamma - \bar{\mathbf{n}}_{,\gamma} \cdot \hat{\mathbf{p}}_0^\alpha \bar{\mathbf{G}}_\alpha \cdot \bar{\mathbf{G}}^\gamma \tag{163}$$

$$= -\bar{\mathbf{n}}_{,\alpha} \cdot \hat{\mathbf{p}}_0^\alpha. \tag{164}$$

Using Eq. (164), we rewrite Eq. (162) as

$$\begin{aligned} & - \int_{\bar{\Gamma}_0} \delta \bar{\mathbf{x}} \cdot \bar{\mathbf{n}} (\bar{\mathbf{n}} \cdot \hat{\mathbf{f}}_0 - \bar{\mathbf{n}}_{,\alpha} \cdot \hat{\mathbf{p}}_0^\alpha) d\Gamma \\ & - \int_{\bar{\Gamma}_0} \delta \bar{\mathbf{x}} \cdot \bar{\mathbf{n}} (\bar{\mathbf{g}}^\beta \cdot (\hat{\mathbf{f}}_1 + (\hat{\mathbf{p}}_1^\alpha \bar{\mathbf{G}}_\alpha)_{,\gamma} \cdot \bar{\mathbf{G}}^\gamma) \bar{\mathbf{G}}_\beta)_{,\delta} \cdot \bar{\mathbf{G}}^\delta d\Gamma \\ & - \int_{\bar{\Gamma}_0} \delta \bar{\mathbf{x}} \cdot \bar{\mathbf{g}}_\delta \bar{\mathbf{g}}^\delta \cdot (\hat{\mathbf{f}}_0 + (\hat{\mathbf{p}}_0^\alpha \bar{\mathbf{G}}_\alpha)_{,\gamma} \cdot \bar{\mathbf{G}}^\gamma) d\Gamma \\ & - \int_{\bar{\Gamma}_0} \delta \bar{\mathbf{x}} \cdot \bar{\boldsymbol{\kappa}} \cdot (\hat{\mathbf{f}}_1 + (\hat{\mathbf{p}}_1^\alpha \bar{\mathbf{G}}_\alpha)_{,\gamma} \cdot \bar{\mathbf{G}}^\gamma) d\Gamma \\ & = \int_{\bar{S}_0} \delta \bar{\mathbf{x}} \cdot \bar{\mathbf{n}} \bar{\mathbf{n}} \cdot \hat{\mathbf{h}}_0^e dS \\ & - \int_{\bar{S}_0} \delta \bar{\mathbf{x}} \cdot \bar{\mathbf{n}} \frac{1}{\lambda_B} \bar{\mathbf{b}}^\star \cdot (\hat{\mathbf{f}}_1 + (\hat{\mathbf{p}}_1^\alpha \bar{\mathbf{G}}_\alpha)_{,\gamma} \cdot \bar{\mathbf{G}}^\gamma) dS \\ & + \int_{\bar{S}_0} \delta \bar{\mathbf{x}} \cdot \bar{\mathbf{n}} \left(\frac{1}{\lambda_T} \bar{\mathbf{t}}^\star \cdot (\hat{\mathbf{h}}_1^e - \hat{\mathbf{p}}_1^\alpha \bar{\mathbf{G}}_\alpha \cdot \bar{\mathbf{B}}) \right)_{,\gamma} \bar{\mathbf{G}}^\gamma \cdot \bar{\mathbf{T}} dS \\ & + \int_{\bar{S}_0} \delta \bar{\mathbf{x}} \cdot (\bar{\mathbf{t}} \bar{\mathbf{t}}^\star + \bar{\mathbf{b}} \bar{\mathbf{b}}^\star) \cdot (\hat{\mathbf{h}}_0^e - \hat{\mathbf{p}}_0^\alpha \bar{\mathbf{G}}_\alpha \cdot \bar{\mathbf{B}}) dS \\ & + \int_{\bar{S}_0} \delta \bar{\mathbf{x}} \cdot \bar{\boldsymbol{\kappa}} \cdot \bar{\mathbf{t}} \bar{\mathbf{t}}^\star \cdot (\hat{\mathbf{h}}_1^e - \hat{\mathbf{p}}_1^\alpha \bar{\mathbf{G}}_\alpha \cdot \bar{\mathbf{B}}) dS \\ & + \int_{\bar{S}_0} \delta \bar{\mathbf{n}} \cdot \bar{\mathbf{b}} \bar{\mathbf{b}}^\star \cdot (\hat{\mathbf{h}}_1^e - \hat{\mathbf{p}}_1^\alpha \bar{\mathbf{G}}_\alpha \cdot \bar{\mathbf{B}}) dS. \end{aligned} \tag{165}$$

From that, the strong form in $\bar{\Gamma}_0$ can be written as

$$\begin{aligned} & - \bar{\mathbf{n}} \cdot \hat{\mathbf{f}}_0 + \bar{\mathbf{n}}_{,\alpha} \cdot \hat{\mathbf{p}}_0^\alpha \\ & - (\bar{\mathbf{g}}^\beta \cdot (\hat{\mathbf{f}}_1 + (\hat{\mathbf{p}}_1^\alpha \bar{\mathbf{G}}_\alpha)_{,\gamma} \cdot \bar{\mathbf{G}}^\gamma) \bar{\mathbf{G}}_\beta)_{,\delta} \cdot \bar{\mathbf{G}}^\delta = 0, \end{aligned} \tag{166}$$

$$\begin{aligned} & - \bar{\mathbf{g}}_\delta \bar{\mathbf{g}}^\delta \cdot (\hat{\mathbf{f}}_0 + (\hat{\mathbf{p}}_0^\alpha \bar{\mathbf{G}}_\alpha)_{,\gamma} \cdot \bar{\mathbf{G}}^\gamma) \\ & - \bar{\boldsymbol{\kappa}} \cdot (\hat{\mathbf{f}}_1 + (\hat{\mathbf{p}}_1^\alpha \bar{\mathbf{G}}_\alpha)_{,\gamma} \cdot \bar{\mathbf{G}}^\gamma) = \mathbf{0}. \end{aligned} \tag{167}$$

We note that we split the strong form into its parts associated with the normal and in-plane directions. Along the boundary \bar{S}_0 , we have

$$\bar{\mathbf{n}} \cdot \hat{\mathbf{h}}_0^e - \frac{1}{\lambda_B} \bar{\mathbf{b}}^\star \cdot (\hat{\mathbf{f}}_1 + (\hat{\mathbf{p}}_1^\alpha \bar{\mathbf{G}}_\alpha)_{,\gamma} \cdot \bar{\mathbf{G}}^\gamma)$$

$$+ \left(\frac{1}{\lambda_T} \hat{\mathbf{t}}^* \cdot \left(\hat{\mathbf{h}}_1^e - \hat{\mathbf{p}}_1^\alpha \overline{\mathbf{G}}_\alpha \cdot \overline{\mathbf{B}} \right) \right)_{,\gamma} \overline{\mathbf{G}}^\gamma \cdot \overline{\mathbf{T}} = 0, \tag{168}$$

$$\begin{aligned} & \left(\hat{\mathbf{t}} \hat{\mathbf{t}}^* + \overline{\mathbf{b}} \overline{\mathbf{b}}^* \right) \cdot \left(\hat{\mathbf{h}}_0^e - \hat{\mathbf{p}}_0^\alpha \overline{\mathbf{G}}_\alpha \cdot \overline{\mathbf{B}} \right) \\ & + \overline{\boldsymbol{\kappa}} \cdot \hat{\mathbf{t}} \hat{\mathbf{t}}^* \cdot \left(\hat{\mathbf{h}}_1^e - \hat{\mathbf{p}}_1^\alpha \overline{\mathbf{G}}_\alpha \cdot \overline{\mathbf{B}} \right) = 0, \end{aligned} \tag{169}$$

$$\overline{\mathbf{b}}^* \cdot \left(\hat{\mathbf{h}}_1^e - \hat{\mathbf{p}}_1^\alpha \overline{\mathbf{G}}_\alpha \cdot \overline{\mathbf{B}} \right) = 0. \tag{170}$$

Here Eqs. (168) and (169) are the parts associated with the normal and in-plane directions.

Remark 20 We can show that the first two terms of Eq. (166) constitute an alternative form of Eq. (155) and therefore give zero. For that, we rewrite $\hat{\mathbf{p}}_0^\alpha$ by using Eqs. (76), (75) and (8):

$$\hat{\mathbf{p}}_0^\alpha = \int_{(h_{th})_0} \left(\overline{\mathbf{g}}_\beta + \overline{\mathbf{n}}_{,\beta} \xi^3 \right) S^{\alpha\beta} \frac{A_0}{A_0} d\xi^3, \tag{171}$$

take the inner product of both sides of that with $-\overline{\mathbf{n}}_{,\alpha}$, and obtain

$$-\overline{\mathbf{n}}_{,\alpha} \cdot \hat{\mathbf{p}}_0^\alpha = -\overline{\mathbf{n}}_{,\alpha} \cdot \int_{(h_{th})_0} \left(\overline{\mathbf{g}}_\beta + \overline{\mathbf{n}}_{,\beta} \xi^3 \right) S^{\alpha\beta} \frac{A_0}{A_0} d\xi^3. \tag{172}$$

We rearrange that by using Eqs. (264) and (13):

$$\begin{aligned} -\overline{\mathbf{n}}_{,\alpha} \cdot \hat{\mathbf{p}}_0^\alpha &= -\overline{\boldsymbol{\kappa}}_{\alpha\delta} \overline{\mathbf{g}}^\delta \cdot \overline{\mathbf{g}}_\beta \int_{(h_{th})_0} S^{\alpha\beta} \frac{A_0}{A_0} d\xi^3 \\ &\quad - \overline{\omega}_{\alpha\beta} \int_{(h_{th})_0} S^{\alpha\beta} \frac{A_0}{A_0} \xi^3 d\xi^3. \end{aligned} \tag{173}$$

Recognizing the terms on the right-hand side from Eqs. (80) and (81), we get

$$-\overline{\mathbf{n}}_{,\alpha} \cdot \hat{\mathbf{p}}_0^\alpha = -\overline{\boldsymbol{\kappa}}_{\alpha\beta} \hat{S}_\varepsilon^{\alpha\beta} - \overline{\omega}_{\alpha\beta} \hat{S}_\kappa^{\alpha\beta}. \tag{174}$$

With that and Eq. (157), Eq. (155) can be rewritten as

$$-\overline{\mathbf{n}} \cdot \hat{\mathbf{f}}_0 + \overline{\mathbf{n}}_{,\alpha} \cdot \hat{\mathbf{p}}_0^\alpha = 0. \tag{175}$$

Combining that with Eq. (166), we obtain

$$-\left(\overline{\mathbf{g}}^\beta \cdot \left(\hat{\mathbf{f}}_1 + \left(\hat{\mathbf{p}}_1^\alpha \overline{\mathbf{G}}_\alpha \right)_{,\gamma} \overline{\mathbf{G}}^\gamma \right) \cdot \overline{\mathbf{G}}^\beta \right)_{,\delta} \overline{\mathbf{G}}^\delta = 0. \tag{176}$$

The equation above represents the rotational balance around the midsurface.

Remark 21 Equation (170) represents the rotation boundary condition along \overline{S}_0 . It is a single-component equation. To determine which component that is, we start with taking the cross product of both sides of Eq. (145) with $\overline{\mathbf{n}}$:

$$\overline{\mathbf{n}} \times \hat{\mathbf{h}}_1^e = \int_{(h_{th})_0} \overline{\mathbf{n}} \xi^3 \times \mathbf{h} \lambda_T \lambda_3 \frac{L_0}{L_0} d\xi^3 \tag{177}$$

and recognizing the right-hand side as the moment acting along \overline{S}_0 . Using Eq. (139), Eq. (170) can be written as

$$\frac{\overline{\mathbf{t}} \times \overline{\mathbf{n}}}{(\overline{\mathbf{b}} \times \overline{\mathbf{t}}) \cdot \overline{\mathbf{n}}} \cdot \left(\hat{\mathbf{h}}_1^e - \hat{\mathbf{p}}_1^\alpha \overline{\mathbf{G}}_\alpha \cdot \overline{\mathbf{B}} \right) = 0, \tag{178}$$

which can be rearranged as

$$\frac{1}{(\overline{\mathbf{b}} \times \overline{\mathbf{t}}) \cdot \overline{\mathbf{n}}} \left(\overline{\mathbf{n}} \times \left(\hat{\mathbf{h}}_1^e - \hat{\mathbf{p}}_1^\alpha \overline{\mathbf{G}}_\alpha \cdot \overline{\mathbf{B}} \right) \right) \cdot \overline{\mathbf{t}} = 0. \tag{179}$$

This means that Eq. (170) represents the tangential component of the rotation boundary condition along \overline{S}_0 . We note that we cannot have a component in the $\overline{\mathbf{n}}$ direction because $(\overline{\mathbf{n}} \times \hat{\mathbf{h}}_1^e) \cdot \overline{\mathbf{n}} = 0$, and we cannot have a component in the $\overline{\mathbf{b}}^*$ direction because of the Kirchhoff–Love assumption.

4 Stress and strain distributions in the out-of-plane direction

We solve for the stress and strain distributions along the out-of-plane direction at a given midsurface point. We use the symbol y^3 to denote the displacement in the out-of-plane direction:

$$y^3 = \xi^3 - \xi_0^3, \tag{180}$$

and write

$$\lambda_3 = 1 + \frac{dy^3}{d\xi_0^3}. \tag{181}$$

The point on the midsurface is like an integration point in a typical finite element formulation. For simplicity, we assume steady state and exclude the body force. In the test computations, which will be reported in Sect. 5, we found out that determining in advance the midsurface variables needed in the equation associated with the out-of-plane direction is not a good path. Therefore, in this section, we treat also $\overline{\varepsilon}_{\alpha\beta}$ and $\overline{\boldsymbol{\kappa}}_{\alpha\beta}$ as unknowns, with total six components. Then, in addition to Eq. (148), we use the first three integrals of δU given by Eq. (79), which are associated with the midsurface deformation, with $\delta \overline{\varepsilon}_{\alpha\beta}$ and $\delta \overline{\boldsymbol{\kappa}}_{\alpha\beta}$ generating six additional equations. We note that other virtual-work terms in Eq. (55) play no role in the midsurface deformation. That is because $\delta T = 0$ from assuming steady state, and in δW_{ext} , $\delta W_{\text{exbody}} = 0$ from excluding the body force, $\delta W_{\text{exsurf}} = 0$ from being for the upper and lower surfaces, and $\delta W_{\text{exedge}} = 0$ from being for the edge surfaces. We also note that $\delta \overline{\omega}_{\alpha\beta}$ appearing in the third integral of Eq. (79) can be represented in terms of $\delta \overline{\varepsilon}_{\alpha\beta}$ and $\delta \overline{\boldsymbol{\kappa}}_{\alpha\beta}$, as described in Remark 7. Some of the six additional equations will be

removed for consistency with the constraints coming from the boundary conditions or geometry, depending on the problem setup.

Remark 22 In the actual computations, which will be presented in the second part of this two-part article, we plan to use a different way of numerically solving the strong form of the equations in the out-of-plane direction. That will involve change of unknown variable. We expect that coupling that solution process with solving for the midsurface deformation will not be computationally burdensome.

At this point, we will change the symbol we use for representing the variation associated with the virtual work, and call it “ δ_a .” That is because in solving the nonlinear equations with the Newton–Raphson method, we will need to take another variation for the linearization in the iterations, and that variation will be denoted by the symbol δ_b . In other words, the linearization for the Newton–Raphson iterations will be in terms of δ_b . Using the test functions of $\delta_a \xi^3$, $\delta_a \bar{\epsilon}_{\alpha\beta}$, and $\delta_a \bar{\kappa}_{\alpha\beta}$, we form the equation system as

$$N(\delta_a \xi^3, \delta_a \bar{\epsilon}_{\alpha\beta}, \delta_a \bar{\kappa}_{\alpha\beta}, y^3, \bar{\epsilon}_{\gamma\delta}, \bar{\kappa}_{\gamma\delta}) = F(\delta_a \xi^3), \tag{182}$$

where

$$\begin{aligned} N(\delta_a \xi^3, \delta_a \bar{\epsilon}_{\alpha\beta}, \delta_a \bar{\kappa}_{\alpha\beta}, y^3, \bar{\epsilon}_{\gamma\delta}, \bar{\kappa}_{\gamma\delta}) &= \bar{\kappa}_{\alpha\beta} \int_{(h_{th})_0} \delta_a \xi^3 S^{\alpha\beta} \frac{A_0}{A_0} d\xi^3 \\ &+ \bar{\omega}_{\alpha\beta} \int_{(h_{th})_0} \delta_a \xi^3 \xi^3 S^{\alpha\beta} \frac{A_0}{A_0} d\xi^3 \\ &+ \int_{(h_{th})_0} \frac{d(\delta_a \xi^3)}{d\xi_0^3} \lambda_3 S^{33} \frac{A_0}{A_0} d\xi^3 \\ &+ \delta_a \bar{\epsilon}_{\alpha\beta} \hat{S}_\epsilon^{\alpha\beta} + \delta_a \bar{\kappa}_{\alpha\beta} \hat{S}_\kappa^{\alpha\beta} + \frac{1}{2} \delta_a \bar{\omega}_{\alpha\beta} \hat{S}_\omega^{\alpha\beta}, \end{aligned} \tag{183}$$

$$F(\delta_a \xi^3) = \left(\delta_a \xi^3 \hat{p} \right) \Big|_{(\xi_0^3)^-} - \left(\delta_a \xi^3 \hat{p} \right) \Big|_{(\xi_0^3)^+}. \tag{184}$$

We note that the undeformed shape is represented by $\bar{G}_{\alpha\beta}$ and $\bar{K}_{\alpha\beta}$, and the current configuration by $\bar{\epsilon}_{\alpha\beta}$ and $\bar{\kappa}_{\alpha\beta}$.

Remark 23 The idea of representing the undeformed shape in terms of the metric tensor is from [42], and in that context the configuration is called the integration-point based zero-stress state (IPBZSS). In the shell model, full representation of the IPBZSS requires also the curvature tensor.

Remark 24 The variables $\bar{\omega}_{\alpha\beta}$ and $\delta_a \bar{\omega}_{\alpha\beta}$ appear in Eq. (183) for notational convenience. They are not independent variables. We can write $\bar{\omega}_{\alpha\beta}$ as given by Eq. (14), and write $\frac{1}{2} \delta_a \bar{\omega}_{\alpha\beta} \hat{S}_\omega^{\alpha\beta}$ by multiplying $\delta_a \bar{\omega}_{\alpha\beta}$ given by Eq. (68) with $\frac{1}{2} \hat{S}_\omega^{\alpha\beta}$:

$$\begin{aligned} \frac{1}{2} \delta_a \bar{\omega}_{\alpha\beta} \hat{S}_\omega^{\alpha\beta} &= -\delta_a \bar{\epsilon}_{\alpha\beta} \left(\bar{g}^{\alpha\gamma} \bar{\kappa}_{\gamma\delta} \hat{S}_\omega^{\delta\zeta} \bar{\kappa}_{\zeta\eta} \bar{g}^{\eta\beta} \right) \\ &+ \delta_a \bar{\kappa}_{\alpha\beta} \frac{1}{2} \left(\hat{S}_\omega^{\alpha\gamma} \bar{\kappa}_{\gamma\delta} \bar{g}^{\delta\beta} + \bar{g}^{\alpha\gamma} \bar{\kappa}_{\gamma\delta} \hat{S}_\omega^{\delta\beta} \right). \end{aligned} \tag{185}$$

We also note that

$$\bar{g}_{\alpha\beta} = 2\bar{\epsilon}_{\alpha\beta} + \bar{G}_{\alpha\beta}, \tag{186}$$

which follows from Eq. (45), and

$$[\bar{g}^{\alpha\beta}] = [2\bar{\epsilon}_{\alpha\beta} + \bar{G}_{\alpha\beta}]^{-1}, \tag{187}$$

which follows from Eq. (254) in Appendix A.

In describing the linearization for the Newton–Raphson iterations, we will first derive the variations needed for that. We start with the variations of $S^{\alpha\beta}$ and S^{33} :

$$\delta_b S^{\alpha\beta} = \frac{\partial S^{\alpha\beta}}{\partial E_{\gamma\delta}} \delta_b E_{\gamma\delta} + \frac{\partial S^{\alpha\beta}}{\partial E_{33}} \delta_b E_{33}, \tag{188}$$

$$\delta_b S^{33} = \frac{\partial S^{33}}{\partial E_{\gamma\delta}} \delta_b E_{\gamma\delta} + \frac{\partial S^{33}}{\partial E_{33}} \delta_b E_{33}, \tag{189}$$

where

$$\frac{\partial S^{\alpha\beta}}{\partial E_{\gamma\delta}} = \mathbb{C}^{\alpha\beta\gamma\delta}, \tag{190}$$

$$\frac{\partial S^{\alpha\beta}}{\partial E_{33}} = \mathbb{C}^{\alpha\beta 33}, \tag{191}$$

$$\frac{\partial S^{33}}{\partial E_{\gamma\delta}} = \mathbb{C}^{33\gamma\delta}, \tag{192}$$

$$\frac{\partial S^{33}}{\partial E_{33}} = \mathbb{C}^{3333}. \tag{193}$$

The elastic moduli $\mathbb{C}^{\alpha\beta\gamma\delta}$, $\mathbb{C}^{\alpha\beta 33}$, $\mathbb{C}^{33\gamma\delta}$, and \mathbb{C}^{3333} can be derived from φ . In Eqs. (59) and (60), using δ_b in place of δ , recognizing that $\delta \xi^3$ and δy^3 are interchangeable, and reordering the terms, we obtain

$$\begin{aligned} \delta_b E_{\gamma\delta} &= \left(\bar{\kappa}_{\gamma\delta} + \bar{\omega}_{\gamma\delta} \xi^3 \right) \delta_b y^3 \\ &+ \delta_b \bar{\epsilon}_{\gamma\delta} + \delta_b \bar{\kappa}_{\gamma\delta} \xi^3 + \frac{1}{2} \delta_b \bar{\omega}_{\gamma\delta} \left(\xi^3 \right)^2 \end{aligned} \tag{194}$$

$$\begin{aligned} &= \bar{\kappa}_{\gamma\delta} \delta_b y^3 + \delta_b \bar{\epsilon}_{\gamma\delta} \\ &+ \left(\bar{\omega}_{\gamma\delta} \delta_b y^3 + \delta_b \bar{\kappa}_{\gamma\delta} \right) \xi^3 + \frac{1}{2} \delta_b \bar{\omega}_{\gamma\delta} \left(\xi^3 \right)^2 \end{aligned} \tag{195}$$

and

$$\delta_b E_{33} = \lambda_3 \delta_b \lambda_3. \tag{196}$$

Taking the variation of Eq. (181), we obtain

$$\delta_b \lambda_3 = \frac{d(\delta_b y^3)}{d\xi_0^3}. \tag{197}$$

From the variations of Eqs. (80), (81) and (82), we obtain

$$\delta_b \hat{S}_\varepsilon^{\alpha\beta} = \int_{(h_{th})_0} \delta_b S^{\alpha\beta} \frac{A_0}{A_0} d\xi^3, \tag{198}$$

$$\begin{aligned} \delta_b \hat{S}_\kappa^{\alpha\beta} &= \int_{(h_{th})_0} \left(S^{\alpha\beta} \delta_b y^3 + \xi^3 \delta_b S^{\alpha\beta} \right) \frac{A_0}{A_0} d\xi^3 \\ &= \int_{(h_{th})_0} S^{\alpha\beta} \delta_b y^3 \frac{A_0}{A_0} d\xi^3 + \int_{(h_{th})_0} \xi^3 \delta_b S^{\alpha\beta} \frac{A_0}{A_0} d\xi^3, \end{aligned} \tag{199}$$

$$\delta_b \hat{S}_\omega^{\alpha\beta} = \int_{(h_{th})_0} \left(2S^{\alpha\beta} \xi^3 \delta_b y^3 + (\xi^3)^2 \delta_b S^{\alpha\beta} \right) \frac{A_0}{A_0} d\xi^3 \tag{200}$$

$$\begin{aligned} &= 2 \int_{(h_{th})_0} \xi^3 S^{\alpha\beta} \delta_b y^3 \frac{A_0}{A_0} d\xi^3 \\ &\quad + \int_{(h_{th})_0} (\xi^3)^2 \delta_b S^{\alpha\beta} \frac{A_0}{A_0} d\xi^3. \end{aligned} \tag{202}$$

Now that we have all the variations we need, we write $\delta_b N$ by taking the variation of Eq. (183). After taking the variation, we substitute into it Eqs. (198), (200) and (202). Then we substitute Eqs. (188), (189), (190), (191), (192), (193) and (196) into that. Also, we recognize the right-hand sides of Eqs. (195) and (197) and δ_a versions of those. At the end, we get

$$\begin{aligned} \delta_b N &(\delta_a \xi^3, \delta_a \bar{\varepsilon}_{\alpha\beta}, \delta_a \bar{\kappa}_{\alpha\beta}, y^3, \bar{\varepsilon}_{\gamma\delta}, \bar{\kappa}_{\gamma\delta}) \\ &= \int_{(h_{th})_0} \delta_a E_{\alpha\beta} \mathbb{C}^{\alpha\beta\gamma\delta} \delta_b E_{\gamma\delta} \frac{A_0}{A_0} d\xi^3 \\ &\quad + \int_{(h_{th})_0} \delta_a E_{\alpha\beta} \lambda_3 \mathbb{C}^{\alpha\beta 33} \delta_b \lambda_3 \frac{A_0}{A_0} d\xi^3 \\ &\quad + \int_{(h_{th})_0} \delta_a \lambda_3 \lambda_3 \mathbb{C}^{33\gamma\delta} \delta_b E_{\gamma\delta} \frac{A_0}{A_0} d\xi^3 \\ &\quad + \int_{(h_{th})_0} \delta_a \lambda_3 \left(S^{33} + \lambda_3^2 \mathbb{C}^{3333} \right) \delta_b \lambda_3 \frac{A_0}{A_0} d\xi^3 \\ &\quad + \int_{(h_{th})_0} \delta_a \xi^3 S^{\gamma\delta} \frac{A_0}{A_0} d\xi^3 \delta_b \bar{\kappa}_{\gamma\delta} \\ &\quad + \delta_a \bar{\kappa}_{\alpha\beta} \int_{(h_{th})_0} S^{\alpha\beta} \delta_b y^3 \frac{A_0}{A_0} d\xi^3 \\ &\quad + \int_{(h_{th})_0} \delta_a \xi^3 \xi^3 S^{\gamma\delta} \frac{A_0}{A_0} d\xi^3 \delta_b \bar{\omega}_{\gamma\delta} \\ &\quad + \delta_a \bar{\omega}_{\alpha\beta} \int_{(h_{th})_0} \xi^3 S^{\alpha\beta} \delta_b y^3 \frac{A_0}{A_0} d\xi^3 \\ &\quad + \frac{1}{2} \delta_a \delta_b \bar{\omega}_{\alpha\beta} \hat{S}_\omega^{\alpha\beta}. \end{aligned} \tag{203}$$

Remark 25 The choices made between using different combinations of variable in Eq. (203) were driven by having

visible symmetry in δ_a and δ_b and reducing the number of terms.

Remark 26 The term $\delta_a \delta_b \bar{\omega}_{\alpha\beta}$ is not zero, because, as explained in Remark 23, $\delta_a \bar{\omega}_{\alpha\beta}$ is not an independent variation. We replace δ with δ_a in Eq. (68), take its δ_b variation, multiply that with $\frac{1}{2} \hat{S}_\omega^{\alpha\beta}$, and obtain

$$\begin{aligned} &\frac{1}{2} \delta_a \delta_b \bar{\omega}_{\alpha\beta} \hat{S}_\omega^{\alpha\beta} \\ &= \delta_a \bar{\kappa}_{\alpha\beta} \frac{1}{2} \left(\hat{S}_\omega^{\alpha\gamma} \bar{g}^{\beta\delta} + \bar{g}^{\alpha\gamma} \hat{S}_\omega^{\beta\delta} \right) \delta_b \bar{\kappa}_{\gamma\delta} \\ &\quad - \delta_a \bar{\varepsilon}_{\alpha\beta} \left(\bar{g}^{\alpha\eta} \bar{\kappa}_{\eta\kappa} \hat{S}_\omega^{\kappa\gamma} \bar{g}^{\beta\delta} + \bar{g}^{\alpha\gamma} \bar{g}^{\beta\kappa} \bar{\kappa}_{\kappa\eta} \hat{S}_\omega^{\eta\delta} \right) \delta_b \bar{\kappa}_{\gamma\delta} \\ &\quad - \delta_a \bar{\kappa}_{\alpha\beta} \left(\hat{S}_\omega^{\alpha\kappa} \bar{\kappa}_{\kappa\eta} \bar{g}^{\eta\delta} \bar{g}^{\beta\gamma} + \bar{g}^{\alpha\delta} \hat{S}_\omega^{\beta\eta} \bar{\kappa}_{\eta\kappa} \bar{g}^{\kappa\gamma} \right) \delta_b \bar{\varepsilon}_{\gamma\delta}. \end{aligned} \tag{204}$$

Remark 27 When the traction conditions on the upper and lower surfaces are coming from the pressure on those surfaces, with the conditions expressed as

$$\mathbf{h}|_{(\xi_0^3)^-} = p^- \bar{\mathbf{n}}, \tag{205}$$

$$\mathbf{h}|_{(\xi_0^3)^+} = -p^+ \bar{\mathbf{n}}, \tag{206}$$

\hat{p}^- and \hat{p}^+ appearing in Eq. (184) can vary because of the midsurface deformation or the displacement in the out-of-plane direction. We can derive an expression for that from Eqs. (113) and (114) by using Eqs. (109), (110), (205) and (206):

$$\hat{p}^- = p^- \frac{A}{A_0} \Big|_{(\xi_0^3)^-}, \tag{207}$$

$$\hat{p}^+ = p^+ \frac{A}{A_0} \Big|_{(\xi_0^3)^+}. \tag{208}$$

We note that A depends on both the midsurface deformation and the displacement in the out-of-plane direction. We derive the expression for $\delta_b A$ based on that dependence and use it in the computations.

5 Test problems

With the method described in Sect. 4, for a set of test problems, we determine the displacement in the out-of-plane direction. In all cases, we use a uniform finite element mesh made of 200 elements with linear functions¹. The lower or

¹ As mentioned in Remark 22, in the actual computations, we will be using a different way of numerically solving the equations in the out-of-plane direction, and that process will involve an order of magnitude less number of points.

inner surface serves² as the “midsurface.” Together with the out-of-plane displacement, the midsurface variables $\bar{\varepsilon}_{\alpha\beta}$ and $\bar{\kappa}_{\alpha\beta}$ are solved for, with different boundary or geometry conditions depending on the problem setup. For comparison, we include in the tests a plane-stress shell model from [5]. The constitutive models, provided in Appendix D, are neo-Hookean and Fung’s models with compressible and incompressible materials.

The stress-related variables are scaled by the shear modulus μ_0 at the undeformed configuration. The Poisson’s ratio ν is defined based on the bulk modulus at the undeformed configuration, with $\nu = 0.50$ indicating incompressible material. We use separate models for compressible and incompressible materials, but the compressible-material model converges to the incompressible-material model in the limit $\nu \rightarrow 0.50$ (see [5]). The scaled stress components we report will be from the Cauchy stress, and the indices will correspond to the coordinate frame defined separately in each problem, but the index 3 will always imply the out-of-plane direction:

$$\sigma_{11}^* = \frac{J^{-1} (S^{11} g_{11} + S^{12} g_{21})}{\mu_0}, \tag{209}$$

$$\sigma_{22}^* = \frac{J^{-1} (S^{21} g_{12} + S^{22} g_{22})}{\mu_0}, \tag{210}$$

$$\sigma_{33}^* = \frac{J^{-1} S^{33}}{\mu_0}. \tag{211}$$

For the length scale, we use the undeformed shell thickness $(h_{th})_0 = (\xi_0^3)^+ - (\xi_0^3)^-$. We note that, with the shell model and method sections behind us, now we are using the symbol $(h_{th})_0$ for the shell thickness, as we stated in Sect. 2.1 that we would. We also note that the current thickness is expressed as $h_{th} = (\xi^3)^+ - (\xi^3)^-$.

We use the principal curvatures at the midsurface to describe the individual problems. The principal curvatures $\bar{\kappa}_1$ and $\bar{\kappa}_2$ are obtained from the generalized eigenvalue problem

$$\bar{\kappa}_{\alpha\beta} t^\beta = \bar{\kappa} \bar{g}_{\alpha\beta} t^\beta, \tag{212}$$

where t^β represents the contravariant components of the principal curvature direction. From Eq. (212), we can get the principal curvatures as

$$\bar{\kappa}_1 = \frac{\bar{g}^{\alpha\beta} \bar{\kappa}_{\alpha\beta} + \sqrt{(\bar{g}^{\alpha\beta} \bar{\kappa}_{\alpha\beta})^2 - 4 \det[\bar{g}^{\alpha\beta}] \det[\bar{\kappa}_{\alpha\beta}]}}{2}, \tag{213}$$

² We note that, as can be inferred from the overall formulation, in the shell model proposed here, the location of the midsurface does not matter. However, it does in the model proposed in [5]. We will be comparing our results to those obtained with that model. This is the reason why the lower or inner surface serves as the midsurface.

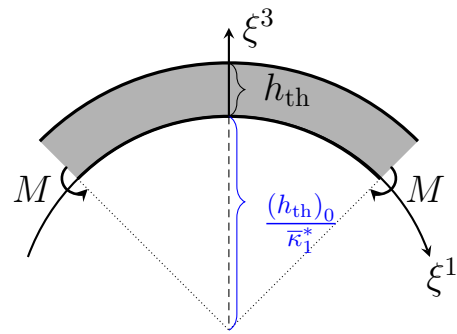


Fig. 7 Unidirectional plate bending. Problem setup. The lower surface is serving as the midsurface. The bending moment M is applied along the midsurface edges. The nondimensional curvature $\bar{\kappa}_1^*$ is given by Eq. (215)

$$\bar{\kappa}_2 = \frac{\bar{g}^{\alpha\beta} \bar{\kappa}_{\alpha\beta} - \sqrt{(\bar{g}^{\alpha\beta} \bar{\kappa}_{\alpha\beta})^2 - 4 \det[\bar{g}^{\alpha\beta}] \det[\bar{\kappa}_{\alpha\beta}]}}{2}. \tag{214}$$

Their nondimensional versions are

$$\bar{\kappa}_1^* = \bar{\kappa}_1 (h_{th})_0, \tag{215}$$

$$\bar{\kappa}_2^* = \bar{\kappa}_2 (h_{th})_0. \tag{216}$$

5.1 Unidirectional plate bending

The bending is only in ξ^1 direction (see Fig. 7). No traction is applied on the upper or lower surface. The bending moment M is applied along the midsurface edges. We select \bar{G}_α to be unit orthogonal basis vectors, and consequently $\bar{G}_{11} = \bar{G}_{22} = 1$, and $\bar{G}_{12} = 0$. We note that, with this selection, we no longer have $-1 \leq \xi^\alpha \leq 1$. In this problem, because it is a plate, $\bar{K}_{11} = \bar{K}_{22} = \bar{K}_{12} = 0$. We constrain the midsurface deformation with $\bar{\varepsilon}_{22} = \bar{\varepsilon}_{12} = 0$ and $\bar{\kappa}_{22} = \bar{\kappa}_{12} = 0$. With these conditions, from Eq. (213) we get

$$\bar{\kappa}_1 = \bar{g}^{11} \bar{\kappa}_{11}, \tag{217}$$

and its nondimensional version is

$$\bar{\kappa}_1^* = \bar{g}^{11} \bar{\kappa}_{11} (h_{th})_0. \tag{218}$$

For any value of $\bar{\kappa}_1^*$, we set $\bar{\kappa}_{11}$ based on that relationship, noting that \bar{g}^{11} is a function of $\bar{\varepsilon}_{11}$. We solve for $\bar{\varepsilon}_{11}$ together with the displacement in the out-of-plane direction. After that, we calculate the required moment around $\xi^3 = 0$:

$$M = \int_{(h_{th})_0} \xi^3 J^{-1} (S^{11} g_{11} + S^{12} g_{21}) \frac{L}{L} d\xi^3, \tag{219}$$

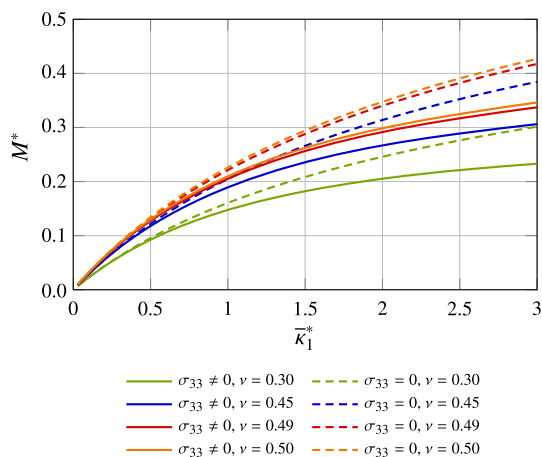


Fig. 8 Unidirectional plate bending. Neo-Hookean material. $\bar{\kappa}_1^*$ and M^*

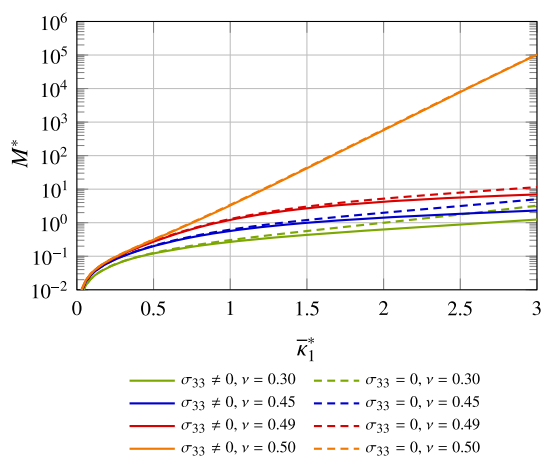


Fig. 9 Unidirectional plate bending. Fung's material. $\bar{\kappa}_1^*$ and M^*

and scale that as

$$M^* = \frac{M}{\mu_0 (h_{th})_0^2}. \tag{220}$$

In this problem, $\frac{L}{L} = 1$ and $g_{21} = 0$, which follow from the constraints listed earlier.

Figures 8 and 9 show, for the neo-Hookean and Fung's materials, M^* as a function of $\bar{\kappa}_1^*$. For both materials, the model with the plane-stress assumption ($\sigma_{33} = 0$) is behaving stiffer than the model with the out-of-plane normal stress ($\sigma_{33} \neq 0$). For the Fung's material, the difference becomes smaller at higher ν values.

We report, for $\bar{\kappa}_1^* = 0.5$ and 1, ξ_0^3 profiles of different variables. We report λ_3 , J , σ_{11}^* , and σ_{33}^* in Figs. 10, 11, 12 and 13 for the neo-Hookean material, and in Figs. 14, 15, 16 and 17 for the Fung's material. For the neo-Hookean material, λ_3 obtained with the $\sigma_{33} = 0$ model is more than it is with the $\sigma_{33} \neq 0$ model. Assuming that the $\sigma_{33} \neq 0$ model is giving the true solution, $\sigma_{33} \leq 0$. This means that the $\sigma_{33} = 0$ model

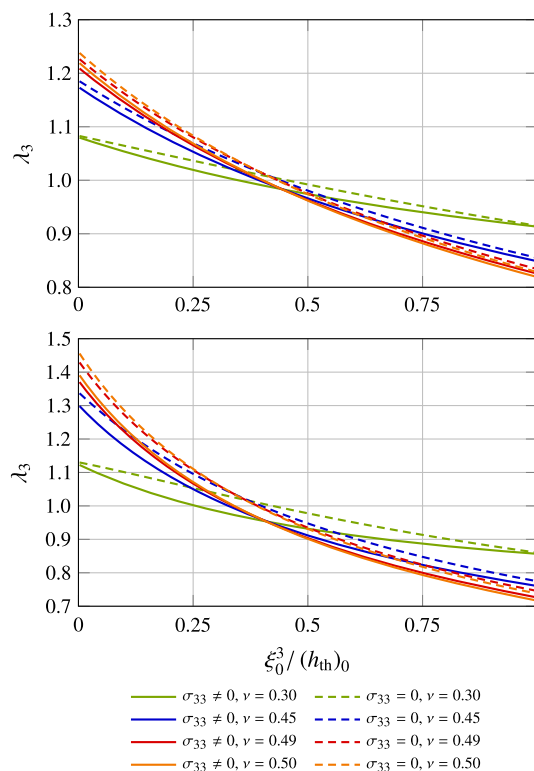


Fig. 10 Unidirectional plate bending. Neo-Hookean material. λ_3 profile. $\bar{\kappa}_1^* = 0.5$ and 1

Table 1 Unidirectional plate bending. Neo-Hookean material. Significance of σ_{33}^*

	$ \sigma_{11}^* _{\max}$	$ \sigma_{33}^* _{\max}$	$ \sigma_{33}^* _{\max} / \sigma_{\text{MAX12}}^*$ (%)
$\bar{\kappa}_1^* = 0.5$	0.816	0.0839	10.3
$\bar{\kappa}_1^* = 1.0$	1.43	0.257	18.0

is behaving in a fashion that inhibits the compressive stress that should be there. The larger λ_3 makes h_{th} higher, and that could be the source of the stiffer response mentioned when Figs. 8 and 9 were discussed. Overall, the Fung's material behaves similar to how the neo-Hookean material behaves. However, because of the strong nonlinearity, the λ_3 profile is more complex. For example, there is a local maximum close to the inner surface. Also, at high values of ν , σ_{11} becomes very high at both the lower and upper surfaces. That is making σ_{33} higher.

To have a better understanding of the significance of σ_{33}^* , we scale it by using, in general, $|\sigma_{11}^*|_{\max}$ and $|\sigma_{22}^*|_{\max}$, where “max” denotes the maximum over both ξ_0^3 and ν . To be on the conservative side in not overrating that significance, we scale σ_{33}^* with $\sigma_{\text{MAX12}}^* = \max(|\sigma_{11}^*|_{\max}, |\sigma_{22}^*|_{\max})$. We note that in this case $|\sigma_{22}^*|_{\max} = 0$. Tables 1 and 2 show, for the neo-Hookean and Fung's materials and for $\bar{\kappa}_1^* = 0.5$ and 1, $|\sigma_{11}^*|_{\max}$, $|\sigma_{33}^*|_{\max}$, and $|\sigma_{33}^*|_{\max} / \sigma_{\text{MAX12}}^*$. We see that the

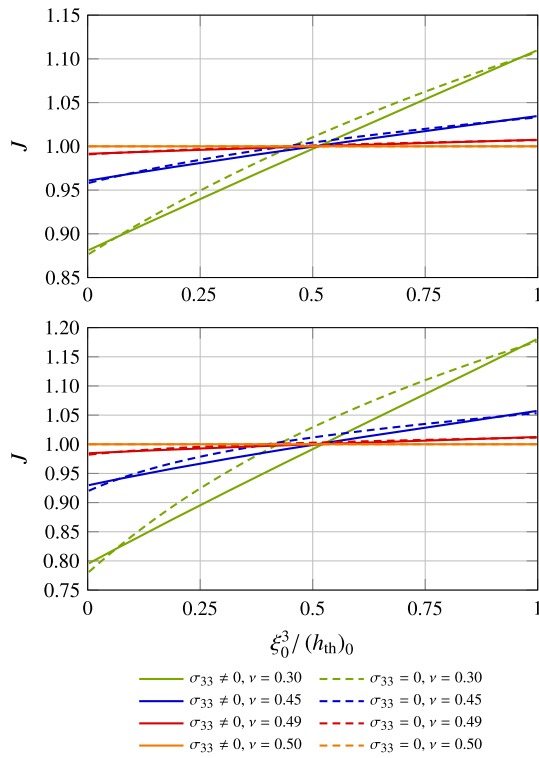


Fig. 11 Unidirectional plate bending. Neo-Hookean material. J profile. $\bar{\kappa}_1^* = 0.5$ and 1

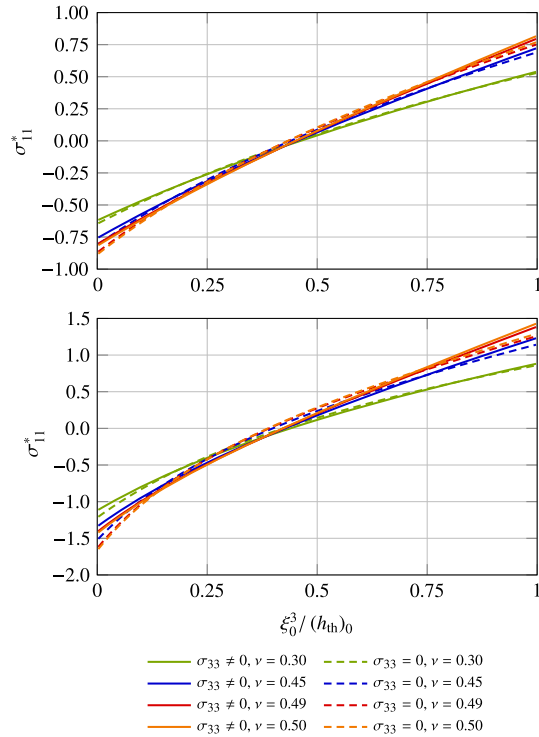


Fig. 12 Unidirectional plate bending. Neo-Hookean material. σ_{11}^* profile. $\bar{\kappa}_1^* = 0.5$ and 1

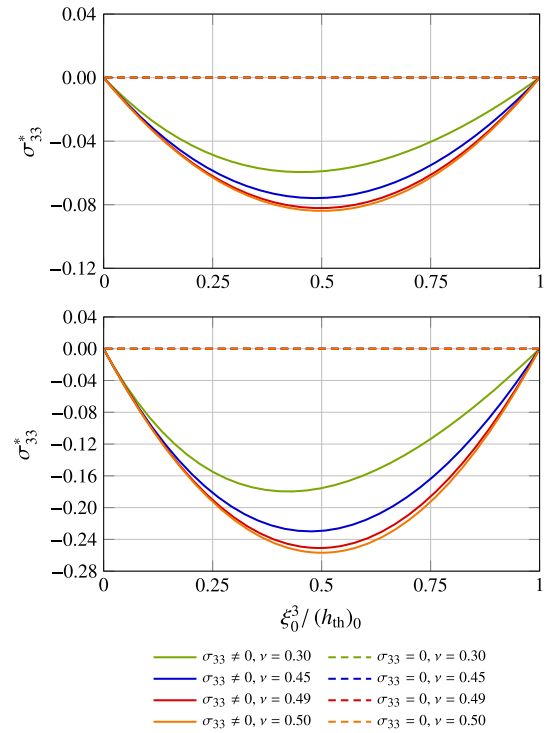


Fig. 13 Unidirectional plate bending. Neo-Hookean material. σ_{33}^* profile. $\bar{\kappa}_1^* = 0.5$ and 1

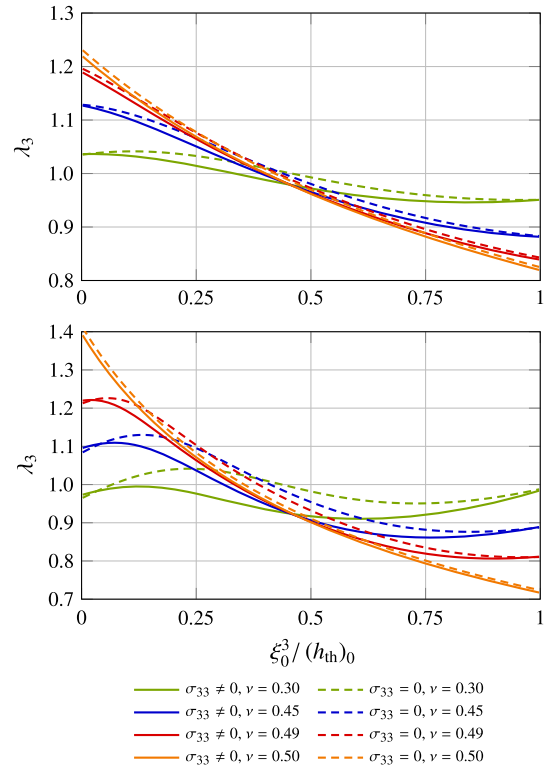


Fig. 14 Unidirectional plate bending. Fung's material. λ_3 profile. $\bar{\kappa}_1^* = 0.5$ and 1

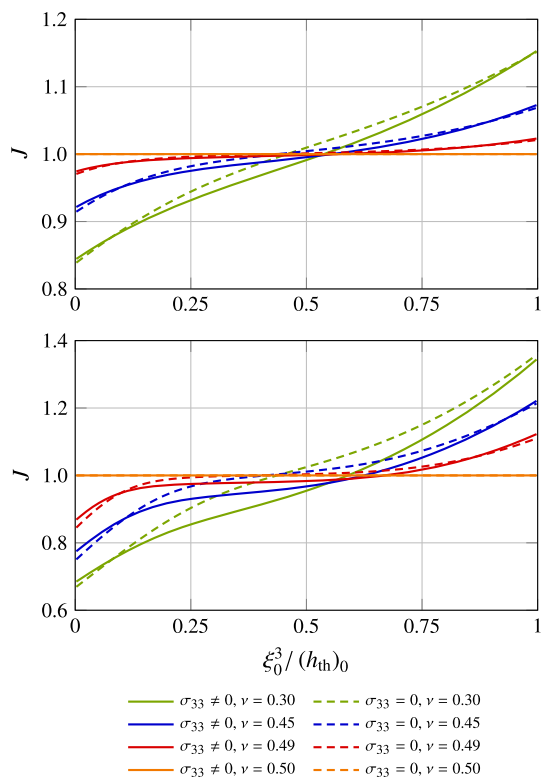


Fig. 15 Unidirectional plate bending. Fung’s material. J profile. $\bar{\kappa}_1^* = 0.5$ and 1

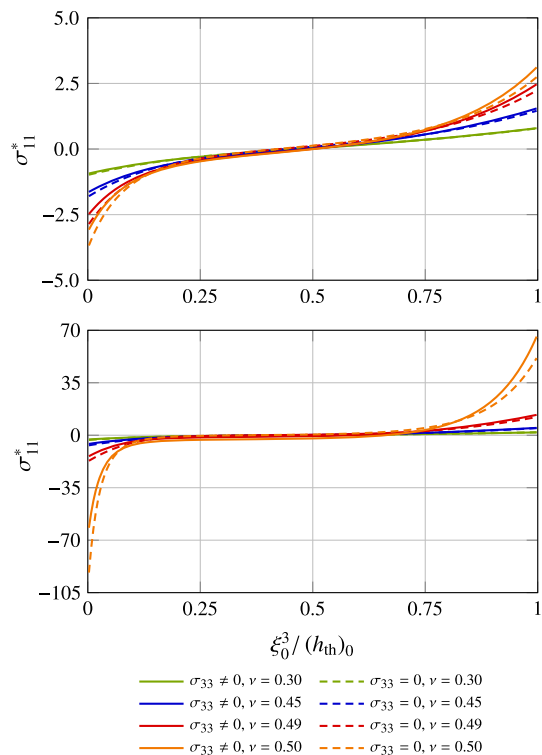


Fig. 16 Unidirectional plate bending. Fung’s material. σ_{11}^* profile. $\bar{\kappa}_1^* = 0.5$ and 1

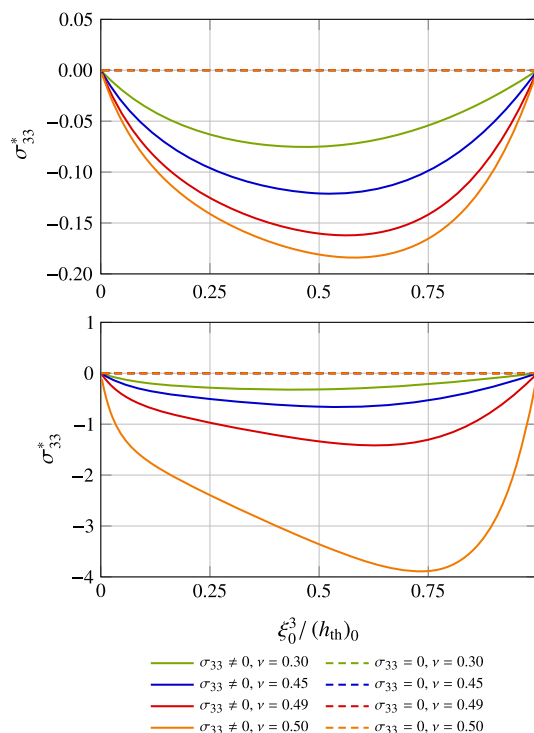


Fig. 17 Unidirectional plate bending. Fung’s material. σ_{33}^* profile. $\bar{\kappa}_1^* = 0.5$ and 1

Table 2 Unidirectional plate bending. Fung’s material. Significance of σ_{33}^*

	$ \sigma_{11}^* _{\max}$	$ \sigma_{33}^* _{\max}$	$ \sigma_{33}^* _{\max} / \sigma_{\text{MAX12}}^*$ (%)
$\bar{\kappa}_1^* = 0.5$	3.11	0.184	5.92
$\bar{\kappa}_1^* = 1.0$	65.8	3.89	5.91

significance, as measured by $|\sigma_{33}^*|_{\max} / \sigma_{\text{MAX12}}^*$, is more than 10 % for the neo-Hookean material and more than 5.9 % for the Fung’s material.

5.2 Plate saddle deformation

Bending moments are applied along the midsurface edges both in ξ^1 and ξ^2 directions to create a saddle deformation. No traction is applied on the upper or lower surface. Again, we select $\bar{G}_{11} = \bar{G}_{22} = 1$, $\bar{G}_{33} = 0$, and $\bar{K}_{11} = \bar{K}_{22} = \bar{K}_{12} = 0$ to represent a plate. We constrain the midsurface deformation with $\bar{\epsilon}_{12} = 0$ and $\bar{\kappa}_{12} = 0$. With these conditions, from Eqs. (213) and (214) we get

$$\bar{\kappa}_1 = \bar{\kappa}_{11} \bar{g}^{11}, \tag{221}$$

$$\bar{\kappa}_2 = \bar{\kappa}_{22} \bar{g}^{22}, \tag{222}$$

and their nondimensional versions are

$$\bar{\kappa}_1^* = \bar{\kappa}_{11} \bar{g}^{11} (h_{\text{th}})_0, \tag{223}$$

Table 3 Plate saddle deformation. Cases tested

	$\bar{\kappa}_1^*$	$\bar{\kappa}_2^*$
Case 1	0.5	-0.5
Case 2	1.0	-0.5

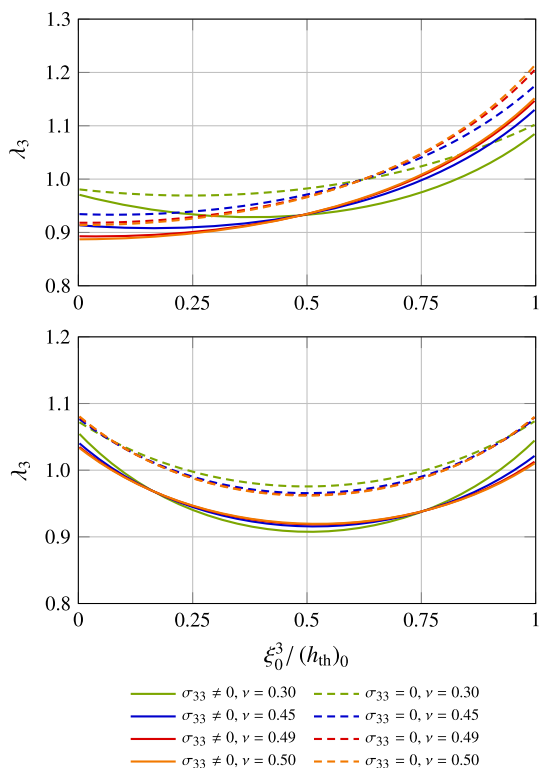


Fig. 18 Plate saddle deformation. Neo-Hookean material. λ_3 profile. Case 1 and Case 2

$$\bar{\kappa}_2^* = \bar{\kappa}_{22} \bar{g}^{22} (h_{th})_0. \tag{224}$$

For any values of $\bar{\kappa}_1^*$ and $\bar{\kappa}_2^*$, we set $\bar{\kappa}_{11}$ and $\bar{\kappa}_{22}$ based on these relationships, noting that \bar{g}^{11} is a function of $\bar{\epsilon}_{11}$ and \bar{g}^{22} is a function of $\bar{\epsilon}_{22}$. We solve for $\bar{\epsilon}_{11}$ and $\bar{\epsilon}_{22}$ together with the displacement in the out-of-plane direction.

The saddle deformation is obtained by specifying the two principal curvatures to be $\bar{\kappa}_1^* > 0$ and $\bar{\kappa}_2^* < 0$. The curvature at the upper surface can be written as

$$\kappa_2|_{(\xi^3)^+} = \frac{1}{\frac{1}{\bar{\kappa}_2} + h_{th}} \tag{225}$$

$$= \frac{\bar{\kappa}_2}{1 + \bar{\kappa}_2 h_{th}}, \tag{226}$$

and this needs to be finite. That requirement brings the restriction $\bar{\kappa}_2 h_{th} = \bar{\kappa}_2^* \frac{h_{th}}{(h_{th})_0} > -1$. Considering that, we set $\bar{\kappa}_2^* = -\frac{1}{2}$.

We report, for the two test cases given in Table 3, ξ_0^3 profiles of λ_3 , J , σ_{11}^* , σ_{22}^* , and σ_{33}^* . Figures 18, 19, 20, 21 and 22

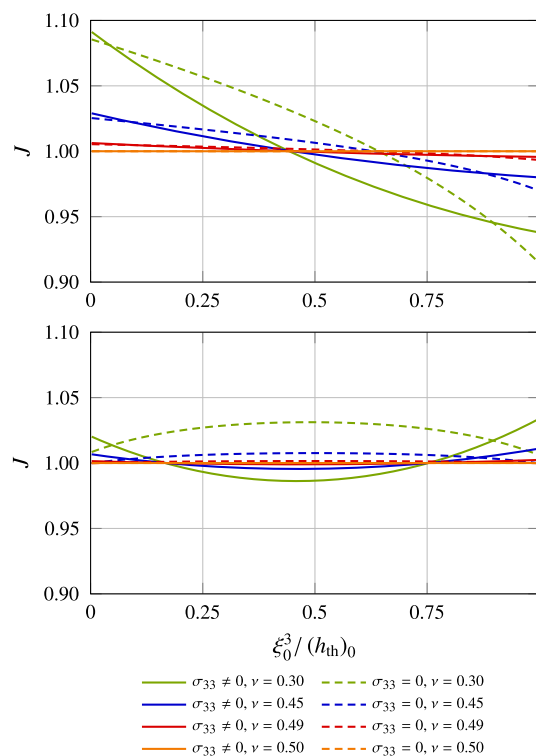


Fig. 19 Plate saddle deformation. Neo-Hookean material. J profile. Case 1 and Case 2

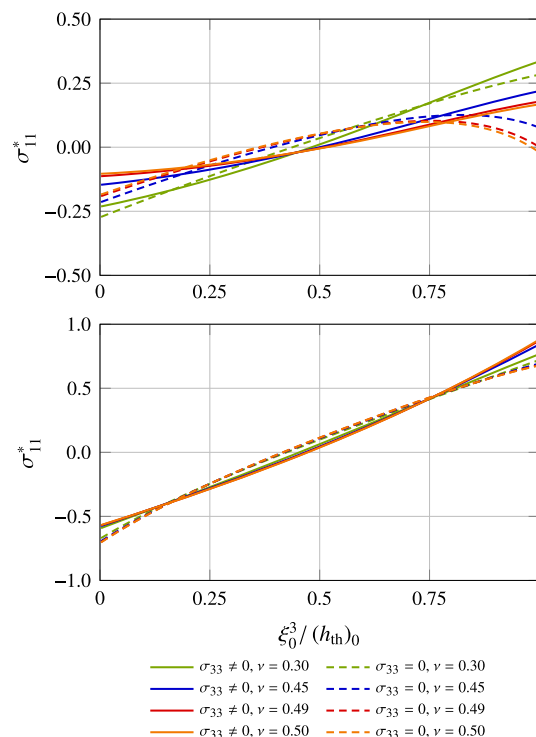


Fig. 20 Plate saddle deformation. Neo-Hookean material. σ_{11}^* profile. Case 1 and Case 2

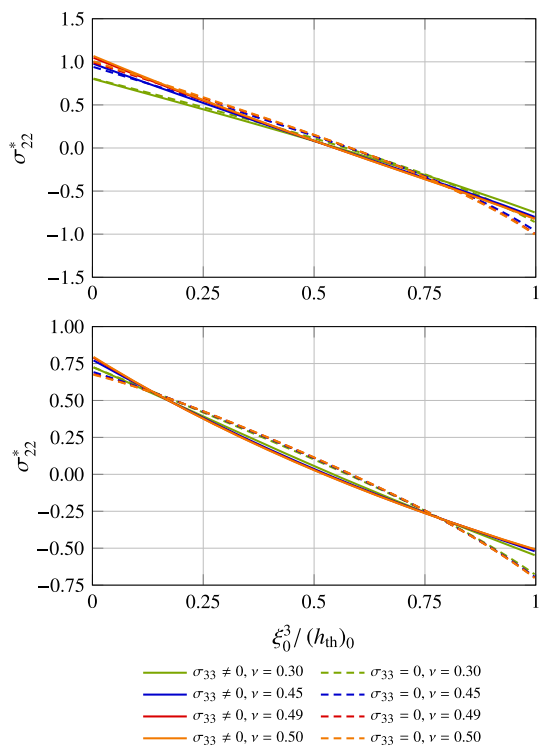


Fig. 21 Plate saddle deformation. Neo-Hookean material. σ_{22}^* profile. Case 1 and Case 2

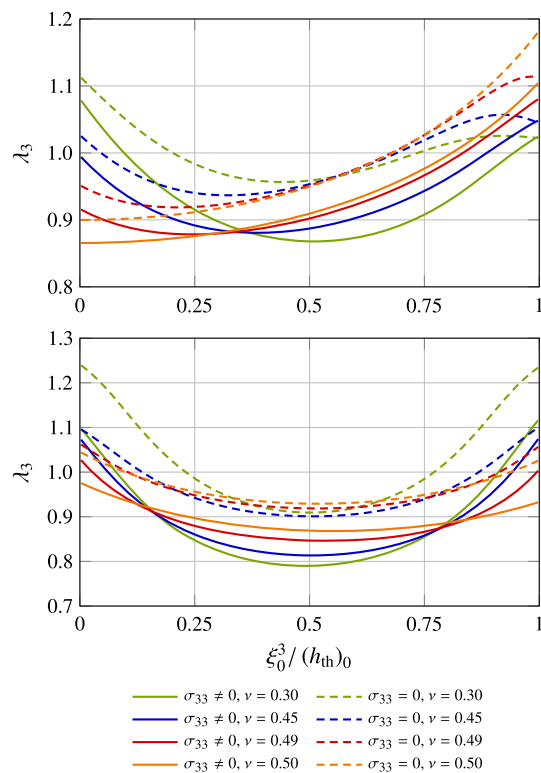


Fig. 23 Plate saddle deformation. Fung's material. λ_3 profile. Case 1 and Case 2

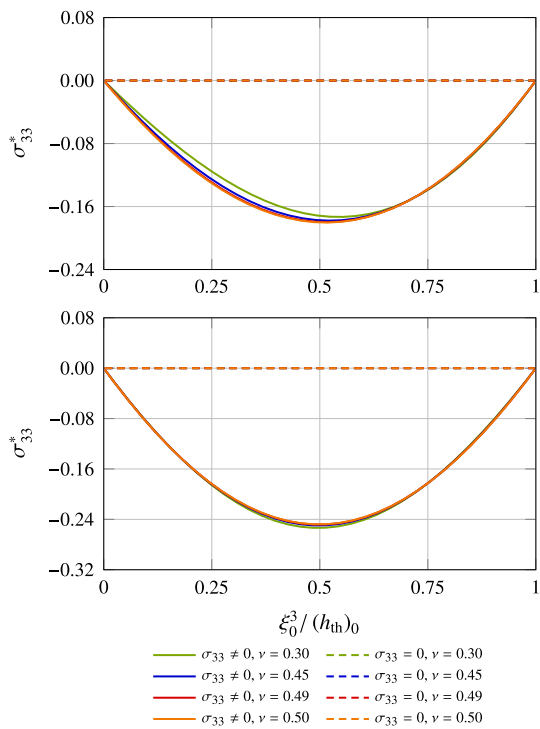


Fig. 22 Plate saddle deformation. Neo-Hookean material. σ_{33}^* profile. Case 1 and Case 2

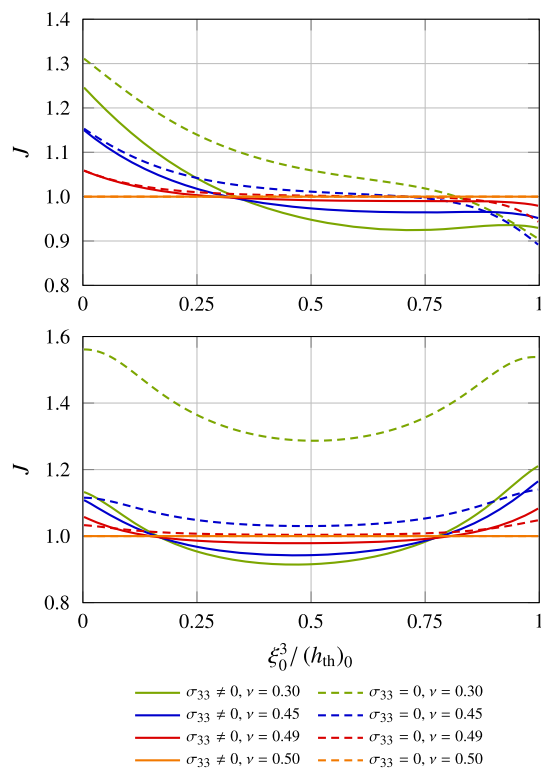


Fig. 24 Plate saddle deformation. Fung's material. J profile. Case 1 and Case 2

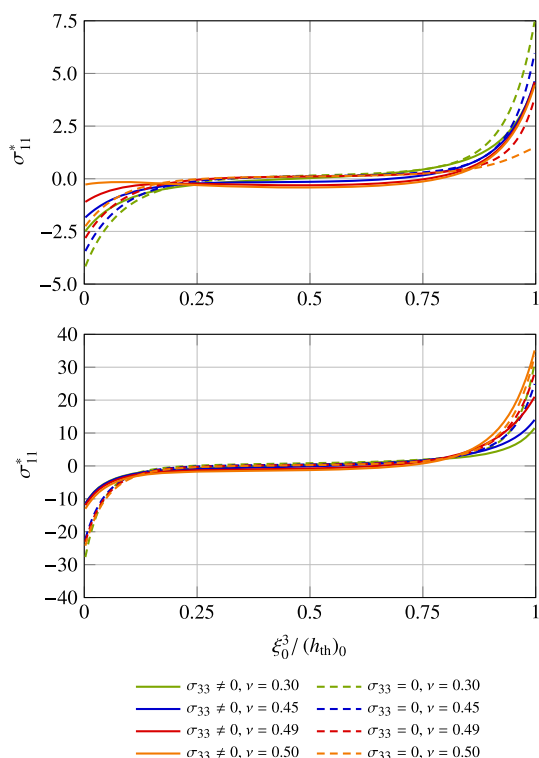


Fig. 25 Plate saddle deformation. Fung’s material. σ_{11}^* profile. Case 1 and Case 2

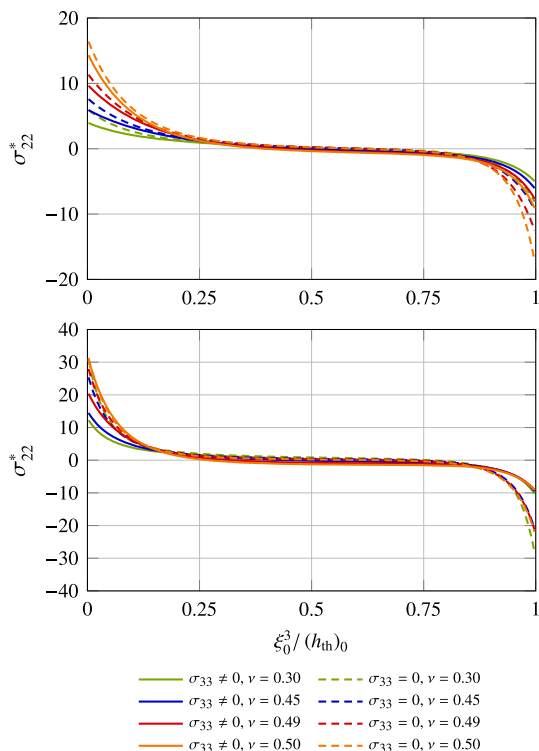


Fig. 26 Plate saddle deformation. Fung’s material. σ_{22}^* profile. Case 1 and Case 2

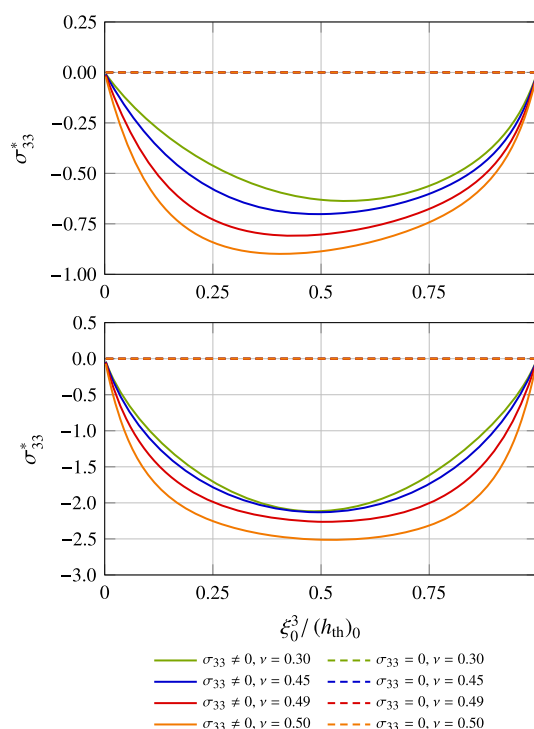


Fig. 27 Plate saddle deformation. Fung’s material. σ_{33}^* profile. Case 1 and Case 2

Table 4 Unidirectional plate saddle. Neo-Hookean material. Significance of σ_{33}^*

	$ \sigma_{11}^* _{\max}$	$ \sigma_{22}^* _{\max}$	$ \sigma_{33}^* _{\max}$	$ \sigma_{33}^* _{\max} / \sigma_{\text{MAX12}}^*$ (%)
Case 1	0.166	1.07	0.180	16.8
Case 2	0.875	0.795	0.248	28.3

show those profiles for the neo-Hookean material, and Figs. 23, 24, 25, 26 and 27 for the Fung’s material.

Case 2 is closer to having $\kappa_1^* = -\kappa_2^*$ at $\xi_0^3 / (h_{th})_0 = 0.5$. This is the reason behind the near symmetry between the σ_{11}^* and σ_{22}^* profiles (see Case 2 of Figs. 20 and 21, and Case 2 of Figs. 25 and 26). Looking at the λ_3 profiles (see Figs. 18 and 23), there is more difference between what we get from the $\sigma_{33} \neq 0$ and $\sigma_{33} = 0$ models than between what we get from different ν values. In other words, the shell models being different is more significant than the ν values being different. Tables 4 and 5 show, for the neo-Hookean and Fung’s materials and for Case 1 and Case 2, $|\sigma_{11}^*|_{\max}$, $|\sigma_{22}^*|_{\max}$, $|\sigma_{33}^*|_{\max}$, and $|\sigma_{33}^*|_{\max} / \sigma_{\text{MAX12}}^*$. This time $|\sigma_{33}^*|_{\max} / \sigma_{\text{MAX12}}^*$ is more than 16 % for the neo-Hookean material and more than 6.2 % for the Fung’s material. These numbers are higher compared to what we had in the unidirectional plate bending.

5.3 Pressurized cylindrical and spherical shells

The inner and outer pressures are p_I and p_O , and the inner and outer radii are R_I and R_O in the undeformed configuration

Table 5 Unidirectional plate saddle. Fung’s material. Significance of σ_{33}^*

	$ \sigma_{11}^* _{\max}$	$ \sigma_{22}^* _{\max}$	$ \sigma_{33}^* _{\max}$	$ \sigma_{33}^* _{\max} / \sigma_{\text{MAX12}}^*$ (%)
Case 1	4.44	14.3	0.899	6.29
Case 2	35.1	30.9	2.51	7.15

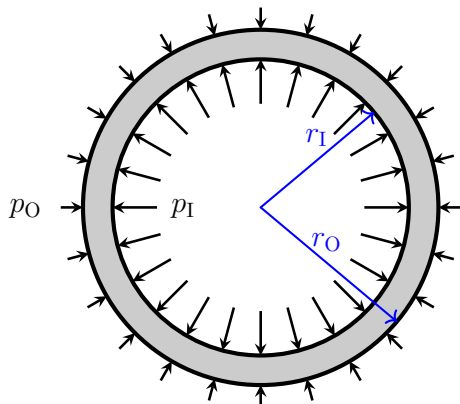


Fig. 28 Pressurized cylindrical and spherical shells. The symbols p_I and p_O represent the pressures acting on the inner and outer surfaces in the actual problem. The symbols r_1 and r_O represent the inner and outer radii in the deformed configuration, and R_1 and R_O in the undeformed configuration

Table 6 Pressurized cylindrical and spherical shells. Three methods, characterized by selecting between the $\sigma_{33} \neq 0$ and $\sigma_{33} = 0$ models and whether p_O is applied at the outer or inner surface

	p_I	p_O	σ_{33}
Method 1	Inner	Inner	$\sigma_{33} = 0$
Method 2	Inner	Outer	$\sigma_{33} = 0$
Method 3	Inner	Outer	$\sigma_{33} \neq 0$

and r_1 and r_O in the deformed configuration (see Fig. 28). We note that $R_O = R_1 + (h_{th})_0$ and $r_O = r_1 + h_{th}$. We set $\frac{(h_{th})_0}{2R_1} = 0.1$, the same value used for the undeformed configurations in [5].

We compute with three different methods, characterized by selecting between the $\sigma_{33} \neq 0$ and $\sigma_{33} = 0$ models and whether p_O is applied at the outer or inner surface (see Table 6). In Method 1, by applying both p_I and p_O at the inner surface, which serves as the midsurface, the difference between the inner and outer surface areas is not taken into account in calculating the net force acting on the shell. That is taken into account in Method 2 by applying p_O at the outer surface. Method 3 also takes that into account, but with the $\sigma_{33} \neq 0$ model. We measure the deformation by $\bar{\lambda}_1$. For the cylindrical shell, we set $\lambda_2 = 1$. We set $p_I = 2p$ and $p_O = p$, and p is scaled as $p^* = \frac{p}{\mu_0}$.

5.3.1 Pressurized cylindrical shell

We select the undeformed configuration as

$$\bar{G}_{11} = 1, \tag{227}$$

$$\bar{G}_{22} = 1, \tag{228}$$

$$\bar{G}_{12} = 0, \tag{229}$$

$$\bar{K}_{11} = \frac{1}{R_1}, \tag{230}$$

$$\bar{K}_{22} = 0, \tag{231}$$

$$\bar{K}_{12} = 0, \tag{232}$$

and constrain the midsurface deformation with

$$\bar{\epsilon}_{11} = \frac{1}{2} \left(\left(\frac{r_1}{R_1} \right)^2 - 1 \right), \tag{233}$$

$$\bar{\epsilon}_{22} = 0, \tag{234}$$

$$\bar{\epsilon}_{12} = 0, \tag{235}$$

$$\bar{\kappa}_{11} = \frac{1}{r_1} \left(\frac{r_1}{R_1} \right)^2, \tag{236}$$

$$\bar{\kappa}_{22} = 0, \tag{237}$$

$$\bar{\kappa}_{12} = 0. \tag{238}$$

In representing the mutual dependence between $\bar{\kappa}_{11}$ and $\bar{\epsilon}_{11}$ based on the constraints above, we select the form $\bar{\kappa}_{11}$ being a function of $\bar{\epsilon}_{11}$. We solve for $\bar{\epsilon}_{11}$ together with the displacement in the out-of-plane direction, with the conditions $p_O^* = p^*$ and $p_I^* = 2p^*$ (see Remark 27 for the way the pressure conditions are specified).

Figures 29 and 30 show, for both the neo-Hookean and Fung’s materials, p^* as a function of $\bar{\lambda}_1$. We first compare Method 1 and Method 2. With Method 1, because p_O acts on the inner surface, the net force in the inflation direction is more. Consequently, in all cases, for a given p^* , Method 1 has higher $\bar{\lambda}_1$. Next we compare Method 2 and Method 3. For the neo-Hookean material, in all cases, for a given $\bar{\lambda}_1$, Method 2 has higher p^* , meaning that it is stiffer than Method 3. For the Fung’s material, we do not see that in all cases. When $\nu = 0.5$, Method 2 is stiffer for all values of $\bar{\lambda}_1$, but at lower ν values, beyond a high-enough $\bar{\lambda}_1$ value, Method 2 switches to being less stiff. We will discuss that more when we report the ξ_0^3 profiles.

Remark 28 It is clear from Figs. 29 and 30 that when $\nu = 0.5$, for both the neo-Hookean and Fung’s materials, there is no $\bar{\lambda}_1$ value that would make Method 2 less stiff. In other words, if the behavior is incompressible, Method 2, i.e. the $\sigma_{33} = 0$ model, is stiffer.

We report, for $\lambda_1 = 1.3$, ξ_0^3 profiles of λ_3 , J , σ_{11}^* , and σ_{33}^* . Figures 31, 32, 33 and 34 show those profiles for the neo-

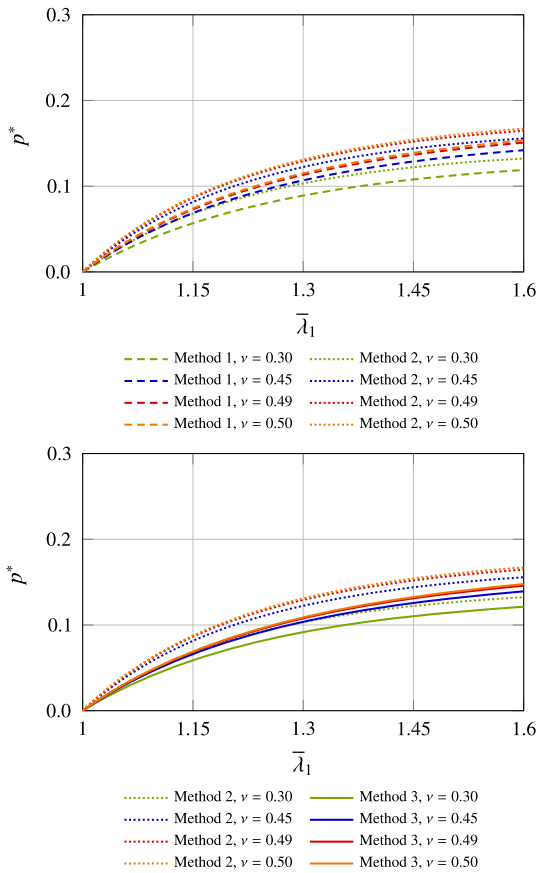


Fig. 29 Pressurized cylindrical shell. Neo-Hookean material. $\bar{\lambda}_1$ and p^* . Comparison between Method 1 and Method 2, and Method 2 and Method 3

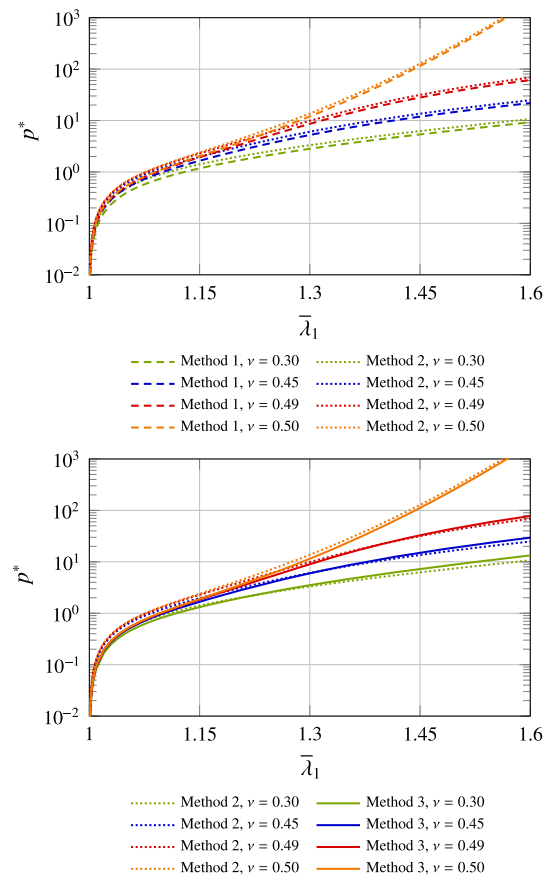


Fig. 30 Pressurized cylindrical shell. Fung's material. $\bar{\lambda}_1$ and p^* . Comparison between Method 1 and Method 2, and Method 2 and Method 3

Hookean material, and Figs. 35, 36, 37 and 38 for the Fung's material. Because the only difference between Method 1 and Method 2 is how the net force acting on the midsurface is calculated, when we look at the ξ_3^0 profiles coming from the two methods at a given $\bar{\lambda}_1$, meaning at the same midsurface deformation, we are already beyond how the net force acting on the midsurface was calculated. The midsurface deformations are the same, and therefore the ξ_3^0 profiles will be the same. For that reason, the ξ_3^0 profiles are reported under the labels " $\sigma_{33} = 0$ " and " $\sigma_{33} \neq 0$."

When $\nu = 0.5$, the deformation patterns obtained with the $\sigma_{33} = 0$ and $\sigma_{33} \neq 0$ models are the same (see Figs. 31, 32, 35, 36). This is expected because when $\nu = 0.5$, the constraint $J = 1$ determines the profile for a given midsurface deformation.

For the Neo-Hookean material, as can be seen in Fig. 33, the $\sigma_{33} = 0$ model yields higher σ_{11}^* values at all ν values and for the full range of ξ_0^3 . Remembering that these profiles are for a given value of λ_1 , higher σ_{11}^* means that $\sigma_{33} = 0$ model stiffer. This is consistent with the observation we made when we discussed Fig. 29.

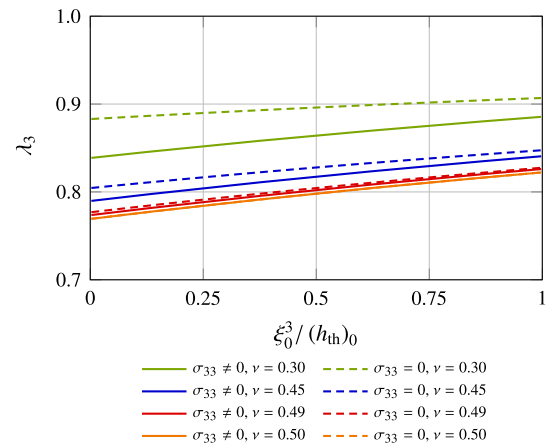


Fig. 31 Pressurized cylindrical shell. Neo-Hookean material. λ_3 profile

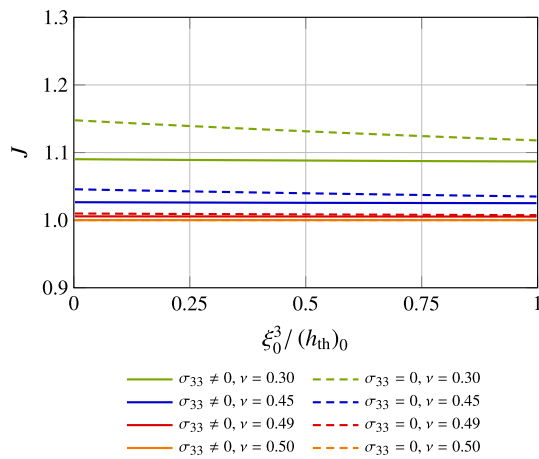


Fig. 32 Pressurized cylindrical shell. Neo-Hookean material. J profile

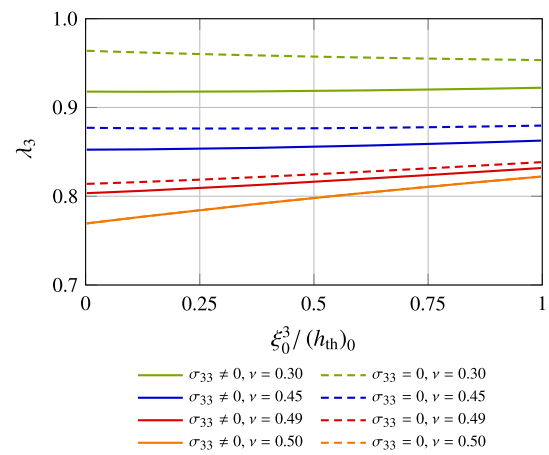


Fig. 35 Pressurized cylindrical shell. Fung's material. λ_3 profile

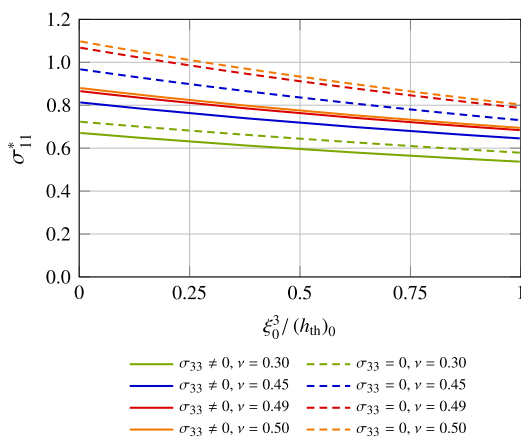


Fig. 33 Pressurized cylindrical shell. Neo-Hookean material. σ_{11}^* profile

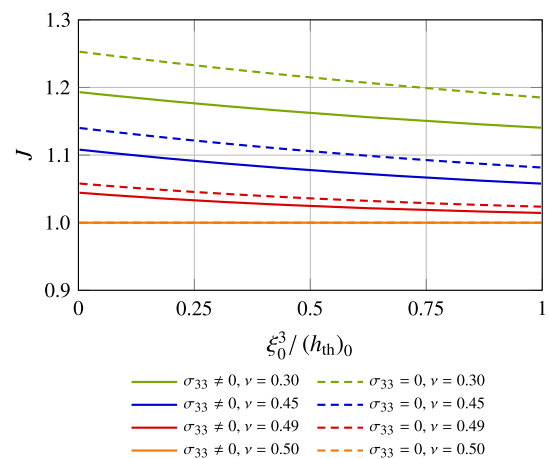


Fig. 36 Pressurized cylindrical shell. Fung's material. J profile

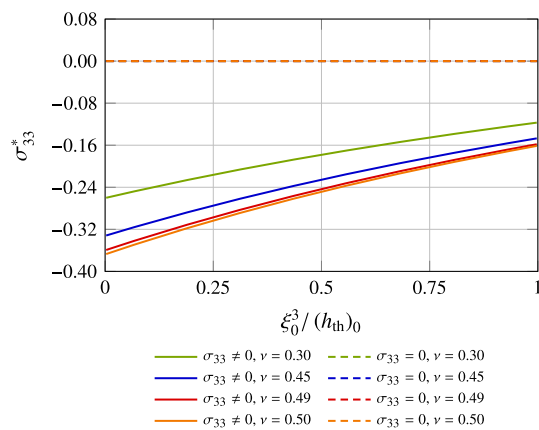


Fig. 34 Pressurized cylindrical shell. Neo-Hookean material. σ_{33}^* profile

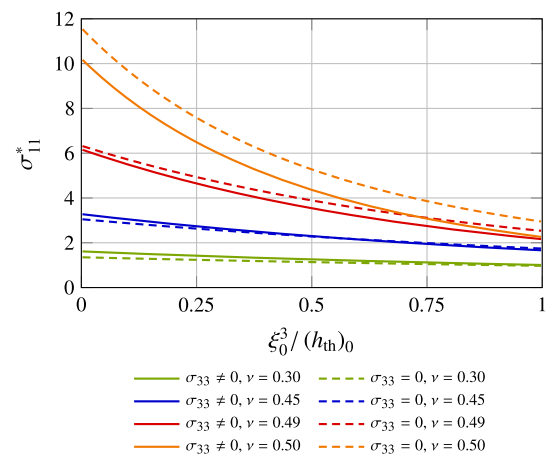


Fig. 37 Pressurized cylindrical shell. Fung's material. σ_{11}^* profile

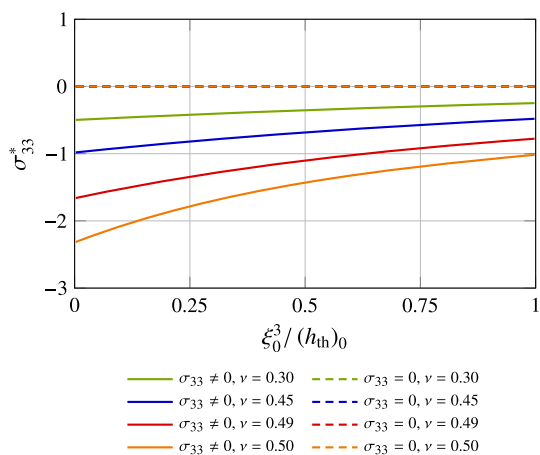


Fig. 38 Pressurized cylindrical shell. Fung’s material. σ_{33}^* profile

For the Fung’s material, we do not see that in Fig. 37 at all ν values. Consistent with the observation we made when we discussed Fig. 30, when $\nu = 0.5$, the $\sigma_{33} = 0$ model yields higher σ_{11}^* values, and therefore is stiffer, for the full range of range of ξ_0^3 . For this specific value of $\bar{\lambda}_1$ we are reporting the ξ_0^3 profiles, the $\sigma_{33} = 0$ model is also stiffer when $\nu = 0.49$ and for the full range of ξ_0^3 . At lower ν values, however, the $\sigma_{33} = 0$ model does not yield higher σ_{11}^* values for the full range of ξ_0^3 , and at even lower ν values, it yields lower σ_{11}^* values for the full range of ξ_0^3 , and therefore is less stiff than the $\sigma_{33} \neq 0$ model. This can be explained by the shifting balance between the bulk and shear moduli as $\bar{\lambda}_1$ varies. At ν values not far from 0.5, when $\bar{\lambda}_1$ is not so high, the bulk modulus is dominant, the material behavior is closer to being incompressible, and therefore, from Remark 28, the $\sigma_{33} = 0$ model is stiffer. However, even at ν values not far from 0.5, due to the exponential form of the constitutive model, when $\bar{\lambda}_1$ is high enough, the shear modulus is dominant and not the bulk modulus, the material behavior is not close enough to being incompressible, and therefore the $\sigma_{33} = 0$ model is less stiff.

5.3.2 Pressurized spherical shell

We select the undeformed configuration as

$$\bar{G}_{11} = 1, \tag{239}$$

$$\bar{G}_{22} = 1, \tag{240}$$

$$\bar{G}_{12} = 0, \tag{241}$$

$$\bar{K}_{11} = \frac{1}{R_1}, \tag{242}$$

$$\bar{K}_{22} = \frac{1}{R_1}, \tag{243}$$

$$\bar{K}_{12} = 0, \tag{244}$$

and constrain the midsurface deformation with

$$\bar{\epsilon}_{11} = \frac{1}{2} \left(\left(\frac{r_1}{R_1} \right)^2 - 1 \right), \tag{245}$$

$$\bar{\epsilon}_{22} = \frac{1}{2} \left(\left(\frac{r_1}{R_1} \right)^2 - 1 \right), \tag{246}$$

$$\bar{\epsilon}_{12} = 0, \tag{247}$$

$$\bar{\kappa}_{11} = \frac{1}{r_1} \left(\frac{r_1}{R_1} \right)^2, \tag{248}$$

$$\bar{\kappa}_{22} = \frac{1}{r_1} \left(\frac{r_1}{R_1} \right)^2, \tag{249}$$

$$\bar{\kappa}_{12} = 0. \tag{250}$$

In representing the mutual dependence between $\bar{\kappa}_{11}$, $\bar{\kappa}_{22}$, $\bar{\epsilon}_{22}$, and $\bar{\epsilon}_{11}$ based on the constraints above, we select the form $\bar{\kappa}_{11}$, $\bar{\kappa}_{22}$, and $\bar{\epsilon}_{22}$ being functions of $\bar{\epsilon}_{11}$. We solve for $\bar{\epsilon}_{11}$ together with the displacement in the out-of-plane direction, with the conditions $p_0^* = p^*$ and $p_1^* = 2p^*$. Figures 39 and 40 show, for both the neo-Hookean and Fung’s materials, p^* as a function of $\bar{\lambda}_1$. Our observations are essentially the same as those we made for the cylindrical shell, except the differences are more pronounced, because, with the same radius, the sphere has overall higher curvature effects.

We report, for $\lambda_1 = 1.3$, ξ_0^3 profiles of λ_3 , J , σ_{11}^* , and σ_{33}^* . Figures 41, 42, 43 and 44 show those profiles for the neo-Hookean material, Figs. 45, 46, 47 and 48 for the Fung’s material. We again note that the ξ_0^3 profiles coming from Method 1 and Method 2 at a given $\bar{\lambda}_1$ will be the same and therefore the ξ_0^3 profiles are again reported under the labels “ $\sigma_{33} = 0$ ” and “ $\sigma_{33} \neq 0$.” We note in Fig. 47 that, although it is not all discernible, except for the full range of $\xi_0^3 / (h_{th})_0$ when $\nu = 0.5$ and for $\xi_0^3 / (h_{th})_0 > 0.5$ when $\nu = 0.49$, the $\sigma_{33} = 0$ model yields lower σ_{11}^* values and therefore is less stiff than the $\sigma_{33} \neq 0$ model. The substance of the observations we made for the cylindrical shell remains applicable.

6 Concluding remarks

This was the first part of a two-part article on a hyperelastic extended Kirchhoff–Love shell model with out-of-plane normal stress. We have presented the derivation of the new model, with focus on the mechanics of the out-of-plane deformation. To determine the out-of-plane stress, we solve the linear-momentum-balance equation in the out-of-plane direction. Accounting for the out-of-plane normal stress distribution in the out-of-plane direction affects the accuracy in calculating the deformed-configuration out-of-plane position, and consequently the nonlinear response of the shell. The improvement is beyond what was achieved with the

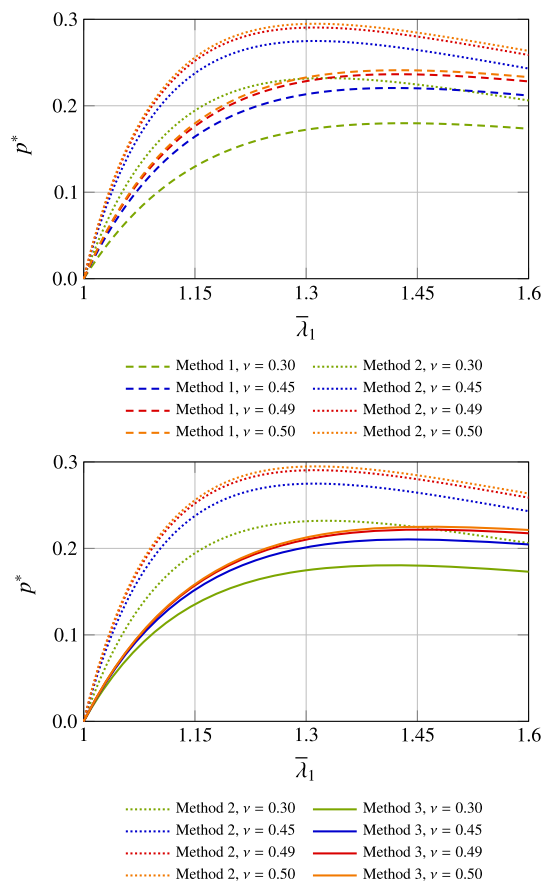


Fig. 39 Pressurized spherical shell. Neo-Hookean material. $\bar{\lambda}_1$ and p^* . Comparison between Method 1 and Method 2, and Method 2 and Method 3

new model’s precursor [5] by accounting for the out-of-plane deformation mapping. Continuing what was started with the precursor, the new model is extending the range of applicability of the Kirchhoff–Love shell theory to the situations where the Kirchhoff–Love shell kinematics is still valid yet the thickness or the curvature change is significant enough to make a difference in the response.

By accounting for the out-of-plane normal stress, the traction acting on the shell can be specified on the upper and lower surfaces separately. This enables more accuracy in the linear-momentum balance in the out-of-plane direction. For example, we can accurately model cases that might have nonzero net force even when those out-of-plane tractions have equal magnitudes and opposite directions. Accounting for the out-of-plane normal stress also enables more accuracy in representation of the moment the shear tractions on the upper and lower surfaces generate around the midsurface. To accurately account for the moment generated by the separate shear tractions on the upper and lower surfaces, we have also improved the rotational kinematics in the model. Accounting for the out-of-plane stress improves the out-of-plane deformation mapping also in cases with no traction on

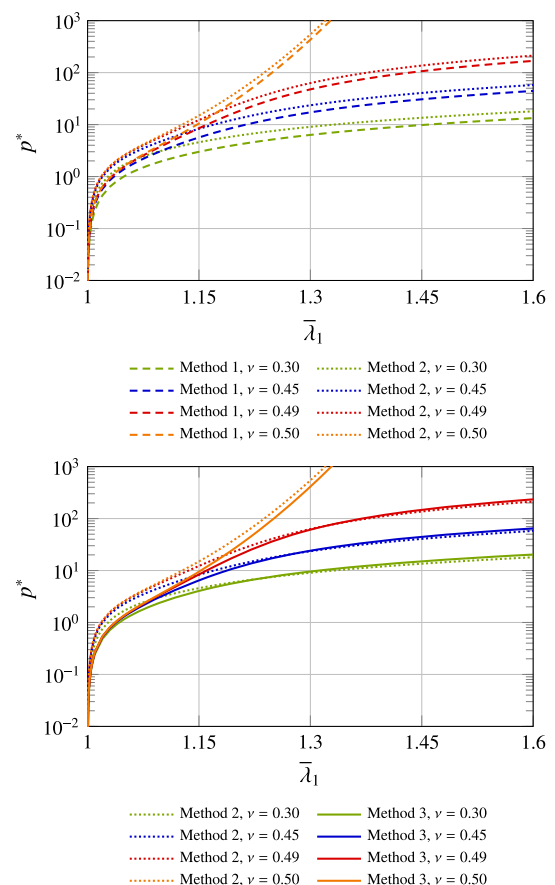


Fig. 40 Pressurized spherical shell. Fung’s material. $\bar{\lambda}_1$ and p^* . Comparison between Method 1 and Method 2, and Method 2 and Method 3

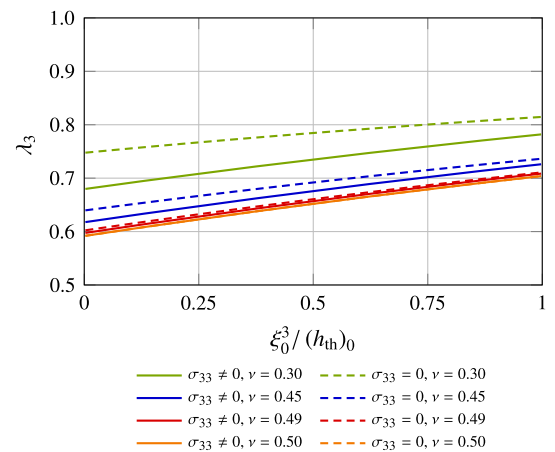


Fig. 41 Pressurized spherical shell. Neo-Hookean material. λ_3 profile

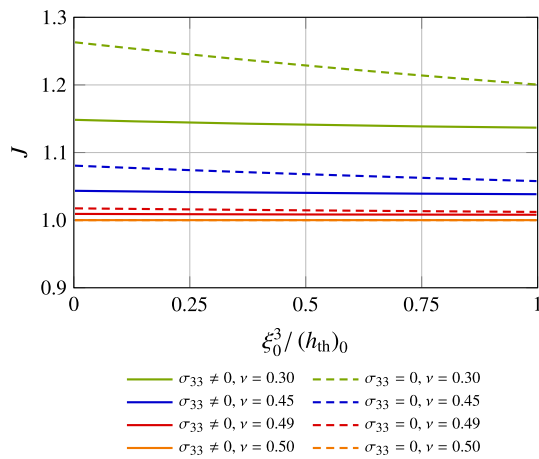


Fig. 42 Pressurized spherical shell. Neo-Hookean material. J profile

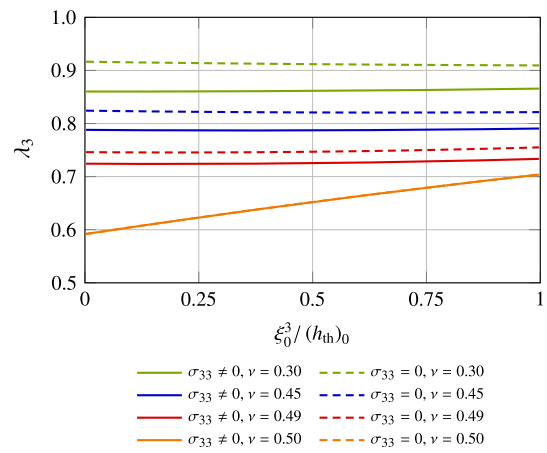


Fig. 45 Pressurized spherical shell. Fung's material. λ_3 profile

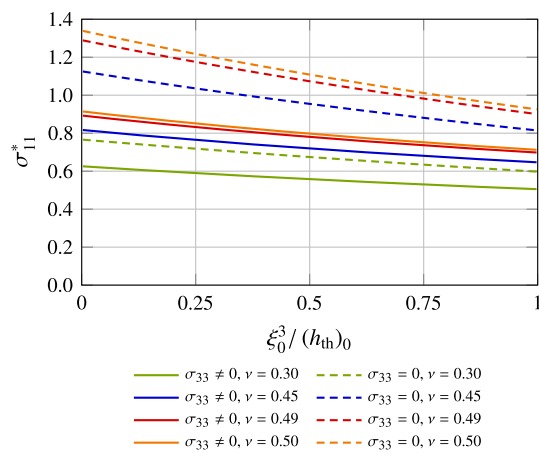


Fig. 43 Pressurized spherical shell. Neo-Hookean material. σ_{11}^* profile

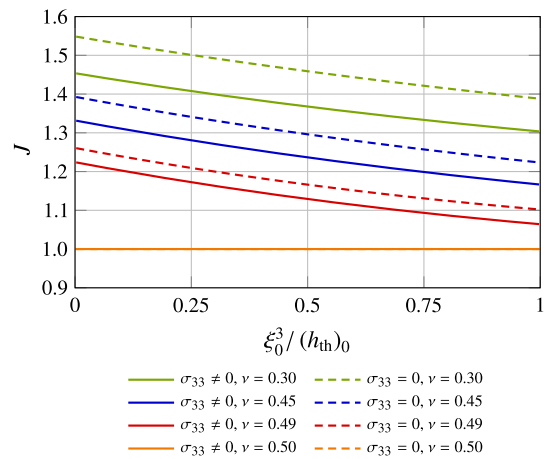


Fig. 46 Pressurized spherical shell. Fung's material. J profile

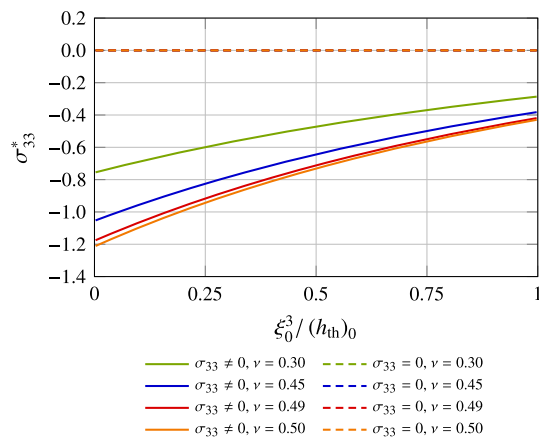


Fig. 44 Pressurized spherical shell. Neo-Hookean material. σ_{33}^* profile

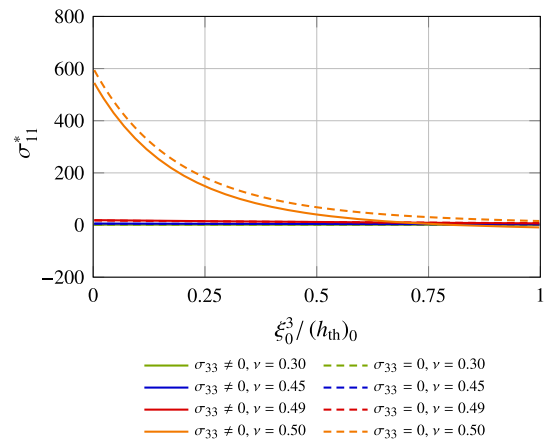


Fig. 47 Pressurized spherical shell. Fung's material. σ_{11}^* profile

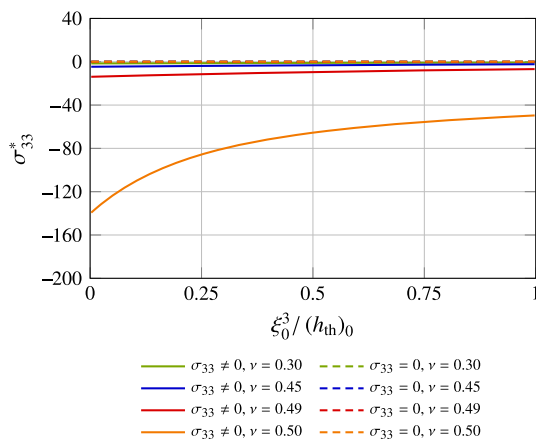


Fig. 48 Pressurized spherical shell. Fung’s material. σ_{33}^* profile

the upper or lower surfaces and no body force. Those would be the cases when the shell deformation is driven by the displacements and slopes specified along the shell edges.

We presented test computations for unidirectional plate bending, plate saddle deformation, and pressurized cylindrical and spherical shells. We tested the neo-Hookean and Fung’s material models, for the compressible and incompressible materials, and with the out-of-plane normal stress and without, which is the plane-stress case. The test computations show that the differences between the shell models with and without the out-of-plane normal stress are more pronounced i) for plate saddle deformation than unidirectional plate bending, ii) when we have higher curvature effects, and iii) for cylindrical or spherical shells at high ν values. We leave it to the reader to judge how significant these differences are.

The level of accuracy we are striving for in representing the tractions on the upper and lower surfaces would be meaningful in an FSI computation only if the flow solution method can deliver those tractions with a comparable level of accuracy. That level of flow solution accuracy, especially in representing the shear stress, requires moving-mesh methods, where the high mesh resolution near solid surfaces follows the fluid–solid interface as it moves. That is now possible even in flow computations with actual contact between solid surfaces or some other topology change. The space–time computational methods introduced in the last decade enable that, as can be seen, for example, in [43,44].

Acknowledgements This work was supported in part by JST-CREST; Grant-in-Aid for Scientific Research (A) 18H04100 from Japan Society for the Promotion of Science; and Rice–Waseda research agreement and International Technology Center Indo-Pacific (ITC IPAC) Contract FA520921C0010. This work was also supported (first author) in part by Pioneering Research Program for a Waseda Open Innovation Ecosystem (W-SPRING). The mathematical model and computational method parts of the work were also supported (fourth author) in part

by ARO Grant W911NF-17-1-0046, Contract W911NF-21-C-0030 and Top Global University Project of Waseda University.

Open Access This article is licensed under a Creative Commons Attribution 4.0 International License, which permits use, sharing, adaptation, distribution and reproduction in any medium or format, as long as you give appropriate credit to the original author(s) and the source, provide a link to the Creative Commons licence, and indicate if changes were made. The images or other third party material in this article are included in the article’s Creative Commons licence, unless indicated otherwise in a credit line to the material. If material is not included in the article’s Creative Commons licence and your intended use is not permitted by statutory regulation or exceeds the permitted use, you will need to obtain permission directly from the copyright holder. To view a copy of this licence, visit <http://creativecommons.org/licenses/by/4.0/>.

A Dual basis system

The description given here for the relationship between a basis system and its dual is applicable to all the basis systems we work with, where we use the symbols $g, \bar{g}, G,$ and \bar{G} .

For the covariant basis vectors \mathbf{g}_α , the components of the metric tensor are

$$g_{\alpha\beta} = \mathbf{g}_\alpha \cdot \mathbf{g}_\beta. \tag{251}$$

We define the contravariant basis vectors as

$$\mathbf{g}^\alpha \cdot \mathbf{g}_\beta = \delta_\beta^\alpha. \tag{252}$$

This implies

$$\mathbf{g}^\alpha = [g_{\alpha\beta}]^{-1} \mathbf{g}_\beta, \tag{253}$$

where the brackets denote the matrix formed from its components, and the contravariant components of the metric tensor are given as

$$[g^{\alpha\beta}] = [g_{\alpha\beta}]^{-1}. \tag{254}$$

We note that, with $n_{sd} = 3$ and $n_{pd} = 2$, one of the ways to express the unit tensor is

$$\mathbf{I} = \mathbf{g}_\alpha \mathbf{g}^\alpha + \mathbf{nn}, \tag{255}$$

where

$$\mathbf{n} = \frac{\mathbf{g}_1 \times \mathbf{g}_2}{\|\mathbf{g}_1 \times \mathbf{g}_2\|}. \tag{256}$$

B Derivative and variation of the normal vector in the shell model

B.1 Derivative of the normal vector

Derivative of the normal vector with respect to ξ^α can be obtained as follows:

$$\bar{\mathbf{n}}_{,\alpha} = \frac{\partial}{\partial \xi^\alpha} \left(\frac{\bar{\mathbf{g}}_1 \times \bar{\mathbf{g}}_2}{(\bar{\mathbf{g}}_1 \times \bar{\mathbf{g}}_2) \cdot \bar{\mathbf{n}}} \right) \tag{257}$$

$$= (\mathbf{I} - \bar{\mathbf{n}}\bar{\mathbf{n}}) \cdot \frac{\bar{\mathbf{g}}_{1,\alpha} \times \bar{\mathbf{g}}_2 + \bar{\mathbf{g}}_1 \times \bar{\mathbf{g}}_{2,\alpha}}{(\bar{\mathbf{g}}_1 \times \bar{\mathbf{g}}_2) \cdot \bar{\mathbf{n}}} \tag{258}$$

$$= (\mathbf{I} - \bar{\mathbf{n}}\bar{\mathbf{n}}) \cdot \frac{\bar{\mathbf{g}}_{1,\alpha} \times (\bar{\mathbf{n}} \times \bar{\mathbf{g}}^1) + \bar{\mathbf{g}}_{2,\alpha} \times (\bar{\mathbf{n}} \times \bar{\mathbf{g}}^2)}{(\bar{\mathbf{g}}^1 \times \bar{\mathbf{g}}^2) \cdot \bar{\mathbf{n}}(\bar{\mathbf{g}}_1 \times \bar{\mathbf{g}}_2) \cdot \bar{\mathbf{n}}} \tag{259}$$

$$= (\mathbf{I} - \bar{\mathbf{n}}\bar{\mathbf{n}}) \cdot (\bar{\mathbf{g}}_{\beta,\alpha} \times (\bar{\mathbf{n}} \times \bar{\mathbf{g}}^\beta)) \tag{260}$$

$$= (\mathbf{I} - \bar{\mathbf{n}}\bar{\mathbf{n}}) \cdot ((\bar{\mathbf{g}}_{\beta,\alpha} \cdot \bar{\mathbf{g}}^\beta) \bar{\mathbf{n}} - (\bar{\mathbf{g}}_{\beta,\alpha} \cdot \bar{\mathbf{n}}) \bar{\mathbf{g}}^\beta) \tag{261}$$

$$= -(\bar{\mathbf{g}}_{\beta,\alpha} \cdot \bar{\mathbf{n}}) \underbrace{\bar{\mathbf{g}}^\beta + \bar{\mathbf{n}}(\bar{\mathbf{n}} \cdot \bar{\mathbf{g}}^\beta)}_{=0} (\bar{\mathbf{g}}_{\beta,\alpha} \cdot \bar{\mathbf{n}}) \tag{262}$$

$$= -\bar{\mathbf{g}}^\beta \bar{\mathbf{g}}_{\beta,\alpha} \cdot \bar{\mathbf{n}} \tag{263}$$

$$= \bar{\mathbf{g}}^\beta \bar{\kappa}_{\alpha\beta} \tag{264}$$

$$= \bar{\boldsymbol{\kappa}} \cdot \bar{\mathbf{g}}_\alpha \tag{265}$$

We note that $\bar{\kappa}_{\alpha\beta}$ is equal to the second fundamental form with a negative sign. In the derivation, we used the following relationships, which generally hold:

$$\mathbf{g}_1 = \frac{\mathbf{g}^2 \times \mathbf{g}^3}{(\mathbf{g}^1 \times \mathbf{g}^2) \cdot \mathbf{g}^3}, \tag{266}$$

$$\mathbf{g}_2 = \frac{\mathbf{g}^3 \times \mathbf{g}^1}{(\mathbf{g}^1 \times \mathbf{g}^2) \cdot \mathbf{g}^3}, \tag{267}$$

$$(\mathbf{g}^1 \times \mathbf{g}^2) \cdot \mathbf{g}^3 = ((\mathbf{g}_1 \times \mathbf{g}_2) \cdot \mathbf{g}_3)^{-1}. \tag{268}$$

B.2 Variation of the normal vector

From the steps given by Eqs. (257)–(263), the variation of the normal vector can be written as

$$\delta \bar{\mathbf{n}} = -\bar{\mathbf{g}}^\beta \delta \bar{\mathbf{g}}_\beta \cdot \bar{\mathbf{n}}. \tag{269}$$

B.3 Rearrangement of the form $\delta \bar{\mathbf{n}} \cdot \mathbf{h}$

From Eq. (269), we write

$$\delta \bar{\mathbf{n}} \cdot \mathbf{h} = -\bar{\mathbf{g}}^\beta \cdot \mathbf{h} \delta \bar{\mathbf{g}}_\beta \cdot \bar{\mathbf{n}}. \tag{270}$$

We recall the Lagrange’s identity

$$(\mathbf{a} \times \mathbf{b}) \cdot (\mathbf{c} \times \mathbf{d}) = \mathbf{a} \cdot \mathbf{c} \mathbf{b} \cdot \mathbf{d} - \mathbf{a} \cdot \mathbf{d} \mathbf{b} \cdot \mathbf{c}. \tag{271}$$

With that, we obtain

$$(\bar{\mathbf{g}}^\beta \times \delta \bar{\mathbf{g}}_\beta) \cdot (\bar{\mathbf{n}} \times \mathbf{h}) = \underbrace{\bar{\mathbf{g}}^\beta \cdot \bar{\mathbf{n}}}_{=0} \delta \bar{\mathbf{g}}_\beta \cdot \mathbf{h} - \bar{\mathbf{g}}^\beta \cdot \mathbf{h} \delta \bar{\mathbf{g}}_\beta \cdot \bar{\mathbf{n}} \tag{272}$$

$$= -\bar{\mathbf{g}}^\beta \cdot \mathbf{h} \delta \bar{\mathbf{g}}_\beta \cdot \bar{\mathbf{n}}. \tag{273}$$

For notational convenience, we introduce

$$\delta \bar{\mathbf{r}} \equiv \bar{\mathbf{g}}^\beta \times \delta \bar{\mathbf{g}}_\beta, \tag{274}$$

and

$$\delta \bar{\mathbf{n}} \cdot \mathbf{h} = \delta \bar{\mathbf{r}} \cdot (\bar{\mathbf{n}} \times \mathbf{h}). \tag{275}$$

C Integration with variation of the normal vector

C.1 Dual basis system for the midsurface edges

We have a set of orthonormal basis vectors: $\bar{\mathbf{B}}$, $\bar{\mathbf{T}}$, and $\bar{\mathbf{N}}$. After the deformation:

$$\bar{\lambda}_B \bar{\mathbf{b}} = \bar{\mathbf{F}} \cdot \bar{\mathbf{B}}, \tag{276}$$

$$\bar{\lambda}_T \bar{\mathbf{t}} = \bar{\mathbf{F}} \cdot \bar{\mathbf{T}}, \tag{277}$$

$$\bar{\lambda}_3 \bar{\mathbf{n}} = \bar{\mathbf{F}} \cdot \bar{\mathbf{N}}. \tag{278}$$

Here the unit vectors $\bar{\mathbf{b}}$ and $\bar{\mathbf{t}}$ may not be orthogonal. To overcome the difficulty of using a set of non-orthogonal basis vectors, we introduced in Remark 17

$$\bar{\mathbf{t}}^\star = \frac{\bar{\mathbf{n}} \times \bar{\mathbf{b}}}{(\bar{\mathbf{b}} \times \bar{\mathbf{t}}) \cdot \bar{\mathbf{n}}}, \tag{279}$$

$$\bar{\mathbf{b}}^\star = \frac{\bar{\mathbf{t}} \times \bar{\mathbf{n}}}{(\bar{\mathbf{b}} \times \bar{\mathbf{t}}) \cdot \bar{\mathbf{n}}}. \tag{280}$$

We repeat them here from Eqs. (138) and (139) for the reader’s convenience. The denominator, a triple scalar product, represents the volume of the parallelepiped based on the three vectors. With that, the counterparts of Eq. (252) can be written as

$$\bar{\mathbf{t}}^\star \cdot \bar{\mathbf{t}} = 1, \tag{281}$$

$$\bar{\mathbf{t}}^\star \cdot \bar{\mathbf{b}} = 0, \tag{282}$$

$$\bar{\mathbf{b}}^\star \cdot \bar{\mathbf{t}} = 0, \tag{283}$$

$$\bar{\mathbf{b}}^\star \cdot \bar{\mathbf{b}} = 1. \tag{284}$$

The counterpart of Eq. (255) is

$$\mathbf{I} = \bar{\mathbf{b}} \bar{\mathbf{b}}^\star + \bar{\mathbf{t}} \bar{\mathbf{t}}^\star + \bar{\mathbf{n}} \bar{\mathbf{n}}. \tag{285}$$

With the set of basis vectors and stretches, we can express the deformation gradient tensor and its inverse. The deformation gradient tensor can be expressed as

$$\bar{\mathbf{F}} = \bar{\lambda}_B \bar{\mathbf{b}} \bar{\mathbf{B}} + \bar{\lambda}_T \bar{\mathbf{t}} \bar{\mathbf{T}} + \bar{\lambda}_3 \bar{\mathbf{n}} \bar{\mathbf{N}}. \tag{286}$$

The inverse of $\bar{\mathbf{F}}$ can be written as

$$\bar{\mathbf{F}}^{-1} = \frac{1}{\bar{\lambda}_B} \bar{\mathbf{B}} \bar{\mathbf{b}}^* + \frac{1}{\bar{\lambda}_T} \bar{\mathbf{T}} \bar{\mathbf{t}}^* + \frac{1}{\bar{\lambda}_3} \bar{\mathbf{N}} \bar{\mathbf{n}}, \tag{287}$$

and we have two alternative ways of verifying that. We can show that

$$\bar{\mathbf{F}} \cdot \bar{\mathbf{F}}^{-1} = \mathbf{I} \tag{288}$$

by remembering that $\bar{\mathbf{B}}, \bar{\mathbf{T}},$ and $\bar{\mathbf{N}}$ are orthonormal and using Eq. (285), or show that

$$\bar{\mathbf{F}}^{-1} \cdot \bar{\mathbf{F}} = \mathbf{I} \tag{289}$$

by using Eqs. (281), (282), (283) and (284) and remembering that $\mathbf{I} = \bar{\mathbf{B}} \bar{\mathbf{B}} + \bar{\mathbf{T}} \bar{\mathbf{T}} + \bar{\mathbf{N}} \bar{\mathbf{N}}$. By excluding the normal-direction terms in Eqs. (286) and (287), we obtain

$$\bar{\mathbf{g}}_\alpha \bar{\mathbf{G}}^\alpha = \bar{\lambda}_B \bar{\mathbf{b}} \bar{\mathbf{B}} + \bar{\lambda}_T \bar{\mathbf{t}} \bar{\mathbf{T}}, \tag{290}$$

$$\bar{\mathbf{G}}_\alpha \bar{\mathbf{g}}^\alpha = \frac{1}{\bar{\lambda}_B} \bar{\mathbf{B}} \bar{\mathbf{b}}^* + \frac{1}{\bar{\lambda}_T} \bar{\mathbf{T}} \bar{\mathbf{t}}^*. \tag{291}$$

Depending on the context, we use either the left- or right-hand side of Eqs. (290) and (291).

We can write \mathbf{C} at the midsurface as

$$\bar{\mathbf{C}} = (\bar{\lambda}_B \bar{\mathbf{B}} \bar{\mathbf{b}} + \bar{\lambda}_T \bar{\mathbf{T}} \bar{\mathbf{t}} + \bar{\lambda}_3 \bar{\mathbf{N}} \bar{\mathbf{n}}) \cdot (\bar{\lambda}_B \bar{\mathbf{b}} \bar{\mathbf{B}} + \bar{\lambda}_T \bar{\mathbf{t}} \bar{\mathbf{T}} + \bar{\lambda}_3 \bar{\mathbf{n}} \bar{\mathbf{N}}) \tag{292}$$

$$= \bar{\lambda}_B^2 \bar{\mathbf{B}} \bar{\mathbf{B}} + \bar{\lambda}_T^2 \bar{\mathbf{T}} \bar{\mathbf{T}} + \bar{\lambda}_3^2 \bar{\mathbf{N}} \bar{\mathbf{N}} + \bar{\lambda}_B \bar{\lambda}_T (\bar{\mathbf{t}} \cdot \bar{\mathbf{b}}) (\bar{\mathbf{B}} \bar{\mathbf{T}} + \bar{\mathbf{T}} \bar{\mathbf{B}}), \tag{293}$$

and its determinant as

$$\bar{J}^2 = \bar{\lambda}_B^2 \bar{\lambda}_T^2 \bar{\lambda}_3^2 (1 - (\bar{\mathbf{t}} \cdot \bar{\mathbf{b}})^2) \tag{294}$$

$$= \bar{\lambda}_B^2 \bar{\lambda}_T^2 \bar{\lambda}_3^2 ((\bar{\mathbf{b}} \times \bar{\mathbf{t}}) \cdot \bar{\mathbf{n}})^2, \tag{295}$$

where $\bar{J} = \det \bar{\mathbf{F}}$. Because $(\bar{\mathbf{b}} \times \bar{\mathbf{t}}) \cdot \bar{\mathbf{n}} > 0$, we get

$$(\bar{\mathbf{b}} \times \bar{\mathbf{t}}) \cdot \bar{\mathbf{n}} = \frac{\bar{J}}{\bar{\lambda}_B \bar{\lambda}_T \bar{\lambda}_3} = \frac{\bar{A}}{\bar{\lambda}_B \bar{\lambda}_T \bar{A}_0} = \frac{\bar{A}/\bar{L}}{\bar{A}_0/\bar{L}_0} \frac{1}{\bar{\lambda}_B}. \tag{296}$$

We note that, in Eq. (296), the second and third equalities are based on Eqs. (38) and (131), respectively. Thus, Eqs. (279)

and (280) can be expressed as

$$\bar{\mathbf{t}}^* = \bar{\mathbf{n}} \times \bar{\mathbf{b}} \frac{\bar{\lambda}_3 \bar{\lambda}_B \bar{\lambda}_T}{\bar{J}}, \tag{297}$$

$$\bar{\mathbf{b}}^* = \bar{\mathbf{t}} \times \bar{\mathbf{n}} \frac{\bar{\lambda}_3 \bar{\lambda}_B \bar{\lambda}_T}{\bar{J}}. \tag{298}$$

C.2 Integration over the midsurface

We first rearrange the variation of the normal vector from Eq. (269):

$$\delta \bar{\mathbf{n}} = -\delta \bar{\mathbf{g}}_\gamma \cdot \bar{\mathbf{n}} \delta_\beta^\gamma \bar{\mathbf{g}}^\beta \tag{299}$$

$$= -\delta \bar{\mathbf{g}}_\gamma \cdot \bar{\mathbf{n}} \bar{\mathbf{G}}^\gamma \cdot \bar{\mathbf{G}}_\beta \bar{\mathbf{g}}^\beta. \tag{300}$$

From that, for any vector \mathbf{q} , we have

$$\int_{\bar{\Gamma}_0} \delta \bar{\mathbf{n}} \cdot \mathbf{q} d\Gamma = - \int_{\bar{\Gamma}_0} \bar{\mathbf{G}}^\gamma \cdot (\delta \bar{\mathbf{g}}_\gamma \cdot \bar{\mathbf{n}} \bar{\mathbf{G}}_\beta \bar{\mathbf{g}}^\beta \cdot \mathbf{q}) d\Gamma \tag{301}$$

$$= - \int_{\bar{\Gamma}_0} \bar{\mathbf{G}}^\gamma \cdot (\delta \bar{\mathbf{x}}_{,\gamma} \cdot \bar{\mathbf{n}} \bar{\mathbf{G}}_\beta \bar{\mathbf{g}}^\beta \cdot \mathbf{q}) d\Gamma. \tag{302}$$

We integrate the right-hand side of Eq. (302) by parts and obtain

$$\int_{\bar{\Gamma}_0} \delta \bar{\mathbf{n}} \cdot \mathbf{q} d\Gamma = - \int_{\bar{S}_0} \delta \bar{\mathbf{x}} \cdot \bar{\mathbf{n}} \mathbf{q} \cdot \bar{\mathbf{g}}^\beta \bar{\mathbf{G}}_\beta \cdot \bar{\mathbf{B}} dS + \int_{\bar{\Gamma}_0} \delta \bar{\mathbf{x}} \cdot (\bar{\mathbf{n}} \bar{\mathbf{G}}_\beta \bar{\mathbf{g}}^\beta \cdot \mathbf{q})_{,\gamma} \cdot \bar{\mathbf{G}}^\gamma d\Gamma. \tag{303}$$

The last integral of the above equation can further be arranged by using the product rule as

$$\int_{\bar{\Gamma}_0} \delta \bar{\mathbf{x}} \cdot (\bar{\mathbf{n}} \bar{\mathbf{G}}_\beta \bar{\mathbf{g}}^\beta \cdot \mathbf{q})_{,\gamma} \cdot \bar{\mathbf{G}}^\gamma d\Gamma = \int_{\bar{\Gamma}_0} \delta \bar{\mathbf{x}} \cdot \bar{\mathbf{n}}_{,\gamma} \bar{\mathbf{g}}^\gamma \cdot \mathbf{q} d\Gamma + \int_{\bar{\Gamma}_0} \delta \bar{\mathbf{x}} \cdot \bar{\mathbf{n}} (\mathbf{q} \cdot \bar{\mathbf{g}}^\beta \bar{\mathbf{G}}_\beta)_{,\gamma} \cdot \bar{\mathbf{G}}^\gamma d\Gamma. \tag{304}$$

Substituting Eq. (265) into this, we obtain

$$\int_{\bar{\Gamma}_0} \delta \bar{\mathbf{x}} \cdot (\bar{\mathbf{n}} \bar{\mathbf{G}}_\beta \bar{\mathbf{g}}^\beta \cdot \mathbf{q})_{,\gamma} \cdot \bar{\mathbf{G}}^\gamma d\Gamma = \int_{\bar{\Gamma}_0} \delta \bar{\mathbf{x}} \cdot \bar{\boldsymbol{\kappa}} \cdot \mathbf{q} d\Gamma + \int_{\bar{\Gamma}_0} \delta \bar{\mathbf{x}} \cdot \bar{\mathbf{n}} (\mathbf{q} \cdot \bar{\mathbf{g}}^\beta \bar{\mathbf{G}}_\beta)_{,\gamma} \cdot \bar{\mathbf{G}}^\gamma d\Gamma. \tag{305}$$

Combining Eqs. (303) and (305) and recognizing the left-hand side of Eq. (291) in the integral over \bar{S}_0 , we obtain

$$\int_{\bar{\Gamma}_0} \delta \bar{\mathbf{n}} \cdot \mathbf{q} d\Gamma = - \int_{\bar{S}_0} \delta \bar{\mathbf{x}} \cdot \bar{\mathbf{n}} \frac{1}{\bar{\lambda}_B} \bar{\mathbf{b}}^* \cdot \mathbf{q} dS + \int_{\bar{\Gamma}_0} \delta \bar{\mathbf{x}} \cdot \bar{\boldsymbol{\kappa}} \cdot \mathbf{q} d\Gamma$$

$$+ \int_{\bar{\Gamma}_0} \delta \bar{\mathbf{x}} \cdot \bar{\mathbf{n}} (\mathbf{q} \cdot \bar{\mathbf{g}}^\beta \bar{\mathbf{G}}_\beta)_{,\gamma} \cdot \bar{\mathbf{G}}^\gamma d\Gamma. \tag{306}$$

C.3 Integration over the midsurface edges

From Eq. (300), we get

$$\delta \bar{\mathbf{n}} = -\delta \bar{\mathbf{g}}_\gamma \cdot \bar{\mathbf{n}} \bar{\mathbf{G}}^\gamma \cdot \underbrace{(\bar{\mathbf{N}}\bar{\mathbf{N}} + \bar{\mathbf{T}}\bar{\mathbf{T}} + \bar{\mathbf{B}}\bar{\mathbf{B}})}_{=\mathbf{I}} \cdot \bar{\mathbf{G}}_\beta \bar{\mathbf{g}}^\beta. \tag{307}$$

Because of the orthogonality of $\bar{\mathbf{G}}_\beta$ and $\bar{\mathbf{N}}$, we obtain

$$\delta \bar{\mathbf{n}} = -\delta \bar{\mathbf{g}}_\gamma \cdot \bar{\mathbf{n}} \bar{\mathbf{G}}^\gamma \cdot (\bar{\mathbf{T}}\bar{\mathbf{T}} + \bar{\mathbf{B}}\bar{\mathbf{B}}) \cdot \bar{\mathbf{G}}_\beta \bar{\mathbf{g}}^\beta \tag{308}$$

$$= -\delta \bar{\mathbf{g}}_\gamma \cdot \bar{\mathbf{n}} \bar{\mathbf{G}}^\gamma \cdot \bar{\mathbf{T}}\bar{\mathbf{T}} \cdot \bar{\mathbf{G}}_\beta \bar{\mathbf{g}}^\beta - \delta \bar{\mathbf{g}}_\gamma \cdot \bar{\mathbf{n}} \bar{\mathbf{G}}^\gamma \cdot \bar{\mathbf{B}}\bar{\mathbf{B}} \cdot \bar{\mathbf{G}}_\beta \bar{\mathbf{g}}^\beta. \tag{309}$$

Taking the inner product of $\bar{\mathbf{g}}_\gamma$ with Eq. (269):

$$\delta \bar{\mathbf{n}} \cdot \bar{\mathbf{g}}_\gamma = -\delta \bar{\mathbf{g}}_\gamma \cdot \bar{\mathbf{n}}, \tag{310}$$

recognizing the right-hand side of that in two places in Eq. (309) and replacing only the second one, we obtain

$$\delta \bar{\mathbf{n}} = -\bar{\mathbf{T}} \cdot \bar{\mathbf{G}}^\gamma \delta \bar{\mathbf{g}}_\gamma \cdot \bar{\mathbf{n}} \bar{\mathbf{T}} \cdot \bar{\mathbf{G}}_\beta \bar{\mathbf{g}}^\beta + \delta \bar{\mathbf{n}} \cdot \bar{\mathbf{g}}_\gamma \bar{\mathbf{G}}^\gamma \cdot \bar{\mathbf{B}}\bar{\mathbf{B}} \cdot \bar{\mathbf{G}}_\beta \bar{\mathbf{g}}^\beta. \tag{311}$$

With that, for any vector \mathbf{q} , we have

$$\begin{aligned} \int_{\bar{S}_0} \delta \bar{\mathbf{n}} \cdot \mathbf{q} dS &= - \int_{\bar{S}_0} \bar{\mathbf{T}} \cdot \bar{\mathbf{G}}^\gamma \delta \bar{\mathbf{g}}_\gamma \cdot \bar{\mathbf{n}} \bar{\mathbf{T}} \cdot \bar{\mathbf{G}}_\beta \bar{\mathbf{g}}^\beta \cdot \mathbf{q} dS \\ &+ \int_{\bar{S}_0} \delta \bar{\mathbf{n}} \cdot \bar{\mathbf{g}}_\gamma \bar{\mathbf{G}}^\gamma \cdot \bar{\mathbf{B}}\bar{\mathbf{B}} \cdot \bar{\mathbf{G}}_\beta \bar{\mathbf{g}}^\beta \cdot \mathbf{q} dS. \end{aligned} \tag{312}$$

We apply integration by parts to the first integral on the right-hand side after recognizing from Eq. (2) that $\bar{\mathbf{T}} \cdot \bar{\mathbf{G}}^\gamma \delta \bar{\mathbf{g}}_\gamma = \bar{\mathbf{T}} \cdot \bar{\mathbf{G}}^\gamma (\delta \bar{\mathbf{x}})_{,\gamma}$ and realizing that $\bar{\mathbf{T}} \cdot \bar{\mathbf{G}}^\gamma (\delta \bar{\mathbf{x}})_{,\gamma}$ is the spatial derivative along the line of integration. Keeping in mind that \bar{S}_0 is a closed curve in the integration by parts, we obtain

$$\begin{aligned} \int_{\bar{S}_0} \delta \bar{\mathbf{n}} \cdot \mathbf{q} dS &= \int_{\bar{S}_0} \delta \bar{\mathbf{x}} \cdot (\bar{\mathbf{n}} \bar{\mathbf{T}} \cdot \bar{\mathbf{G}}_\beta \bar{\mathbf{g}}^\beta \cdot \mathbf{q})_{,\gamma} \bar{\mathbf{G}}^\gamma \cdot \bar{\mathbf{T}} dS \\ &+ \int_{\bar{S}_0} \delta \bar{\mathbf{n}} \cdot \bar{\mathbf{g}}_\gamma \bar{\mathbf{G}}^\gamma \cdot \bar{\mathbf{B}}\bar{\mathbf{B}} \cdot \bar{\mathbf{G}}_\beta \bar{\mathbf{g}}^\beta \cdot \mathbf{q} dS. \end{aligned} \tag{313}$$

Using the product rule in the first integral on the right, we get

$$\int_{\bar{S}_0} \delta \bar{\mathbf{x}} \cdot (\bar{\mathbf{n}} \bar{\mathbf{T}} \cdot \bar{\mathbf{G}}_\beta \bar{\mathbf{g}}^\beta \cdot \mathbf{q})_{,\gamma} \bar{\mathbf{G}}^\gamma \cdot \bar{\mathbf{T}} dS$$

$$\begin{aligned} &= \int_{\bar{S}_0} \delta \bar{\mathbf{x}} \cdot \bar{\mathbf{n}}_{,\gamma} \bar{\mathbf{T}} \cdot \bar{\mathbf{G}}_\beta \bar{\mathbf{g}}^\beta \cdot \mathbf{q} \bar{\mathbf{G}}^\gamma \cdot \bar{\mathbf{T}} dS \\ &+ \int_{\bar{S}_0} \delta \bar{\mathbf{x}} \cdot \bar{\mathbf{n}} (\bar{\mathbf{T}} \cdot \bar{\mathbf{G}}_\beta \bar{\mathbf{g}}^\beta \cdot \mathbf{q})_{,\gamma} \bar{\mathbf{G}}^\gamma \cdot \bar{\mathbf{T}} dS, \end{aligned} \tag{314}$$

and by substituting for $\bar{\mathbf{n}}_{,\gamma}$ from Eq. (265), we obtain

$$\begin{aligned} &\int_{\bar{S}_0} \delta \bar{\mathbf{x}} \cdot (\bar{\mathbf{n}} \bar{\mathbf{T}} \cdot \bar{\mathbf{G}}_\beta \bar{\mathbf{g}}^\beta \cdot \mathbf{q})_{,\gamma} \bar{\mathbf{G}}^\gamma \cdot \bar{\mathbf{T}} dS \\ &= \int_{\bar{S}_0} \delta \bar{\mathbf{x}} \cdot \bar{\boldsymbol{\kappa}} \cdot \bar{\mathbf{g}}_\gamma \bar{\mathbf{G}}^\gamma \cdot \bar{\mathbf{T}}\bar{\mathbf{T}} \cdot \bar{\mathbf{G}}_\beta \bar{\mathbf{g}}^\beta \cdot \mathbf{q} dS \\ &+ \int_{\bar{S}_0} \delta \bar{\mathbf{x}} \cdot \bar{\mathbf{n}} (\bar{\mathbf{T}} \cdot \bar{\mathbf{G}}_\beta \bar{\mathbf{g}}^\beta \cdot \mathbf{q})_{,\gamma} \bar{\mathbf{G}}^\gamma \cdot \bar{\mathbf{T}} dS. \end{aligned} \tag{315}$$

Combining Eqs. (313) and (315) and recognizing the left-hand sides of Eqs. (290) and (291), we obtain

$$\begin{aligned} \int_{\bar{S}_0} \delta \bar{\mathbf{n}} \cdot \mathbf{q} dS &= \int_{\bar{S}_0} \delta \bar{\mathbf{x}} \cdot \bar{\mathbf{n}} \left(\frac{1}{\lambda_T} \bar{\mathbf{t}}^* \cdot \mathbf{q} \right)_{,\gamma} \bar{\mathbf{G}}^\gamma \cdot \bar{\mathbf{T}} dS \\ &+ \int_{\bar{S}_0} \delta \bar{\mathbf{x}} \cdot \bar{\boldsymbol{\kappa}} \cdot \bar{\mathbf{t}} \bar{\mathbf{t}}^* \cdot \mathbf{q} dS \\ &+ \int_{\bar{S}_0} \delta \bar{\mathbf{n}} \cdot \bar{\mathbf{b}} \bar{\mathbf{b}}^* \cdot \mathbf{q} dS. \end{aligned} \tag{316}$$

D Constitutive models

We test two constitutive models: neo-Hookean and Fung’s materials. The strain-energy density functions are

$$\varphi_{\text{NH}}(\mathbf{C}) = \frac{1}{2} \mu (\text{tr} \mathbf{C} - 3), \tag{317}$$

$$\varphi_{\text{F}}(\mathbf{C}) = D_1 \left(e^{(D_2(\text{tr} \mathbf{C} - 3))} - 1 \right), \tag{318}$$

where μ is the shear modulus, and D_1 and $D_2 = 8.365$ are the coefficients of the Fung’s material model. The shear modulus at the undeformed configuration is $\mu_0 = \mu$ for the neo-Hookean material and $\mu_0 = 2D_1 D_2$ for the Fung’s material. We determine the bulk modulus from ν and μ_0 as

$$\kappa_{\text{B}} = \frac{2\mu_0 (1 + \nu)}{3(1 - 2\nu)}. \tag{319}$$

D.1 Incompressible material

For incompressible material, we use

$$\varphi_{\text{NHI}}(\mathbf{C}) = \varphi_{\text{NH}}(\mathbf{C}) + p(1 - J), \tag{320}$$

$$\varphi_{\text{FI}}(\mathbf{C}) = \varphi_{\text{F}}(\mathbf{C}) + p(1 - J), \tag{321}$$

and p can be calculated by using the constraint $J = 1$ in the equation associated with the out-of-plane direction.

We use the label “ $\nu = 0.5$ ” in reporting the results for the incompressible-material cases, but we use the forms above in the tests.

D.2 Compressible material

For compressible material, we use

$$\varphi_{\text{NHR}}(\mathbf{C}) = \varphi_{\text{NH}}\left(J^{-\frac{2}{3}}\mathbf{C}\right) + \varphi_{\text{vol}}(J), \quad (322)$$

$$\varphi_{\text{FR}}(\mathbf{C}) = \varphi_{\text{F}}\left(J^{-\frac{2}{3}}\mathbf{C}\right) + \varphi_{\text{vol}}(J), \quad (323)$$

where

$$\varphi_{\text{vol}}(J) = \kappa_{\text{B}}\beta_{\text{B}}^{-2}(\beta_{\text{B}} \ln J + J^{-\beta_{\text{B}}} - 1), \quad (324)$$

and we use $\beta_{\text{B}} = -2$. This form with β_{B} was introduced in [45].

References

- Kiendl J, Bletzinger KU, Linhard J, Wüchner R (2009) Isogeometric shell analysis with Kirchhoff-Love elements. *Comput Methods Appl Mech Eng* 198:3902–3914
- Kiendl J, Bazilevs Y, Hsu M-C, Wüchner R, Bletzinger K-U (2010) The bending strip method for isogeometric analysis of Kirchhoff-Love shell structures comprised of multiple patches. *Comput Methods Appl Mech Eng* 199:2403–2416
- Bazilevs Y, Hsu M-C, Kiendl J, Wüchner R, Bletzinger K-U (2011) 3D simulation of wind turbine rotors at full scale. Part II: Fluid-structure interaction modeling with composite blades. *Int J Numer Methods Fluids* 65:236–253
- Kiendl J, Hsu M-C, Wu MCH, Reali A (2015) Isogeometric Kirchhoff-Love shell formulations for general hyperelastic materials. *Comput Methods Appl Mech Eng* 291:280–303
- Takizawa K, Tezduyar TE, Sasaki T (2019) Isogeometric hyperelastic shell analysis with out-of-plane deformation mapping. *Comput Mech* 63:681–700. <https://doi.org/10.1007/s00466-018-1616-3>
- Bazilevs Y, Hsu M-C, Kiendl J, Benson DJ (2012) A computational procedure for pre-bending of wind turbine blades. *Int J Numer Methods Eng* 89:323–336
- Bazilevs Y, Hsu M-C, Takizawa K, Tezduyar TE (2012) ALE-VMS and ST-VMS methods for computer modeling of wind-turbine rotor aerodynamics and fluid-structure interaction. *Math Models Methods Appl Sci* 22(supp02):1230002. <https://doi.org/10.1142/S0218202512300025>
- Bazilevs Y, Hsu M-C, Scott MA (2012) Isogeometric fluid-structure interaction analysis with emphasis on non-matching discretizations, and with application to wind turbines. *Comput Methods Appl Mech Eng* 24–9252:28–41
- Bazilevs Y, Takizawa K, Tezduyar TE (2013) *Computational Fluid-Structure Interaction: Methods and Applications*. Wiley, ISBN 978-0470978771
- Bazilevs Y, Korobenko A, Deng X, Yan J (2015) Novel structural modeling and mesh moving techniques for advanced FSI simulation of wind turbines. *Int J Numer Methods Eng* 102:766–783. <https://doi.org/10.1002/nme.4738>
- Takizawa K, Tezduyar TE, Kostov N (2014) Sequentially-coupled space-time FSI analysis of bio-inspired flapping-wing aerodynamics of an MAV. *Comput Mech* 54:213–233. <https://doi.org/10.1007/s00466-014-0980-x>
- Hsu M-C, Kamensky D, Bazilevs Y, Sacks MS, Hughes TJR (2014) Fluid-structure interaction analysis of bioprosthetic heart valves: significance of arterial wall deformation. *Comput Mech* 54:1055–1071. <https://doi.org/10.1007/s00466-014-1059-4>
- Hsu M-C, Kamensky D, Xu F, Kiendl J, Wang C, Wu MCH, Mineroff J, Reali A, Bazilevs Y, Sacks MS (2015) Dynamic and fluid-structure interaction simulations of bioprosthetic heart valves using parametric design with T-splines and Fung-type material models. *Comput Mech* 55:1211–1225. <https://doi.org/10.1007/s00466-015-1166-x>
- Wu MCH, Zakerzadeh R, Kamensky D, Kiendl J, Sacks MS, Hsu M-C (2018) An anisotropic constitutive model for immersogeometric fluid-structure interaction analysis of bioprosthetic heart valves. *J Biomech* 74:23–31
- Xu F, Morganti S, Zakerzadeh R, Kamensky D, Auricchio F, Reali A, Hughes TJR, Sacks MS, Hsu M-C (2018) A framework for designing patient-specific bioprosthetic heart valves using immersogeometric fluid-structure interaction analysis. *Int J Numer Methods Biomed Eng* 34:e2938
- Kamensky D, Xu F, Lee C-H, Yan J, Bazilevs Y, Hsu M-C (2018) A contact formulation based on a volumetric potential: application to isogeometric simulations of atrioventricular valves. *Comput Methods Appl Mech Eng* 330:522–546
- Bazilevs Y, Deng X, Korobenko A, di Scalea FL, Todd MD, Taylor SG (2015) Isogeometric fatigue damage prediction in large-scale composite structures driven by dynamic sensor data. *J Appl Mech* 82:091008
- Deng X, Korobenko A, Yan J, Bazilevs Y (2015) Isogeometric analysis of continuum damage in rotation-free composite shells. *Comput Methods Appl Mech Eng* 284:349–372
- Bazilevs Y, Korobenko A, Deng X, Yan J (2016) FSI modeling for fatigue-damage prediction in full-scale wind-turbine blades. *J Appl Mech* 83(6):061010
- Bazilevs Y, Pigazzini MS, Ellison A, Kim H (2017) A new multi-layer approach for progressive damage simulation in composite laminates based on isogeometric analysis and Kirchhoff-Love shells. Part I: Basic theory and modeling of delamination and transverse shear. *Comput Mech*. <https://doi.org/10.1007/s00466-017-1513-1>
- Pigazzini MS, Bazilevs Y, Ellison A, Kim H (2017) A new multi-layer approach for progressive damage simulation in composite laminates based on isogeometric analysis and Kirchhoff-Love shells. Part II: Impact modeling. *Comput Mech*. <https://doi.org/10.1007/s00466-017-1514-0>
- Pigazzini MS, Bazilevs Y, Ellison A, Kim H (2018) Isogeometric analysis for simulation of progressive damage in composite laminates. *J Compos Mater*. <https://doi.org/10.1177/0021998318770723>
- Benzaken J, Herrema AJ, Hsu M-C, Evans JA (2017) A rapid and efficient isogeometric design space exploration framework with application to structural mechanics. *Comput Methods Appl Mech Eng* 316:1215–1256
- Herrema AJ, Wiese NM, Darling CN, Ganapathysubramanian B, Krishnamurthy A, Hsu M-C (2017) A framework for parametric design optimization using isogeometric analysis. *Comput Methods Appl Mech Eng* 316:944–965
- Simo JC, Rifai MS, Fox DD (1990) On a stress resultant geometrically exact shell model. Part IV: variable thickness shells with through-the-thickness stretching. *Comput Methods Appl Mech Eng* 81:91–126
- Bischoff M, Ramm E (1997) Shear deformable shell elements for large strains and rotations. *Int J Numer Methods Eng* 40:4427–4449

27. Pimenta PM, Campello EMB, Wriggers P (2004) A fully nonlinear multi-parameter shell model with thickness variation and a triangular shell finite element. *Comput Mech* 34:181–193
28. Klinkel S, Gruttmann F, Wagner W (2008) A mixed shell formulation accounting for thickness strains and finite strain 3d material models. *Int J Numer Methods Eng* 74:945–970
29. Ivannikov V, Tiago C, Pimenta PM (2014) On the boundary conditions of the geometrically nonlinear Kirchhoff-Love shell theory. *Int J Solids Struct* 51:3101–3112
30. Ivannikov V, Tiago C, Pimenta PM (2015) Generalization of the C^1 TUBA plate finite elements to the geometrically exact Kirchhoff-Love shell model. *Comput Methods Appl Mech Eng* 294:210–244
31. Viebahn N, Pimenta PM, Schröder J (2016) A simple triangular finite element for nonlinear thin shells: statics, dynamics and anisotropy. *Comput Mech* 59:281–297
32. Tezduyar TE, Sathe S, Schwaab M, Conklin BS (2008) Arterial fluid mechanics modeling with the stabilized space-time fluid-structure interaction technique. *Int J Numer Methods Fluids* 57:601–629. <https://doi.org/10.1002/flid.1633>
33. Tezduyar TE, Schwaab M, Sathe S (2009) Sequentially-Coupled Arterial Fluid-Structure Interaction (SCAFSI) technique. *Comput Methods Appl Mech Eng* 198:3524–3533. <https://doi.org/10.1016/j.cma.2008.05.024>
34. Takizawa K, Christopher J, Tezduyar TE, Sathe S (2010) Space-time finite element computation of arterial fluid-structure interactions with patient-specific data. *Int J Numer Methods Biomed Eng* 26:101–116. <https://doi.org/10.1002/cnm.1241>
35. Tezduyar TE, Takizawa K, Moorman C, Wright S, Christopher J (2010) Multiscale sequentially-coupled arterial FSI technique. *Comput Mech* 46:17–29. <https://doi.org/10.1007/s00466-009-0423-2>
36. Takizawa K, Moorman C, Wright S, Christopher J, Tezduyar TE (2010) Wall shear stress calculations in space-time finite element computation of arterial fluid-structure interactions. *Comput Mech* 46:31–41. <https://doi.org/10.1007/s00466-009-0425-0>
37. Takizawa K, Moorman C, Wright S, Purdue J, McPhail T, Chen PR, Warren J, Tezduyar TE (2011) Patient-specific arterial fluid-structure interaction modeling of cerebral aneurysms. *Int J Numer Methods Fluids* 65:308–323. <https://doi.org/10.1002/flid.2360>
38. Tezduyar TE, Takizawa K, Brummer T, Chen PR (2011) Space-time fluid-structure interaction modeling of patient-specific cerebral aneurysms. *Int J Numer Methods Biomed Eng* 27:1665–1710. <https://doi.org/10.1002/cnm.1433>
39. Takizawa K, Brummer T, Tezduyar TE, Chen PR (2012) A comparative study based on patient-specific fluid-structure interaction modeling of cerebral aneurysms. *J Appl Mech* 79:010908. <https://doi.org/10.1115/1.4005071>
40. Takizawa K, Tezduyar TE, Buscher A, Asada S (2014) Space-time interface-tracking with topology change (ST-TC). *Comput Mech* 54:955–971. <https://doi.org/10.1007/s00466-013-0935-7>
41. Benson D, Bazilevs Y, Hsu M-C, Hughes TJR (2011) A large deformation, rotation-free, isogeometric shell. *Comput Methods Appl Mech Eng* 200:1367–1378
42. Sasaki T, Takizawa K, Tezduyar TE (2019) Aorta zero-stress state modeling with T-spline discretization. *Comput Mech* 63:1315–1331. <https://doi.org/10.1007/s00466-018-1651-0>
43. Kuraishi T, Takizawa K, Tezduyar TE (2019) Space-time computational analysis of tire aerodynamics with actual geometry, road contact, tire deformation, road roughness and fluid film. *Comput Mech* 64:1699–1718. <https://doi.org/10.1007/s00466-019-01746-8>
44. Terahara T, Takizawa K, Tezduyar TE, Tsushima A, Shiozaki K (2020) Ventricle-valve-aorta flow analysis with the Space-Time Isogeometric Discretization and Topology Change. *Comput Mech* 65:1343–1363. <https://doi.org/10.1007/s00466-020-01822-4>
45. Takizawa K, Tezduyar TE, Avsar R (2020) A low-distortion mesh moving method based on fiber-reinforced hyperelasticity and optimized zero-stress state. *Comput Mech* 65:1567–1591. <https://doi.org/10.1007/s00466-020-01835-z>

Publisher's Note Springer Nature remains neutral with regard to jurisdictional claims in published maps and institutional affiliations.